

T.R.  
VAN YUZUNCU YIL UNIVERSITY  
INSTITUTE OF NATURAL AND APPLIED SCIENCE  
DEPARTMENT OF MECHANICAL ENGINEERING

**PROCESSING OF POROUS TITANIUM NIOBIUM ALLOYS FOR  
BIOMEDICAL APPLICATIONS**



MASTER'S THESIS

PREPARED BY: DANA KAREEM HAMEED PALANI  
SUPERVISOR: Assoc. Prof. Dr. Tarık AYDOĞMUŞ

VAN-2018



T.R.  
VAN YUZUNCU YIL UNIVERSITY  
INSTITUTE OF NATURAL AND APPLIED SCIENCE  
DEPARTMENT OF MECHANICAL ENGINEERING

**PROCESSING OF POROUS TITANIUM NIOBIUM ALLOYS FOR  
BIOMEDICAL APPLICATIONS**



MASTER'S THESIS

PREPARED BY: DANA KAREEM HAMEED PALANI

VAN-2018

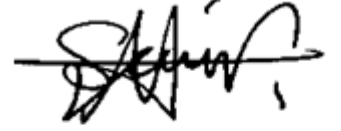


## ACCEPTANCE AND APPROVAL PAGE

Master thesis is entitled "PROCESSING OF POROUS TITANIUM NIOBIUM ALLOYS FOR BIOMEDICAL APPLICATIONS" and prepared by Dana Kareem Hameed PALANI under supervision of Assoc. Prof. Dr. Tarık AYDOĞMUŞ, in the Mechanical Engineering Department has been accepted as M.Sc. thesis according to Guidelines of Graduate School of Higher Education on 22.01.2018 and certified by all the majority jury members, whose signatures are given below.

President: Yrd. Doç. Dr. Hüseyin ŞEVİK

Signature:



Member: Asst. Prof. Dr. Serap KOÇ

Signature:



Member: Assoc. Prof. Dr. Tarık AYDOĞMUŞ

Signature:



This thesis has been approved by committee of The Institute of Natural and Applied Science on / / with decision .

Signature

Prof. Dr. Suat SENSOY

Director of Institute



## **THESIS STATEMENT**

All information presented in the thesis obtained in the frame of ethical behavior and academic rules. In addition, all kind of information that does not belong to me has been cited appropriately in the thesis prepared by the thesis writing rules.

Signature

Dana Kareem Hameed PALANI







## ABSTRACT

### PROCESSING OF POROUS TITANIUM NIOBIUM ALLOYS FOR BIOMEDICAL APPLICATIONS

PALANI Dana Kareem Hameed  
M.Sc. Thesis Mechanical Engineering Department  
Supervisor: Assoc. Prof. Dr. Tarık AYDOGMUŞ  
January 2018, 113 pages

In this study, pure Ti, pure Nb and spherical Mg elemental powders were used to produce  $Ti_{74}Nb_{26}$  alloys having porosities in the range of 43-68% for biomedical bone replacement applications. Space holder technique combined with hot pressing was used to fabricate porous specimens for the first time. Firstly, Ti, Nb and different amount of Mg powders (40%, 50%, 60% and 70% by vol.) were mixed by hand for 15min. Mixed powders were then poured into hollow cylindrical graphite dies with inner diameter of 15mm and hot pressed at 600°C for 1h to prevent melting of Mg (650°C) under a constant pressure of 50MPa to produce samples with a height of 10 mm and argon gas was used during production to prevent oxidation. After hot press samples were sintered in a vertical furnace at 1200°C for 4h under flowing inert argon gas atmosphere. During sintering Mg also (Mg boiling point is 1090°C) was evaporated and removed from the samples and accordingly macro-pores were formed. X-Ray Diffraction and Scanning Electron Microscopy investigations showed that  $\beta$  phase was the main phase in the microstructure of all the samples. A small amount of  $\alpha$  and pure Nb were also observed. Mechanical properties of the porous specimens were sufficient for cancellous bone replacement applications whereas not suitable for the cortical bone replacements. Undesired micro-pores formed as a result of inefficient hot pressing and inadequate sintering temperature caused poor mechanical properties.

**Keywords:** Hot pressing, Magnesium space holder technique, Mechanical properties, Porous Titanium-Niobium alloys, Powder metallurgy.



## ÖZET

### BİYOMEDİKAL UYGULAMALAR İÇİN GÖZENEKLİ TİTANYUM NİYOBYUM ALAŞIMLARININ ÜRETİLMESİ

PALANI, Dana Kareem Hameed  
Yüksek Lisans Tezi, MakineMühendisliği Anabilim Dalı  
Tez Danışmanı : Doç. Dr. Tarık AYDOGMUŞ  
Ocak 2018, 113 sayfa

Bu çalışmada, biyomedikal kemik implant uygulamaları için gözeneklilikleri %43-68 aralığında olan  $Ti_{74}Nb_{26}$  alaşımlarını üretmek için saf Ti, saf Nb ve küresel Mg tozları kullanılmıştır. Gözenekli numuneleri üretmek için ilk kez sıcak presleme işlemi ile boşluk oluşturucu metot birlikte kullanılmıştır. Öncelikle, Ti, Nb ve farklı miktarda Mg tozları (%40, %50, %60 ve %70, hacimce) 15 dakika süre ile karıştırılmıştır. Daha sonra toz karışımları, iç çapı 15 mm olan içi boş silindirik grafit kalıplara doldurulmuş ve 10 mm yüksekliğinde numuneler üretmek için 50 MPa sabit basınç altında Mg'nin erimesini (650 °C) önlemek için 600 °C'de 1 saat süre ile sıcak presleme işlemine tabi tutulmuştur. Oksidasyonu önlemek için üretim sırasında saf argon gazı kullanılmıştır. Sıcak presleme işleminden sonra numuneler dikey bir fırında 1200 °C'de 4 saat boyunca inört argon gazı atmosferi altında sinterlenmiştir. Sinterleme sırasında eşzamanlı olarak Mg da (1090 °C) buharlaştırılmış ve numunelerden uzaklaştırılarak makro gözenekler oluşturulmuştur. X-Işını Kırınımı ve Taramalı Elektron Mikroskobu incelemeleri, tüm numunelerin mikroyapısında ana faz olan  $\beta$  fazının yanı sıra az miktarda  $\alpha$  fazı ve saf Nb'un bulunduğunu göstermiştir. Üretilen gözenekli alaşımların mekanik özelliklerinin süngerimsi kemik implantasyonu uygulamaları için yeterli iken, yoğun (kortikal) kemik implantasyonları için uygun olmadıkları sonucuna ulaşılmıştır. Verimsiz sıcak presleme ve yetersiz sinterleme sıcaklığının bir sonucu olarak oluşan mikro gözeneklerin düşük mekanik özelliklere neden olduğu görülmüştür.

**Anahtar kelimeler:** Gözenekli Titanyum-Niyobyum alaşımları, Mg boşluk oluşturucu yöntemi, Mekanik özellikler, Sıcak presleme, Toz metalurjisi.



## ACKNOWLEDGMENTS

Firstly, I thank (ALLAH) for giving me the opportunities that I have received.

Great thanks to my supervisor, Assoc. Prof. Dr. Tarik AYDOĞMUŞ who was always helpful to me. We had many conversations during the development of ideas.

Great thanks to Mr. Fevzi KELEN who was always helpful to me during production.

Great thanks to my father Kareem Hameed, my mother Samia Mohamad Faraj and my wife Hanar Mohamad for helping to finish my M.Sc. grade.

To my children Yad and Yara

2018

Dana Kareem Hameed PALANI



# CONTENTS

	<b>Pages</b>
ABSTRACT .....	i
ACKNOWLEDGMENTS .....	v
CONTENTS .....	vii
LIST OF TABLES .....	ix
LIST OF FIGURES .....	xi
SYMBOLS AND ABBREVIATIONS .....	xvii
1. INTRODUCTION .....	1
2. LITERATURE REVIEW .....	5
2.1. Basic Material Requirements of Ti-Based Alloys for Biomedical Applications.5	
2.1.1. Mechanical compatibility .....	5
2.1.2. Biocompatibility .....	7
2.2. Ti and Ti Alloys for Biomedical and Implant Applications .....	11
2.2.1. The Ti-Nb phase diagram .....	11
2.2.2. Ti-Nb system: relationship between structure and property .....	13
2.3. Porous TiNb .....	17
2.3.1. General .....	17
2.3.2. Processing and characterization of porous TiNb .....	20
2.3.3. Different fabrication ways for porous Ti-based alloys .....	21
2.3.4. Powder metallurgy .....	25
2.4. Production Methods .....	28
2.4.1. General .....	28
2.4.2. Spark plasma sintering (SPS) .....	29
2.4.3. Microwave sintering .....	31
2.4.4. Space holder technique .....	33
2.4.5. Metal injection molding (MIM) .....	42
2.4.6. Conventional sintering (CS) .....	43
2.4.7. Additive manufacturing (3D printing) .....	44
2.5. Compression Behavior of Porous Metallic Materials .....	44
2.5.1. General .....	44
2.5.2. Compression response .....	45

	<b>Pages</b>
3. MATERIALS AND METHODS .....	49
3.1. Powders Used .....	49
3.2. Experimental Method .....	49
3.3. Space Holder Technique .....	52
3.4. Sample Characterization .....	61
3.4.1. SEM .....	61
3.4.2. XRD .....	63
3.4.3. Density and porosity measurements .....	63
3.4.4. Compression behavior.....	67
4. RESULTS AND DISCUSSION .....	69
4.1. Density and Porosity .....	69
4.2. Microstructure of Porous Ti <sub>74</sub> Nb <sub>26</sub> Alloys .....	71
4.3. Effect of Hot Pressing on Spherical Pore Structure.....	82
4.4. Mechanical Behavior of Porous Ti <sub>74</sub> Nb <sub>26</sub> .....	83
4.4.1. Compression behavior.....	83
4.4.2. Effect of porosity on the mechanical properties .....	86
5. CONCLUSION .....	89
REFERENCES .....	91
APPENDIX: EXTENDED TURKISH SUMMARY (GENİŞLETİLMİŞ TÜRKÇE ÖZET).....	99
CURRICULUM VITAE .....	113



## LIST OF TABLES

<b>Table</b>	<b>Pages</b>
Table 2.1. Physical and mechanical properties of most commonly implant materials in comparison to human bone .....	8
Table 2.2. Mechanical properties of TiNi foams tested in compression, where E is Young's modulus, $\sigma^o$ is yield strength, $\sigma_{max}$ is compressive strength. The values given together with the standard deviations are average of four or more tests .....	47
Table 3.1. Amount of powders used to produce samples .....	53
Table 3.2. $W_{dry}$ for each sample .....	65
Table 3.3. $W_{susp.}$ for each sample.....	66
Table 3.4. $W_{sat.}$ for each sample .....	66
Table 4.1. Bulk density of each sample.....	69
Table 4.2. Percentages of both total porosity and open porosity as a function of Mg addition.....	70
Table 4.3. Percent of closed porosity .....	70
Table 4.4. Mechanical properties of porous $Ti_{74}Nb_{26}$ alloys tested in compression .....	86
Table 4.5. Mechanical properties of macroporous Ti-35Nb (wt.%) alloy .....	86
Table 4.6. Mechanical properties of macroporous Ti40Nb alloy.....	86



## LIST OF FIGURES

<b>Figures</b>	<b>Pages</b>
Figure 1.1. Total hip and knee replacement. ....	1
Figure 2.1. Elastic modulus of some metals and alloys used as implant materials. ....	6
Figure 2.2. Schematic of stress shielding. ....	7
Figure 2.3. Polarization resistance and biocompatibility of metals used for implant materials.....	9
Figure 2.4. Percentage share of metal allergy caused by each metallic element.....	9
Figure 2.5. Debris produce by wear of implant.....	10
Figure 2.6. Equilibrium phase diagram of Ti-Nb system.....	12
Figure 2.7. CCT diagrams for Ti–Nb–Zr–Ta containing approximately 7 wt.% Zr where WQ, OQ, AC, FC and RT are water quenching, oil quenching, air cooling, furnace cooling, and room temperature respectively. ....	13
Figure 2.8. Crystal structure of hcp $\alpha$ phase and bcc $\beta$ phase. ....	14
Figure 2.9. Effect of alloying elements on Ti alloys phase diagrams (schematically)....	15
Figure 2.10. Ti6Al alloys with different V content by three-dimensional phase diagram. ....	16
Figure 2.11. Effect of Nb content on Young’s modulus of quenched Ti-Nb alloys. ....	17
Figure 2.12. Some natural cellular material examples .....	18
Figure 2.13. Some engineering cellular solid structures. ....	19
Figure 2.14. Applications of cellular metals grouped according to functional or structural depending on the degree of “openness” needed.....	19
Figure 2.15. Several applications of porous aluminum. ....	20
Figure 2.16. Overview of classification of production methods for cellular metallic materials.....	21
Figure 2.17. Porosity in metallic bodies processed by sintering of powders with space holder material. ....	23

<b>Figures</b>	<b>Pages</b>
Figure 2.18. Schematic show in some parts of the powder there is particle deformation while other parts are still in a rearrangement stage. ....	24
Figure 2.19. Plastic deformation cause by increase in pressure. ....	24
Figure 2.20. Density distribution (a) single action pressing (b) double action pressing. 25	
Figure 2.21. Effect of H/D on pressure distributions. ....	25
Figure 2.22. Microstructure evolution during sintering of NiAl a) early stage, b) final stage. ....	26
Figure 2.23. Density evolution of pure Al <sub>2</sub> O <sub>3</sub> . ....	27
Figure 2.24. A scheme explain the influence of powder size on pore size. ....	27
Figure 2.25. Relationship between porosity and Young's modulus in porous titanium. 28	
Figure 2.26. Pore morphologies obtained by powder metallurgical processing techniques. ....	29
Figure 2.27. Schematic diagram of spark plasma sintering device. ....	30
Figure 2.28. Spark plasma sintering process. ....	31
Figure 2.29. Schematic diagram of the two-directional microwave used in Gupta and Wong study. ....	32
Figure 2.30. Schematic fabrication process for porous titanium alloy by space holder technique. ....	33
Figure 2.31. SEM images of fractured TiNi foams (1100°C, 1h) showing interconnected pore structure. ....	34
Figure 2.32. Pore characteristics of produced Ti-6Al-4V foams. ....	36
Figure 2.33. SEM micrographs of porous TiNi samples produced with Ti-50.6 at. %Ni powders (1100 °C, 1 h) with the porosity of (a) 37%, (b) 43%, (c) 51%, (d) 59%, (e) 66% and (f) 81%. ....	38
Figure 2.34. Ti – Mg Binary phase diagram. ....	39
Figure 2.35. Nb – Mg Binary phase diagram. ....	39

<b>Figures</b>	<b>Pages</b>
Figure 2.36. XRD patterns of as-quenched sintered Ti40Nb samples a) reference sample without space-holder b) 50% porous sample prepared using Mg as space holder. ....	40
Figure 2.37. XRD pattern of porous Ti35Nb sintered at 1200°C for 2h. ....	41
Figure 2.38. Flow diagram of metal injection molding. ....	42
Figure 2.39. XRD pattern for as-sintered CP Ti, Ti-10Nb, Ti-16Nb and Ti-22Nb.....	43
Figure 2.40. Schematic comparisons of metal AM processes and systems. ....	45
Figure 2.41. Schematic stress-strain curves of porous materials.....	46
Figure 2.42. Porosity versus Young's modulus and compression strength for samples produced with NaCl space-holder.....	47
Figure 2.43. Static compressive stress-strain (s-ε) curves of the porous Ti at different SPS sintering temperatures. ....	48
Figure 3.1. SEM micrographs showing morphology of a) and b) Ti powders c) and d) Nb powders, and e) and f) Mg powders. ....	50
Figure 3.2. XRD patterns for a) Pure Ti b) Pure Nb and c) Pure Mg.....	51
Figure 3.3. Schematic process of hot pressing and space holder technique.....	52
Figure 3.4. Ti, Nb and 70% Mg before mixing. ....	53
Figure 3.5. Graphite die.....	54
Figure 3.6. Powders in a graphite die under pressure inside the hot press furnace.....	54
Figure 3.7. Sample hot pressed at 600°C under a pressure of 50MPa for 1h.....	54
Figure 3.8. a) Grinding machine b) Grinding a sample.....	55
Figure 3.9. a) Sample before grinding b) Sample after grinding.....	56
Figure 3.10. Ti <sub>74</sub> Nb <sub>26</sub> with different amount of Mg spacers (vol.%). ....	56
Figure 3.11. Schematic drawing and picture of the vertical furnace.....	57
Figure 3.12. Ti <sub>74</sub> Nb <sub>26</sub> porous sample with 40% porosity cooled in the hot zone of the furnace after having been sintered for 4h at 1200°C. ....	57

<b>Figures</b>	<b>Pages</b>
Figure 3.13. Temperature-time curves for hot pressing (HP) and sintering (HP+S). ....	58
Figure 3.14. Pure Ti sponge particles used as getter during sintering, a) before sintering, b) after 4h sintering at 1200°C. ....	58
Figure 3.15. An electrical discharge machine (EDM).....	59
Figure 3.16. Ti <sub>74</sub> Nb <sub>26</sub> with 68% porosity sample after cutting by wire EDM with 5x5x10mm in dimension. ....	59
Figure 3.17. Polishing cloth pad (disk form).....	60
Figure 3.18. Cleaning samples by ultrasonic cleaner a) sample inside ethanol b) ultra-sonic cleaning machine. ....	61
Figure 3.19. Scanning electron microscopy. ....	62
Figure 3.20. Ti <sub>74</sub> Nb <sub>26</sub> porous samples inside vacuum chamber. ....	62
Figure 3.21. Types of reflected electrons according to surface of the sample. ....	63
Figure 3.22. Precisa balance (model LS 220A) equipped with a density determination kit. ....	64
Figure 3.23. a) drying oven b) samples inside drying oven. ....	64
Figure 3.24. Samples left at room temperature for 24h. ....	65
Figure 3.25 a) samples impregnated inside pure water b) bubbles on the surface of the porous sample. ....	65
Figure 4.1. Relation between density and porosity. ....	70
Figure 4.2. Closed porosity total porosity relation. ....	71
Figure 4.3. XRD spectra of sintered porous Ti <sub>74</sub> Nb <sub>26</sub> with 43% porosity.....	72
Figure 4.4. XRD spectra of sintered porous Ti <sub>74</sub> Nb <sub>26</sub> alloy with 54% porosity.....	72
Figure 4.5. XRD spectra of sintered porous Ti <sub>74</sub> Nb <sub>26</sub> with 59% porosity content. ....	73
Figure 4.6. XRD spectra of sintered porous Ti <sub>74</sub> Nb <sub>26</sub> alloy with 68% porosity ratio. ....	73
Figure 4.7. SEM micrograph of porous Ti <sub>74</sub> Nb <sub>26</sub> with 43% porosity. ....	75
Figure 4.8. SEM micrograph of porous Ti <sub>74</sub> Nb <sub>26</sub> alloy with 54% porosity. ....	75

<b>Figures</b>	<b>Pages</b>
Figure 4.9. SEM image of porous $Ti_{74}Nb_{26}$ with 59% porosity .....	76
Figure 4.10. SEM micrograph of porous $Ti_{74}Nb_{26}$ with 68% porosity content.....	76
Figure 4.11. BSE micrograph of 43% porous $Ti_{74}Nb_{26}$ .....	77
Figure 4.12. BSE micrograph of 54% porous $Ti_{74}Nb_{26}$ .....	77
Figure 4.13. BSE micrograph of 59% porous $Ti_{74}Nb_{26}$ .....	78
Figure 4.14. BSE micrograph of 68% porous $Ti_{74}Nb_{26}$ .....	78
Figure 4.15. EDS analysis result for region 1 ( $\alpha$ phase), Ti% (atomic) = 96.2 and Nb% (atomic) = 3.8. ....	79
Figure 4.16. EDS micrograph for region 2, Ti% = 79.1 and Nb% = 20.9. ....	80
Figure 4.17. EDS micrograph for region 3, Ti% = 70.2 and Nb% = 29.8. ....	81
Figure 4.18. EDS micrograph for region 4, Ti% = 0 and Nb% = 100. ....	82
Figure 4.19. Effect of hot pressing on pore structure resulting from yielding of Mg powders for, a) 43%, b) 54%, c) 59%, and d) 68% porous samples. ....	83
Figure 4.20. Stress-strain curves for porous samples with different amount of porosity, a) 43%, b) 54%, c) 59% and d) 68% .....	85
Figure 4.21. Compressive stress-strain curves of a) porous $Ti_{74}Nb_{26}$ alloys with different porosity and b) full density $Ti_{74}Nb_{26}$ produced by hot pressing at 800°C for 1h following sintering at 1200°C for 4h.....	87
Figure 4.22. Effect of porosity on elastic moduli in porous $Ti_{74}Nb_{26}$ porous samples with different porosity (43%, 54%, 59% and 68% porosity) sintered at 1200°C for 4h.....	88
Figure 4.23. Effect of porosity on strength in porous $Ti_{74}Nb_{26}$ porous samples with different porosity (43%, 54%, 59% and 68% porosity) sintered at 1200°C for 4h. ....	88





## **SYMBOLS AND ABBREVIATIONS**

Some of the symbols and abbreviations used in this study, along with explanations, it is presented.

<b>Symbols</b>	<b>Explanation</b>
<b>μm</b>	Micrometer
<b>GPa</b>	Giga Pascal
<b>°C</b>	Degree Celsius
<b>K</b>	Kelvin
<b>min</b>	Minute
<b>MPa</b>	Mega Pascal
<b>h</b>	hour
<b>KPa</b>	Kilo Pascal
<b>mm</b>	Millimeter
<b>g</b>	Gram
<b>cm</b>	Centimeter

<b>Abbreviations</b>	<b>Explanation</b>
<b>hcp</b>	Hexagonal close packing
<b>bcc</b>	Body centered cubic
<b>HIP</b>	Hot isostatic pressing
<b>SPS</b>	Spark plasma sintering
<b>SEM</b>	Scanning electron microscopy
<b>XRD</b>	X-ray diffraction
<b>Wt.%</b>	Weight percent
<b>Vol.%</b>	Volume percent
<b>RT</b>	Room temperature
<b>MIM</b>	Metal Injection Molding
<b>CS</b>	Conventional sintering
<b>RP</b>	Rapid prototyping
<b>SHT</b>	Space holder technique
<b>EDM</b>	Electrical discharge machining
<b>SE</b>	Secondary electron
<b>BS</b>	Backscattering electron
<b><math>W_{dry}</math></b>	Dry weight
<b><math>W_{susp}</math></b>	Suspended weight
<b><math>W_{sat}</math></b>	Saturated weight
<b>EDS</b>	Energy dispersive spectroscopy
<b>RP</b>	Rapid prototyping
<b>DMLS</b>	Direct metal laser sintering
<b>SLS</b>	Selective laser sintering
<b>DED</b>	Direct energy deposition

## 1. INTRODUCTION

Need for artificial implants increase with wounded, diseased hard tissue. For different parts of human body biomaterials are used, for example in knees, hips, artificial valves in the heart, stents in blood vessels, elbows, ears, replacement implants in shoulders and or dental structures (Ramakrishna et al., 2001; Aherwar, et al., 2015). Figure 1.1 shows an example of an implant used in hip and knee joints.

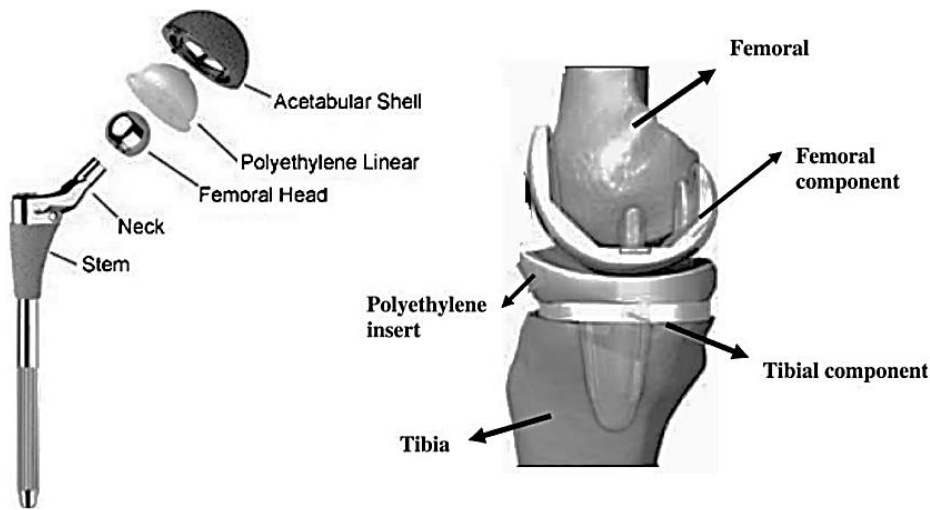


Figure 1.1. Total hip and knee replacement (Geetha, et al., 2009).

Another reason for possibility of hard tissue failure is the age. According to a report by the United Nations in 2013, the population of the age group over 60 years is increasing rapidly and in the more developed regions of the world, the ratio of elderly people is expected to increase by 45% as of 2050 (Ozan et al., 2015).

Simultaneously with the replacement surgeries, revision surgeries of hip and knee implants have also increased. With the pain for the patient, success rate of these revision surgeries are very small and very expensive (Kurtz et al., 2009). In the recent years the transportation volume by cars, bicycles and another movable device such as scooters and motorcycles increased associated traffic accidents. All of these increase the need for orthopedic surgeries and all these increase demand for development of biomedical materials. Implants can be made of ceramic, polymer or composite

materials, also metallic materials are used to produce about 70%-80% of biomaterial implants ( Zhuang et al., 2008; Wu et al., 2014). Characteristics that usually researchers try to follow it for biomedical application in terms of mechanical properties are low elastic modulus, excellent combination strength, superior corrosion resistance in the body environment, high fatigue resistance, high ductility, excellent wear resistance and excellent biocompatibility without cytotoxicity ( Wang, 1996; Long and Rack, 1998).

For load-bearing conditions ceramics or polymers cannot be used as replacement metallic biomaterials because mechanical properties such as strength are the main important properties for safety requirements for biomaterial applications. Metals and their alloys like stainless steels, Co-Cr alloys and commercially pure titanium (CP Ti) are widely used as biomedical materials because they have excellent mechanical properties. Sometimes problems occur when metals are used as biomaterials for example fracture occur due to corrosion and sometimes metals show toxicity, DNA damaging, cytotoxic, carcinogenic (cancer causing), mutagenic, allergenic and neurological effects (Biesiekierski et al., 2012).

Now CP Ti is suggested as an alternative for the stainless steel and Co-Cr alloys. CP Ti has better biocompatibility with human bone and very good corrosion resistance, however, when high strength required CP Ti cannot fulfill requirements of biomaterials (i.e. for hard tissue replacement or when high wear resistance needed). Loosening of implant arise when there is a large mismatch of the Young's moduli between the implant material and bone that is the most critical issue repeatedly faced in bone replacement applications termed "stress shielding". Implant material must have stiffness value which commensurate with that of the bone in order to diminish "stress shielding" effect.

Decrease in Young's modulus of the implant material to a degree similar to that of the bone cannot be reached by changing compositions or heat treatments since it is a basic intrinsic property of material but reduction can be achieved with reasonable loss in strength by producing pores into the sample.

Numerous studies have recently shown that human bones have very low elastic modulus if compared with  $\alpha$  type and  $\alpha + \beta$  type Ti-based alloys, causing stress shielding effect. For example, Young's modulus of the cortical bone tissue (max. 27GPa) is about 4 times smaller than ( $\alpha + \beta$ ) Ti-6Al-4V alloy.  $\beta$  Ti alloys have been

developed for orthopedic implant applications, they have relatively lower Young's modulus of elasticity, improved tissue response, greater strength and increased corrosion resistance in comparison to  $\alpha + \beta$  Ti (Evans, 1976; Ding et al., 1997; Rho et al., 1997; Kuroda et al., 1998; Ozan et al., 2015). For that reason, now  $\beta$  Ti alloys have been widely used to reduce the stress shielding effect (Kuroda et al., 1998; Hao et al., 2003; Sakaguchi et al., 2005), amongst which the representatives are Ti-13Nb-13Zr, Ti-12Mo-6Zr-2Fe, Ti-15Mo, Ti-35Nb-5Ta-7Zr, and Ti-29Nb-13Ta-4.6Zr. Mainly, elastic modulus of Ti-Nb-Ta-Zr alloys is more close to that of bone which is about 60 GPa, it is around half if it compared with pure Ti (Niinomi et al., 2007).

At present, decrease in elastic modulus of bulk Ti-based alloy to lower than 35 GPa is very hard and for this reason to decrease elastic modulus porous Ti-based alloys may be used. High difference in elastic modulus between implant material and bone remains a main problem for good fixation. On the other hand, to bear the physiological loads applied on it or serve for much longer time without failure and revision surgery the implanted materials should be strong and hard-wearing enough.

The demand to decrease elastic modulus, porous material of Ti-based alloys were introduced according to the literatures ( Wang, 1984; Zhu et al., 2005; Xiong et al., 2008). The reason how porous materials have smaller elastic modulus and stiffness is that the total amount of materials supporting the cross section area for bulk material is much higher than porous materials. As a result, if the stress is increased deformation is small for bulk material and high for porous material. Porous alloys are produced to reduce the stiffness. Totally, by helping bone tissue ingrowth into pores, porous materials can provide better biological fixation resulting in better biomechanical compatibility and high resistance to fatigue loading, which allow homogeneous stress transfer between implants and bones. It is, therefore, important for prolonged life to increase the strength of the  $\beta$  Ti alloys of the implant device. Zr, Nb, Mo, and Ta are favorable alloying elements that may increase the strength and decrease the modulus of the  $\beta$  Ti. Interstitial elements, like oxygen undesirable in titanium, were also endeavored as micro alloying additions in Ti alloys (Ouchi et al., 1998). In the work of Hao et al. (2003), increase in the Young's modulus and strength occurred by interstitial oxygen but ductility decreased.

Ti and Nb have high melting points and at high temperatures react with atmospheric gases and crucible materials, for these reasons producing porosity by liquid state is very difficult, although the expensive high temperature tools and high vacuum equipments needed. Powder metallurgy techniques on the other hand, provide low temperature processing, close composition control and physical property alterations by modification of the processing methods and characteristics. So, various powder metallurgy methods, for example, hot isostatic pressing, spark plasma sintering, conventional sintering, microwave sintering, metal or powder injection molding and 3D printing have been used to fabricate TiNb foams.

Most of these production methods produce non-spherical pores that cause stress concentration, nonhomogeneous pore distribution in the structure effective on load distribution and sharp pore edges that act as stress risers, and decrease both strength and ductility of the porous metallic materials. Also, apart from 3D printing method adjustment of the desired porosity levels and pore size were difficult. At this time, for manufacturing porous TiNb with desired pore structures space holder technique appears to be the best method since 3D printing is a very expensive fabrication method. However, space holder technique commonly produces two types of pores: macro-pores produced by removing space holder material and micro-pores produced from incomplete sintering. Micro-pores are not suitable in size to permit bone ingrowth but body fluids can be transported and have influence on mechanical properties. It's possible to remove all micro-pores by using space holder technique with hot pressing. On the other hand, diminish of micro-pores can be achieved by prolonged sintering time or increasing temperature of sintering because diffusion rate is exponentially affected by temperature.

There are many type of space holder materials that can be used to produce pores inside samples such as urea, ammonium hydrogen carbonate, potassium sorbate, sodium chloride, polymeric materials, sodium chloride, tapioca starch and magnesium powder. Magnesium powder was chosen as a new space holder to prevent contamination and produce spherical pore shape and interconnected pores between 100-600  $\mu\text{m}$ .

## **2. LITERATURE REVIEW**

### **2.1. Basic Material Requirements of Ti-Based Alloys for Biomedical Applications**

Several factors have influence on the successful performance of long-term load-bearing metallic implants in the human body. Mechanical compatibility is the most important of them. Biomechanical properties such as stiffness, strength, wear resistance and corrosion resistance, and biomedical properties such as toxicity are the properties must be cared about for any implant material that used in biomedical applications (Wang, 1996; Long and Rack, 1998; Nnamchi et al., 2016). Vital elements is a group of metallic elements can be used for implantation because they have little cytotoxicity and harmless to be put in a body (Niinomi, 2002).

#### **2.1.1. Mechanical compatibility**

Orthopedics metallic biomaterials are used for two types of implants (Frosch and Stürmer, 2006).

- i. As substitutes for bone and joints (i.e. total knee or hip arthroplasty).
- ii. Implants for the fixation of fractured bones (osteosynthesis).

Mechanical properties of Ti-based alloys used in biomedical applications should achieve requirements of human hard tissues. Mechanical properties of the material like titanium and its alloys designed to be satisfied by excellent blend of low modulus and high strength near to the mechanical properties of real human bones. The phenomenon of biomechanical incompatibility refers to insufficient mechanical strength or mismatch in elastic modulus between implant material and human bone tissue. The main motive for stress shielding of human bones are biomechanical incompatibility or difference in elastic modulus between bones and implant materials (Huiskes et al., 1992).

Figure 2.1 shows the elastic modulus of the biomedical alloys that generally used in the biomedical applications compared to elastic modulus of the cancellous and cortical bones. Metallic alloys such as Co-Cr alloy and 316L stainless steel have much higher elastic modulus if they compared to Ti-based alloys. On the other hand, elastic

modulus values of the cancellous and cortical bones are about (0.2 - 2GPa) and (4 - 30GPa), respectively, the magnitude of elastic modulus of bone depends on the direction of measurement and bone type. Implant materials such as Co-Cr alloys (240GPa), 316L (210GPa) and Ti-based alloys (55 - 110GPa) when they compared to the elastic modulus of the bone or the tissue, where they are replacing show a large elastic modulus (Geetha et al., 2009).

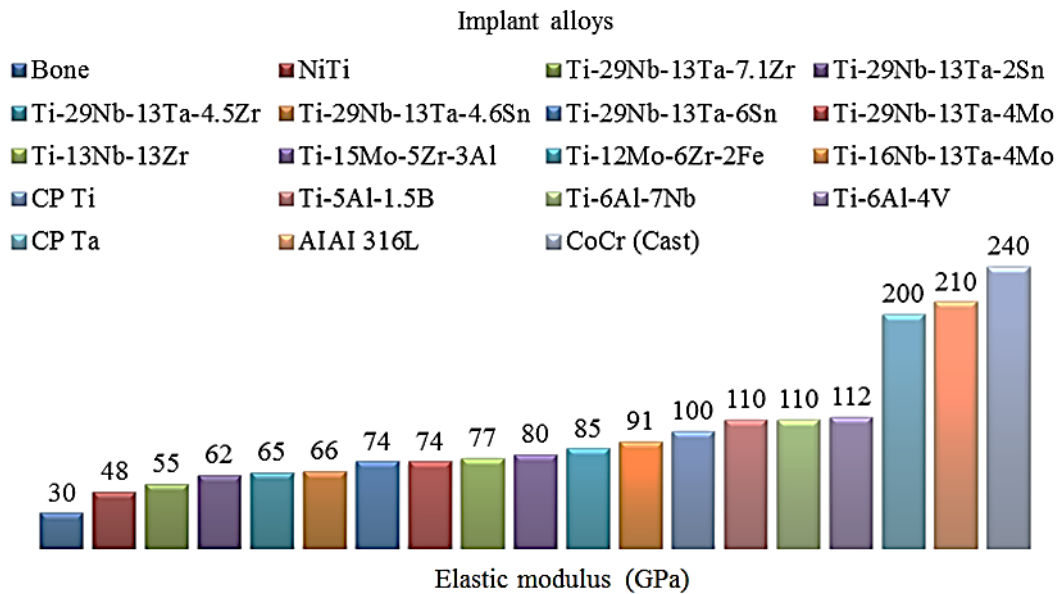


Figure 2.1. Elastic modulus of some metals and alloys used as implant materials (Geetha et al., 2009).

Disuse atrophy Figure 2.2 means bone will resorb back into the body occur due to stress shielding where the metals or alloys that used as implant material carries a most of applied loads, separate the more compliant tissue unstressed (Hrabe, 2010).

When the porous titanium implants introduced into the condyles of tibias and femurs of sheep new bone tissue growth to fill the pores occurred resulting in a titanium-new composite. The formed composites were removed from the bone and subjected to a compression test and for calculating the Young's modulus stress-strain curve was used. The tests show after 4weeks there is no change in elastic properties after that the new bone tissue filled the pores. After 8weeks of composite formation the measurement of the test shows that the composite has a good agreement. After 24 and 52 weeks of the implantation the Young's modulus rises by 21–34% and 62–136%, respectively (Rubshtein et al., 2015).



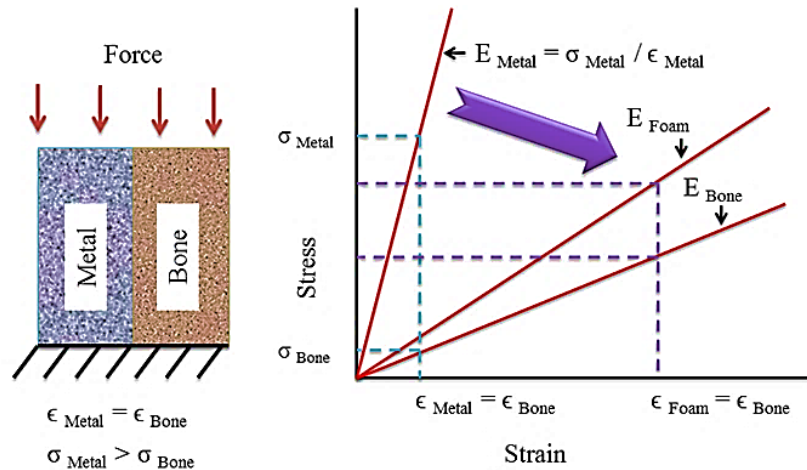


Figure 2.2. Schematic of stress shielding a) schematic of the bone and bulk metallic implant interface with applied stress and b) the stress strain diagram emphasizing that for a given strain, the bone carries negligible stress due to a stress shielding situation caused by the stiffer metal. Also depicted is the lower modulus ( $E_{\text{foam}}$ ) metallic foam and how it would serve to reduce stress shielding (Hrabe, N. W., 2010).

Furthermore, difference in elastic modulus will lead to too much relative movement between bone and implant material. The connection areas between implant materials lose because the implant material inhibits stress transferred from implant material to the neighboring bone and prevent formation of new bone (Moyen et al., 1978).

Good stress transmission between the implant and bone prevent bone resorption, to prevent stress shielding the metal that used as an implant should have low elastic modulus to match elastic modulus of bone. As shown in the Table 2.1 the Young's modulus of the human bone is very low compared to most commonly used implant alloys.

### 2.1.2. Biocompatibility

Metallic implants added into physiological environment, the tissue reaction with the implant and cytotoxicity can be initiated by these materials. Therefore, the most important thing should be cared about is wear and corrosion resistance and this is more important characteristics of long-term load-bearing implant materials.

Table 2.1. Physical and mechanical properties of most commonly implant materials in comparison to human bone ( Wang, 1984; Zhu et al., 2005)

Properties	Natural bone	Stainless steel	Co-Cr alloy	$\alpha$ -type Ti	$\beta$ -Ti-13Nb- 13Zr
Density ( $\text{g/cm}^3$ )	1.8-2.1	7.9-8.1	8.3-9.2	4.4-4.5	4.5-5.5
Elastic modulus (GPa)	3-20	189-205	230	110-117	79
Compressive yield strength (MPa)	130-180	170-310	450-1000	758- 1117	620-900

Very important to understand the effects of an individual alloying element, a series of reactions occur when materials are embedded into human body. Due to wear and corrosion the metals that implanted into the human body can dissolve causing systemic toxicity and this refers to the acceptability of these materials by our system. Safety of metals in the biological system including cytotoxicity of pure metals and the relationship between polarization resistance and biocompatibility of pure metals, Co-Cr alloy and stainless steels as shown in Figure 2.3.

In the physiological environment polarization resistance corresponds to the metal ion release rate. We can classify most commonly used metals in the implantation to three groups according to their biocompatibility (see Figure 2.3) vital, neutral and harmful. Vital elements are Ti, Ta, Zr, Pt and Nb. Elements like Ti, Ta and Nb can be used for long-term implantation because they have very high corrosion resistance and they have very low metal release rate (Kuroda et al., 1998).

From the previous studies Ta, B, Au, Si, Pt, Ca, Sr, Zr, Nb, Mo, Pd, In, Sn, Ti, P, and Mg are biocompatible elements and can be used as implant metals, on the other hand, harmful elements include Be, Ag, V, Cr, Mn, Fe, Cu, Ni, Co, Zn, and Al (Calin et al., 2013). Fe and V cannot be used as implant materials because they are cytotoxic elements, while Zr, Ta, Nb, Ti and Sn selected as non-cytotoxic elements (Kuroda et al., 1998). Because human body composite of complex electrochemical system and body fluids have dissimilar types of corrosive substances composed of an aggressive corrosion environment for implants and implants exposed to them. The main factor causing allergic and toxic reactions is the release of metals used in implant, the reason for that is bad corrosion resistance in the body fluids (Hallab et al., 2005).

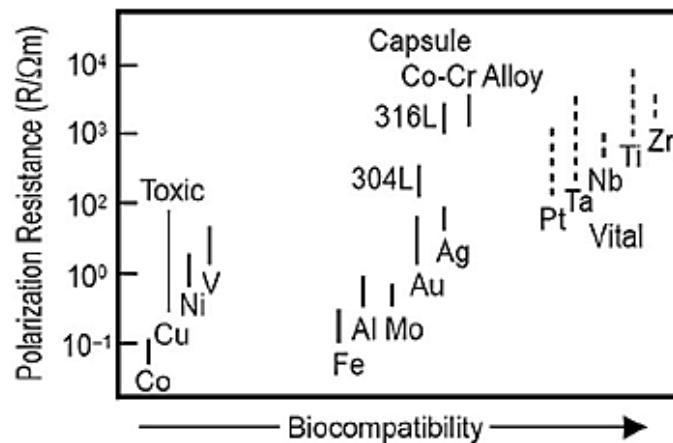


Figure 2.3. Polarization resistance and biocompatibility of metals used for implant materials (Liang et al., 2016).

Co, Cr, and Ni have been pointed out in dentistry and they have high associated with metal allergy, and the use of Ni is rapidly being disused. Figure 2.4 shows the percentage of metal allergy caused by each metallic element (Niinomi, 2002). Nb, Ta, and Zr look like to be the safest alloying elements for biocompatible titanium alloy it is very important to neglect metallic elements that cause metal allergy.

Also, wear resistance is another important factor for losing implants and determines the service period of an implant, wear debris produced with friction results in inflammatory reactions causing pain and loosening of implants where they are placed as shown in Figure 2.5 (Geetha et al., 2009; Hussein et al., 2015).

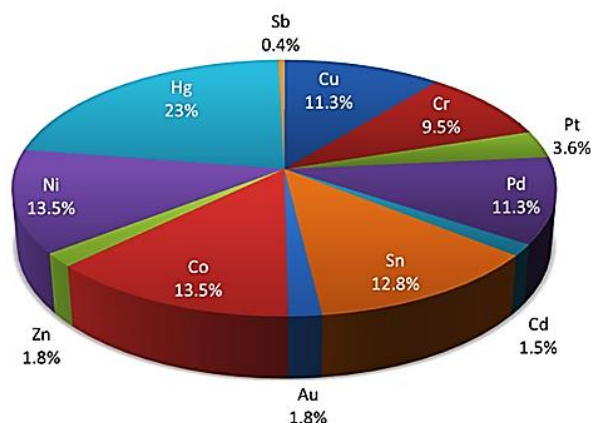


Figure 2.4. Percentage share of metal allergy caused by each metallic element (Niinomi, 2002).

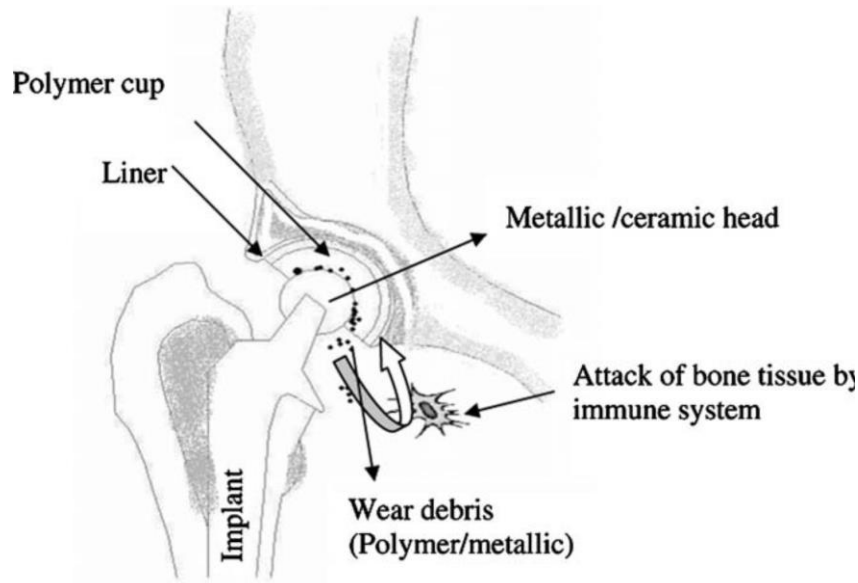


Figure 2.5. Debris produce by wear of implant (Geetha et al., 2009).

Li et al. (2004) found that improving the wear resistance can be achieved by increasing the Nb content. After implanting some surface contact takes place, friction between natural joints is much lower than in artificial materials and non-recoverable wear of the artificial joint materials takes place.

Another reason for loosening the implant is incapability of surface of an implant to mix with the tissues and bone due to micro motions (Viceconti et al., 2000). If the bone is not well joined with the implant a fibrous tissue is formed between them (Viceconti et al., 2000).

For both permanent and temporary material formation of fibrous tissue between the implant and surrounding tissue is not desired. Calcium phosphate precipitates on the surface of the implant material increase the rate of formation of the fixation between the bones and implant material. However, to reduce the bone conductance of the implant material, and to prevent adjustment between the implant material and bone tissue the reverse is required in removable implant applications and calcium phosphate precipitates are undesirable on the surface of removable.

Disagreeing to permanent implants, weak enough bonding between bone and implant requires to prevent refracture of the bone during removal surgery. Therefore, implant removal becomes necessary especially in the cases of implants used for children or athletes engaged in contact sports after a period the implant may be removed.

Problems that arise during implant removal surgery, to prevent bone atrophy during the time the implant material that used must have low Young's modulus (Niinomi and Nakai, 2011). Niobium (Nb) was used as a  $\beta$  isomorphous alloy element and the effect of Nb on the microstructures, mechanical properties were investigated (Ozan et al, 2015).

To get better connection between bone and implant introducing porosity in the implant plays a vital role because bone and tissues ingrowth into porous surface causing better biomechanical compatibility and high resistance to fatigue loading and strong interlocking implant with surrounding bone tissue (Gepreela and Niinomi, 2013).

## **2.2. Ti and Ti Alloys for Biomedical and Implant Applications**

### **2.2.1. The Ti-Nb phase diagram**

High biological compatibility and good corrosion resistance properties made Ti usage widely for biomedical applications (see section 2.1.2 Biocompatibility). For improvement in mechanical properties many new Ti-alloys have been developed for the biomedical applications because Ti implants have some problems like high Young's modulus, low wear resistance and low shear strength (He and Hagiwara, 2006).

In the equilibrium Ti-Nb phase diagram there are only two stable solid phases (Moffat and Larbalestier, 1988) as shown in Figure 2.6 the hcp  $\alpha$ -phase and the bcc  $\beta$ -phase (Moffat and Larbalestier 1988). In the equilibrium Ti-Nb phase diagram, at three percent Nb at 400°C hcp  $\alpha$ -phase is stable. At 400°C  $\alpha + \beta$  phase mixture becomes stable when Nb content increased. By increasing the Nb content to about 38 at %Nb at 400°C the phase that is stable is  $\beta$  phase. Generally, pure Ti in the  $\beta$  phase is at high temperature by adding the Nb and increasing the Nb content transformation temperature from hcp  $\alpha$  phase to bcc  $\beta$  phase decrease. In pure Ti transformation happens by increasing the temperature higher than 882°C from hcp  $\alpha$  phase to bcc  $\beta$  phase. There are two melting points for the system, for pure Ti the temperature that requires converting solid bcc  $\beta$  phase to liquid phase is 1670°C and for pure Nb is 2460°C.

In the Ti-Nb system various metastable phases can occur due to non-equilibrium conditions during quenching. The product from non-equilibrium depends on both the

cooling rate and the amount of Nb in the composition. These products are two martensites (hexagonal ( $\alpha'$ ) and orthorhombic ( $\alpha''$ )) produced from rapidly quenched from the  $\beta$  phase, the composition of the alloy must be known to determine which martensite is formed and  $\omega$  phase precipitates may form from  $\beta$  phase during a slow quenching or isothermal aging (Moffat and Larbalestier, 1988; Moffat and Kattner, 1988).

In the work of Tang et al. (2000) the phase transformations in solid solutions for quenched and treated Ti-(13-26)Nb-(22-38)Ta (wt.%) alloys were investigated. Phase transformations in such alloys were sensitive to both alloy cooling rate and composition. The oil and water quenching techniques resulted in the formation of  $\beta + \omega$  athermal matrix and orthorhombic martensite ( $\alpha''$ ) and the slow cooling technique such as furnace cooling showed the fine  $\alpha$  and  $\omega$  isothermal formation within the  $\beta$  matrix.

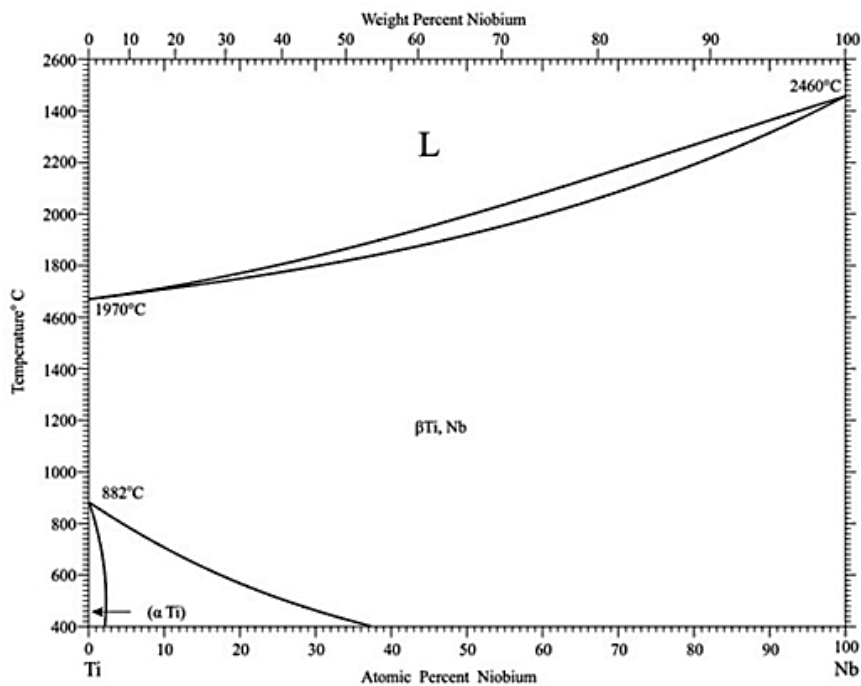


Figure 2.6. Equilibrium phase diagram of Ti-Nb system (Aleksanyan et al., 2012).

Studies about Ti-Nb-Ta-(Zr) system have shown that cooling rate and chemical composition have effect on phase transformations. Figure 2.7 shows continuous cooling transformation (CCT) diagrams for the Ti-Nb-Ta-Zr alloys containing approximately 7 wt.% Zr (Elias et al., 2006).

### 2.2.2. Ti-Nb system: relationship between structure and property

For better understanding a brief introduction to physical metallurgy of Ti-based alloys is required as a background. For the first time in 1791 titanium was discovered by William Gregor the British reverend, mineralogist and chemist. He examined the magnetic sand and isolated black sand (ilmenite). A new impure oxide element was produced by removing the magnet, iron and treating the sand with hydrochloric acid. He named it mechanite. In 1910 in a steel bomb titanium tetrachloride was heated with sodium to isolate the metal by Matthew Albert Hunter from Rensselaer Polytechnic Institute in Troy, N.Y.. Finally, in 1932 father of the titanium industry Wilhelm Justin Kroll from Luxembourg by combining  $\text{TiCl}_4$  with calcium he produced significant quantities of titanium (Leyens and Peters, 2003).

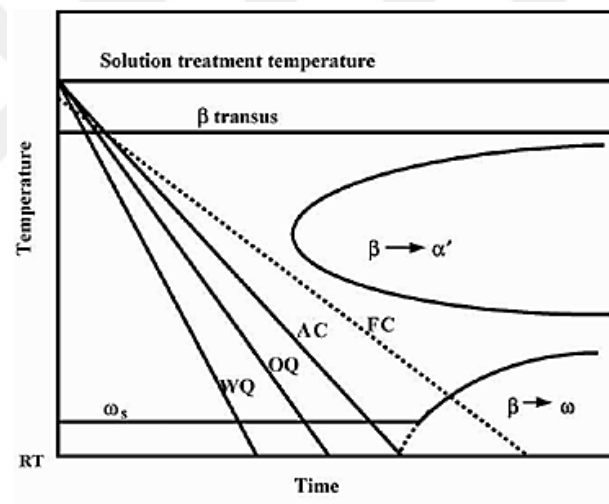


Figure 2.7. CCT diagrams for Ti–Nb–Zr–Ta containing approximately 7 wt.% Zr where WQ, OQ, AC, FC and RT are water quenching, oil quenching, air cooling, furnace cooling, and room temperature respectively (Elias et al., 2006).

The metallic bonding of the atoms in the crystal lattice specify the properties of metals. Mobile valence electrons in the crystal lattice result in common properties such as plastic deformation by atomic slip in crystal lattices and alloying by combination of impurity atoms into the crystal lattice with the consequence of improved hardness and strength.

As said before, Ti suffers an allotropic transformation at  $882 \pm 2^\circ\text{C}$ , at this temperature for pure Ti  $\alpha$  phase converts to  $\beta$  phase. Under  $882 \pm 2^\circ\text{C}$ , it has  $\alpha$ -phase

closed packed hexagonal crystal (HCP) structure, although above  $882\pm 2^\circ\text{C}$  it has  $\beta$  phase body centered cubic (BCC) structure (see Figure 2.6 equilibrium phase diagram of Ti-Nb system) The atomic unit cells of  $\alpha$  and  $\beta$  phases are showed in Figure 2.8 (Leyens and Peters, 2003).

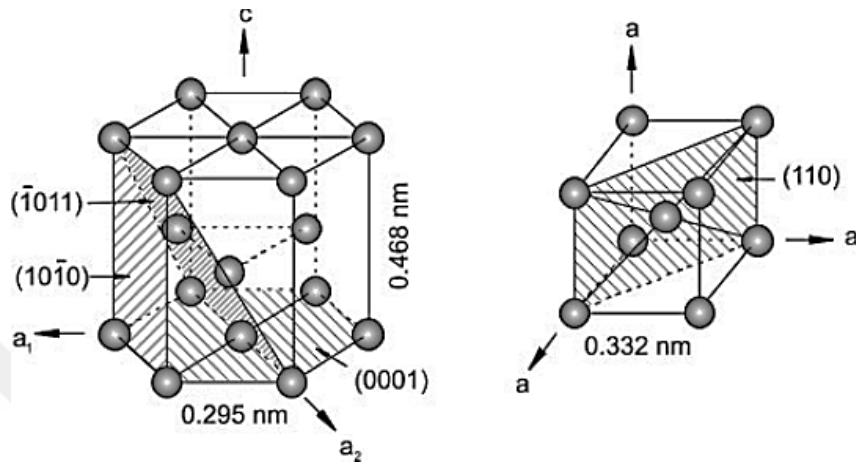


Figure 2.8. Crystal structure of hcp  $\alpha$  phase and bcc  $\beta$  phase (Leyens and Peters, 2003).

Because of the densely packed atoms in bcc  $\beta$  phase, diffusion is considerably higher than in hcp  $\alpha$  phase. The different diffusion coefficients of  $\alpha$  and  $\beta$  phase is influenced by the microstructure and thus influences the mechanical behavior of the two phases, such as superplasticity, creep performance and hot workability. The alloying elements of titanium can be classified into three types depending on their influence on the  $\beta$ -transus temperature, as shown in Figure 2.9. These types are  $\beta$ -stabilizers,  $\alpha$ -stabilizers and neutral. It's possible at room temperature stabilize a single  $\beta$  phase or it can change the temperature that used to transfer  $\alpha$  phase to  $\beta$  phase by adding different elements to pure Ti to produce Ti alloys.

Carbon, aluminum, nitrogen and oxygen are the examples of  $\alpha$ -stabilizing elements as shown in Figure 2.9. Depending on their effect on the phase transformation in the alloy  $\beta$ -stabilizing elements classify as  $\beta$ -isomorphous and  $\beta$ -eutectoid. As presented in Figure 2.9 Vanadium, molybdenum, tantalum and niobium are examples of  $\beta$ -isomorphous elements that fully dissolvable in the  $\beta$  phase. It is possible to decrease  $\beta$ -transition temperature more by increasing the rate of these elements to the alloy. Manganese, chromium, cobalt, copper, silicone, iron, nickel and hydrogen are examples of the  $\beta$ -eutectoid elements that solubility of these elements in Ti is limited. As shown



in Figure 2.9 these elements form intermetallic phases by eutectoid decomposition of the  $\beta$  phase. For neutral elements, they do not have significant influence on the transformation temperature. Zr and Sn are the example of these elements; they are soluble in  $\alpha$  phases and  $\beta$  phases. The use of these elements is useful especially for  $\beta$ -stabilizing elements to reduce the Young's modulus of Ti alloy (see 2.1.1 Mechanical compatibility) but those alloying elements that used with Ti for biomedical applications should be "vital" and do not react with tissue and body fluids (see 2.1.2 Biocompatibility).

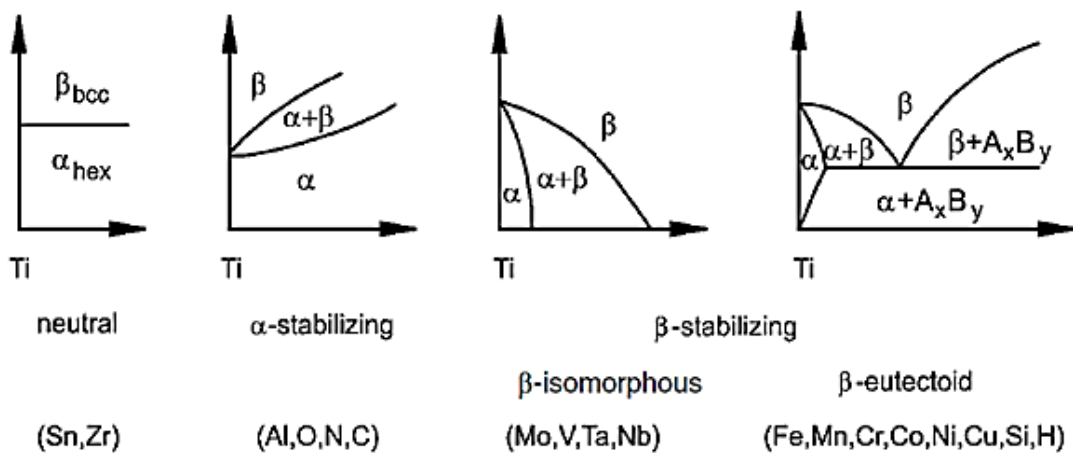


Figure 2.9. Effect of alloying elements on Ti alloys phase diagrams (schematically) (Leyens and Peters, 2003).

Generally titanium alloys are classified as  $\alpha$ ,  $\alpha+\beta$ , and  $\beta$  alloys, with more subdivision into near- $\alpha$  and metastable  $\beta$  or stable  $\beta$  alloys (Liu et al., 2004) This is schematically drawn in a three dimensional phase diagram as shown in Figure 2.10. This three dimensional phase diagram contains two phases with an  $\alpha$ - and a  $\beta$ -stabilizing element respectively. Generally, the  $\alpha$  alloys include pure (cp) titanium, neutral elements and/or alloys with  $\alpha$ -stabilizing. Near - $\alpha$  alloys occur by adding minor fractions of  $\beta$ -stabilizing elements and exhibit superior corrosion resistance. If  $\beta$  volume fraction ranging from about 5 to 40% in the alloy at room temperature the component of this type is  $\alpha+\beta$  alloys and this class is the most widely used alloy group because this group exhibits highest strength due to the presence of both  $\alpha$  and  $\beta$  phases. If the range of  $\beta$ -stabilizing elements is more increased to a level where with fast quenching  $\beta$  no longer transforms to martensite, the class of metastable  $\beta$  alloys is reached. Final class is

the single-phase  $\beta$  alloys mark the end of the alloying scale of the conventional titanium alloys (Leyens and Peters, 2003). Both metastable and stable  $\beta$  alloys have high strength, high hardenability, good formability, superior corrosion resistance and low elastic modulus (Long and Rack, 1998).

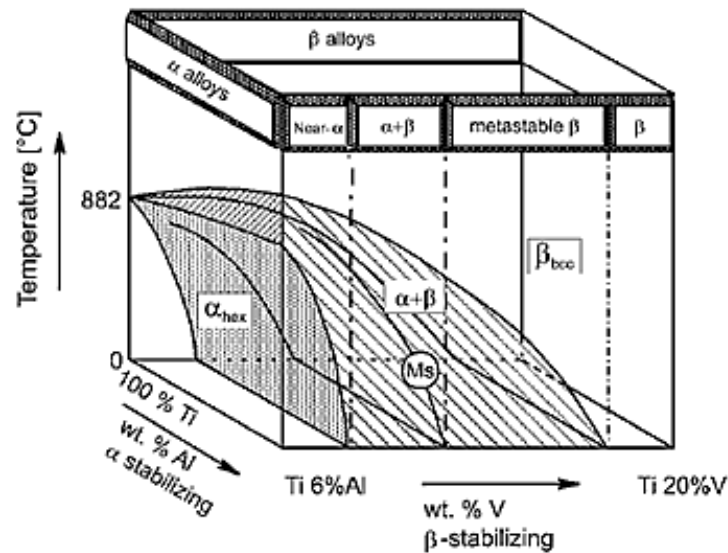


Figure 2.10. Ti6Al alloys with different V content by three-dimensional phase diagram (Leyens and Peters, 2003).

Relationship between the amount of Nb and Young's modulus of the alloy is revealed. Quenching Ti-Nb alloys display change in the Young's modulus by increasing the rate of Nb as shown in Figure 2.11 (Ozaki et al., 2004). As shown in the Figure 2.11 from the beginning after adding a small amount of Nb to Ti the Young's modulus of Ti-Nb alloys are close to the pure Ti Young's modulus, i.e.  $\approx 110$  GPa. Close to 15 mass %Nb Young's modulus is around 68 GPa.

At around the composition of Ti-40 mass %Nb lowest in Young's modulus observed. Nnamchi et al., (2016) reported that between  $\beta$ -stability and high mechanical strength there are excellent agreement and strength increase with increasing Nb addition. Moreover, the alloys have excellent corrosion resistance and low Young's modulus. Nnamchi et al., (2016) reported that Ti-8Mo-4Nb-2Zr alloy, which consists of  $\beta+\alpha''$  phases, exhibits a low Young's modulus of 35 GPa, which is lower than those of the commercial alloys already used in biomedical implantation.

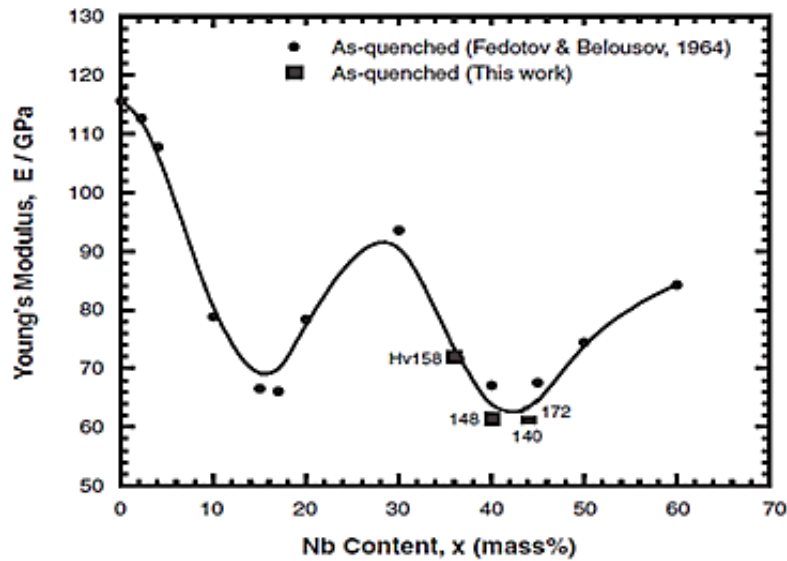


Figure 2.11. Effect of Nb content on Young's modulus of quenched Ti-Nb alloys (Ozaki et al., 2004).

## 2.3. Porous TiNb

### 2.3.1. General

In 1970 for the first time for the problems occurring in the skeletal system such as bone fracture, the concept of using porous structure to achieve adequate and permanent fixation of a bone implant was investigated (Qi et al., 2016).

Introducing a certain amount of porosity in the implant material to get customized mechanical properties, to achieve optimum load transfer from the artificial implant to the adjacent bone allows copycatting bone structures at the same time (Oliveira et al., 2015). Good fixation of the implant is expected with porous surface of solid core  $\beta$  phase. However, the problems with the high stiffness of solid core material occur. Moreover, increases in age decrease the ability of new bone formation and loss of bone mass occurs (Kains et al., 1994). Higher degree of osseointegrated fixation and decrease of the Young's modulus of the implant can be achieved by highly open porous structure than a solid implant with porous surface (Wu et al., 2014). On the other hand, introduction of pores into the bulk material allows ingrowth of living tissues into the porous implant and strong fixation in addition to reducing the alloy density. Limited strength in the porous implant is the main disadvantage (Esen, 2007). There are many

factors that have effect on the compressive strength of the porous structure. These factors are level of porosity, pore shape, pore size, and interconnectivity of the structure. The strength of the structure also depends on the properties of pore walls.

There are many common examples for cellular structured materials in nature as shown in Figure 2.12.

There are generally three types of artificial cellular solid structure produced:

- i. Two dimensional honeycombs.
- ii. Three dimensional porous structures with open cells.
- iii. Three dimensional porous structures with closed cells.

Prismatic cells of honeycombs is an example of two dimensional cellular solids structures, while porous structure, with their polyhedral cells, are three dimensional cellular solid structures, that used for lightweight structural components. Several engineering cellular solid structures are shown in Figure 2.13 (Esen, 2007).

There is a wide range of applications for cellular metallic materials. Many applications require that a medium, either liquid or gaseous, be able to pass through the cellular material. There may be a need for various degrees of “openness”, it can be classified in three steps depending on the range of porosity starting from “very open” for high rate fluid movement to “completely closed” for load-bearing structural applications and partially open between very open and completely closed. Figure 2.14 shows what types of porosity used by various application fields (Banhart, 2001).

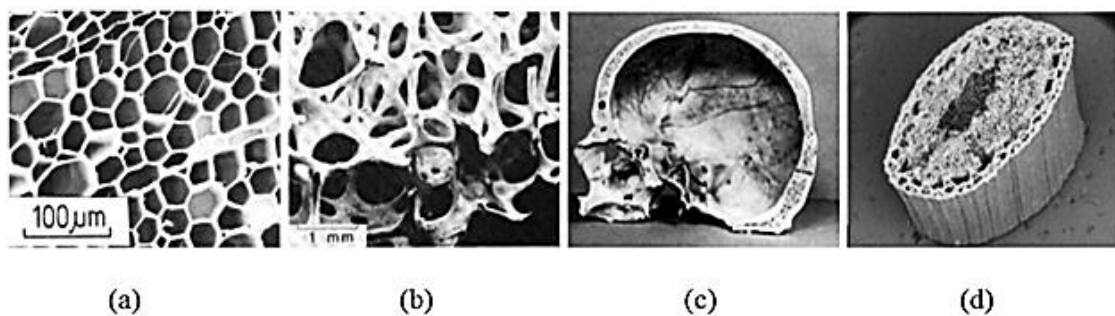


Figure 2.12. Some natural cellular material examples, a) balsa wood, b) trabecular bone, c) skull, d) plant stem (Esen, 2007).

Also, it is very important to decide what type of metals and alloys can be used to manufacture cellular structure. The structural, load bearing parts have to be light because otherwise they would be made from conventional massive metals or alloys.

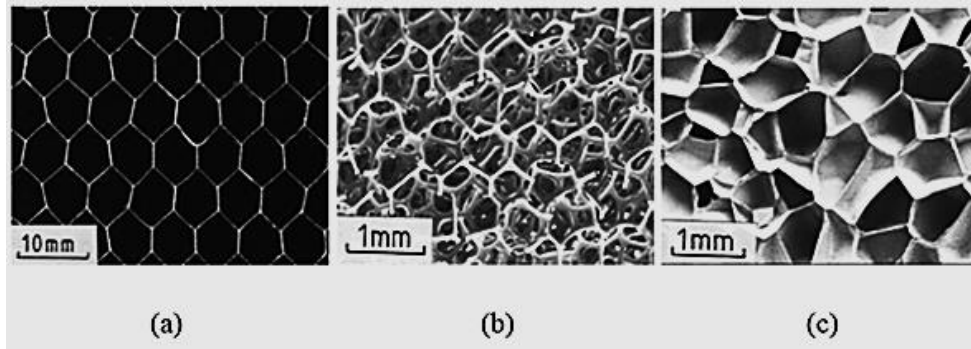


Figure 2.13. Some engineering cellular solid structures a) aluminum honeycomb b) open-cell porous polyurethane c) closed-cell porous polyethylene (Esen, 2007).

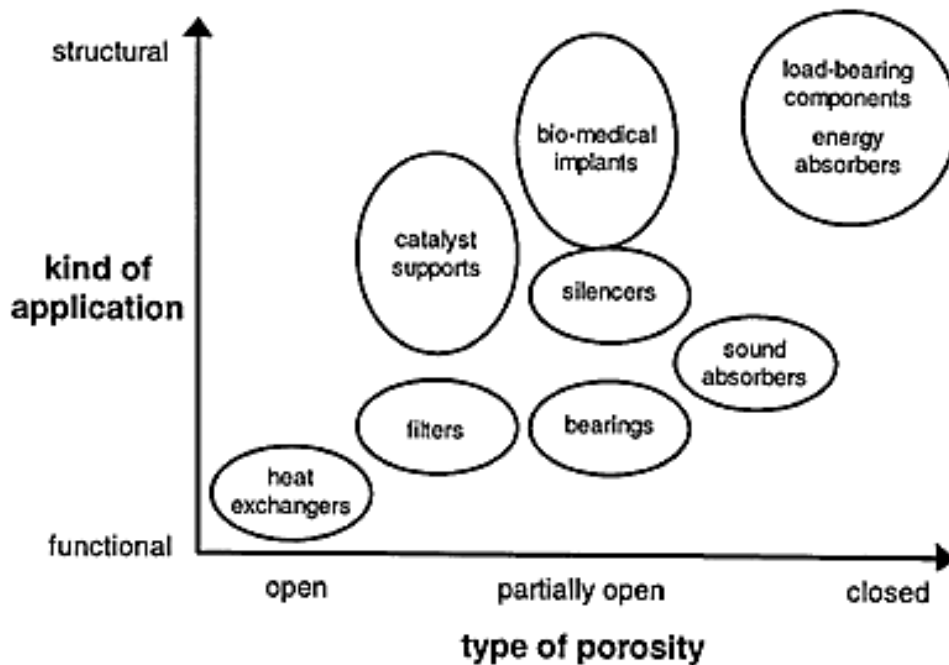


Figure 2.14. Applications of cellular metals grouped according to functional or structural depending on the degree of “openness” needed (Banhart, 2001).

Therefore, for such applications metals like aluminum, magnesium or titanium in porous form are required. Metals like titanium more favorites for biomedical applications because of its compatibility with tissue. Stainless steel or titanium is used for applications where high temperatures required. Figure 2.15 shows various applications of metallic foams.

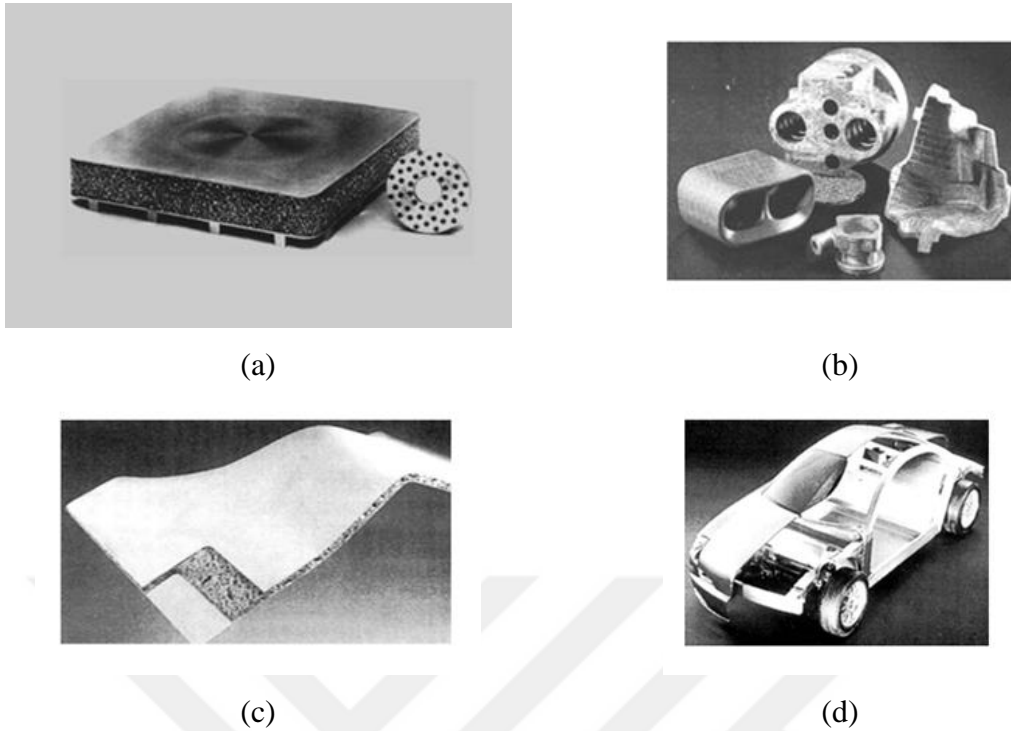


Figure 2.15. Several applications of porous aluminum a) Porous aluminum used as the structural core of a lightweight composite mirror, b) porous metal components with integral skins, c) sunshade for an optical telescope made from foamed aluminum, d) Pressed porous panel (Ashby et al., 2000).

### 2.3.2. Processing and characterization of porous TiNb

There are many methods developed for fabricating porous metal materials, some manufacturing methods used for foaming aqueous or polymer liquids, whereas some methods are specially designed to produce porosity in a metal sample, other methods can be electrically deposited. The basic methods for manufacturing cellular metallic materials are briefed in Figure 2.16 according to the state of the metal are processed (Banhart, 2001).

The liquid state techniques are unsuitable for the fabricating of porous titanium and its alloys because at high temperature titanium reacts with atmospheric gases i.e. oxygen. It can be used for fabricating porous materials that have simple processes and low melting point such as aluminum, zinc and magnesium (Banhart, 2001) but solid processing techniques such as powder metallurgy are more stable for fabricating porous Ti alloys. On the other hand, powder metallurgy methods (Leyens and Peters, 2003) can fabricate porous titanium parts under lower temperatures and less chemical reactivity

with atmospheric gases and it is easy to control of process, pore size and pore shape. Moreover, other advantages of powder metallurgy methods are the ability of near-net-shaping and low cost. Therefore, manufacture methods of porous Ti-based materials are commonly based on powder metallurgy.

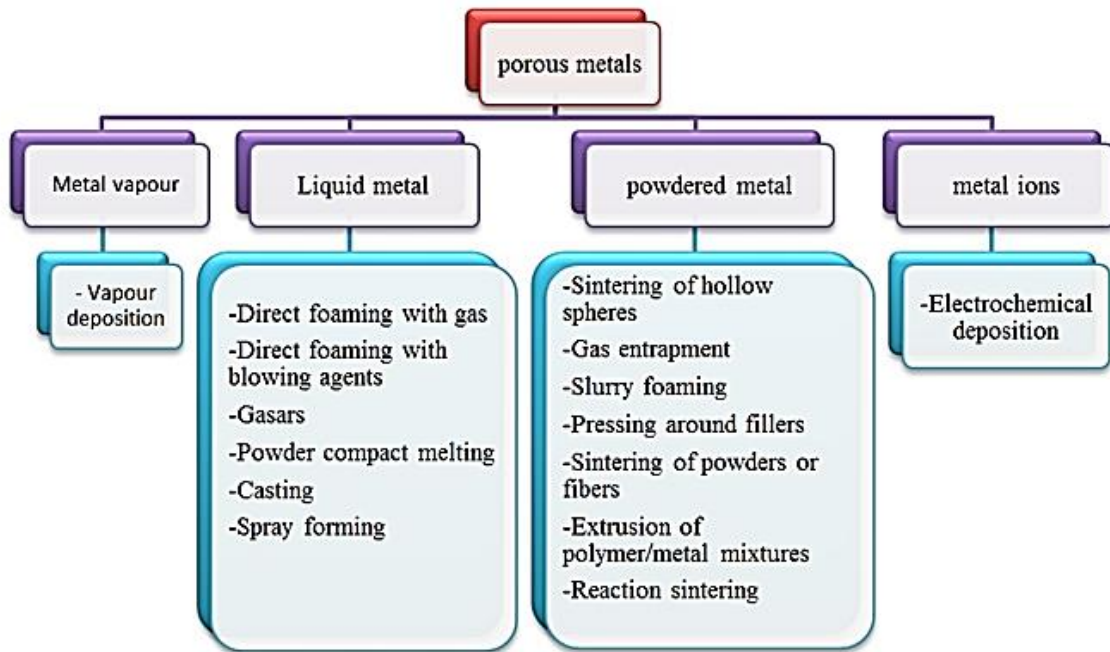


Figure 2.16. Overview of classification of production methods for cellular metallic materials (Banhart, 2001).

### 2.3.3. Different fabrication ways for porous Ti-based alloys

Powder preparation is the main processing step in powder metallurgy and includes mechanical, chemical or thermal treatments or alloying of the powders. The importance of powder treatment can be better understood from the powder shape, size, and surface conditions having a major effect on the processing. To improve or change the physical or chemical properties, the powders prepared by various techniques are subjected to a diversity of treatments. For instance, mechanical fabrication techniques like milling are used to make changes in physical characteristics like particle size and shape. Especially for sintering to avoid any problems during processing wet powders are dried. Generally, the powders are classified into two major groups:

- i. Elemental powders: powders of a single metallic element. For example, elemental powders can be used for manufacturing magnets from iron powder, or two or more types of elemental powders can be mixed to form an alloy.
- ii. Prealloyed powders: powders containing more than one element, in other words alloy powders.

Mainly for compaction and sintering depending on the nature of the powder and on the type of applications elemental or prealloyed powders must be subjected to one or more treatments such as: the particle size must be categorized to achieve desired particle size distribution, for improvement of compaction annealing can be used, crushing or grinding to get acceptable sizes, drying to remove moisture, coating of powder, lubricant or binder for compaction of the powder and mixing of powders for alloying and blending of alloying to achieve a homogenous mixture.

Powder metallurgy can be used to produce porous structure, this porous structure contains various types of pores (Aguilar et al., 2016). For sintered porous material that produced by space holder methods there are two types of pores and they cannot be defined by a single parameter because there are two different length scales for pores in those materials. These scales are:

- i. Micro-scale pores: these types of pores arise due to insufficient compaction or incomplete sintering of the powders Figure 2.17 (a). The size and shape of these small pores depend on the size of the basic powder particles, and the level of compression and sintering. The size is around several microns. New bone tissues and vascularization may be ingrowth into such kind of bimodal porous structure (Zhang et al., 2010; Terayama et al., 2013).
- ii. Macro-scale pores: these types of pores can be seen by eye formed by removal of the space-holder materials (Lewis, 2013), which controls the size and shape of these large pores are shown in Figure 2.17 (b) For example, TiZr alloy were used to fabricate a sample to use in biomedical applications, after sintering the TiZr alloy foam was interconnected throughout the whole sample and the sizes of the pores around 200–500  $\mu\text{m}$  (Terayama et al., 2013).

Due to high melting temperature of some metals, surface contamination, growth of the grain size in the pieces due to holding at high temperatures, the reaction of these metals with the environment or the mold, and their low applicability to the production



of parts with special forms have reduced their large-scale application in the industry. For that reason, hot isostatic pressing (HIP) is a powder forming process developed in the 50s. To achieving densities close to 100%, pressure and temperature are applied at the same time to compacts in certain periods of time (Bolzoni, et al., 2012a; Gómez and Palma, 2015).

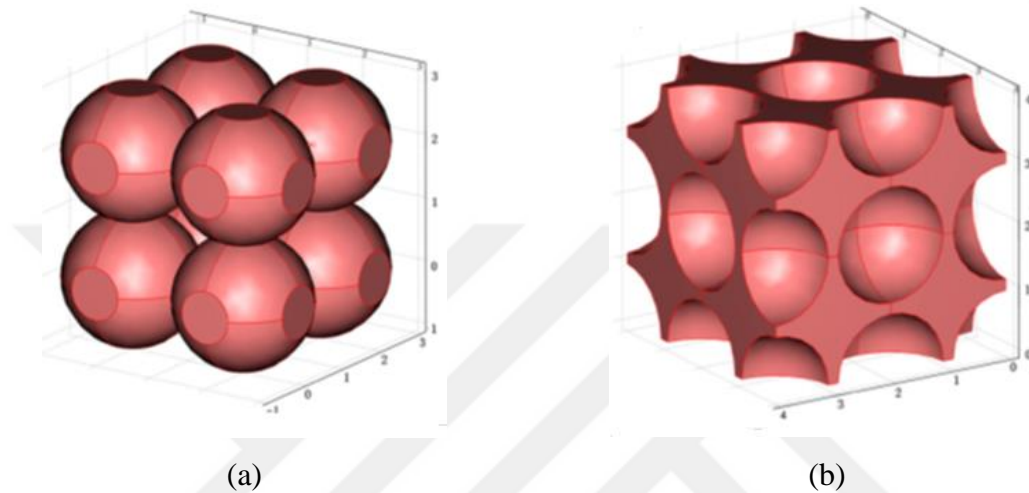


Figure 2.17. Porosity in metallic bodies processed by sintering of powders with space holder material a) micro porosity between the sintered powder particles b) macro porosity after the space-holder particle removal (Niu et al., 2010).

Some mechanisms contribute to densification during hot-isostatic pressing (HIP) (Arzt et al., 1983). When external source of pressure is applied to packed powder particles, the pressure transmitted from the die walls of the capsule to the powders the first response is rearrangement of the particles (Chandler et al., 2008). The point contacts increase due to the increase in pressure, there is a distribution of pressure throughout the powder. At this stage, we can consider that some local points of the powder may still in the rearrangement stage whereas another point enter in the deformation stage as shown in Figure 2.18 (Aryanpour and Farzaneh, 2015). Bolzoni et al. (2012b) used HIP process to fabricate samples from elemental titanium and titanium alloys with relative densities as high as 99% where relative density is the ratio of the compact density to the density of the same material without porosity.

At the beginning elastic deformation occurs at the contact points, the contact points expanding into contact area, when the pressure increase cause rises in contact area, elastic deformation change to plastic deformation as shown in Figure 2.19.

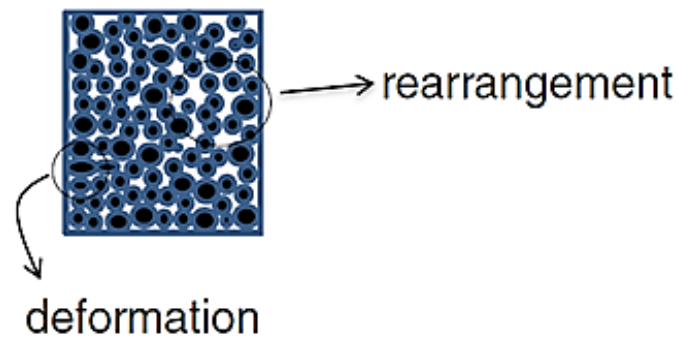


Figure 2.18. Schematic show in some parts of the powder there is particle deformation while other parts are still in a rearrangement stage (Aryanpour and Farzaneh, 2015).

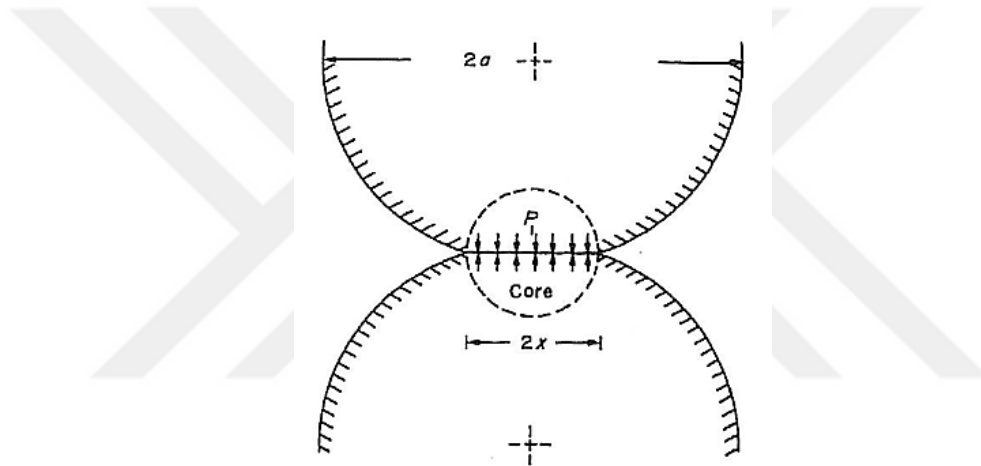


Figure 2.19. Plastic deformation cause by increase in pressure (Swinkels et al., 1983).

In the compaction of metal powders when the pressure is transmitted from top punches, the process is termed single action pressing alternative to double action pressing. These types of pressure applications control the density in the compact and its strength. As shown in Figure 2.20 (a) in single ended pressing, the density is the lowest at the bottom of the compact and increase towards the top. But, in a double-ended pressing compared to the single pressing distribution of density is more homogenous and the minimum density is reached at the center of the compact Figure 2.20 (b) (German, 1984).

The height to diameter ratio of the compact also has influence on the densification. With increasing the height to diameter ratio densities of the compacts decrease as shown in Figure 2.21 (German, 1984).

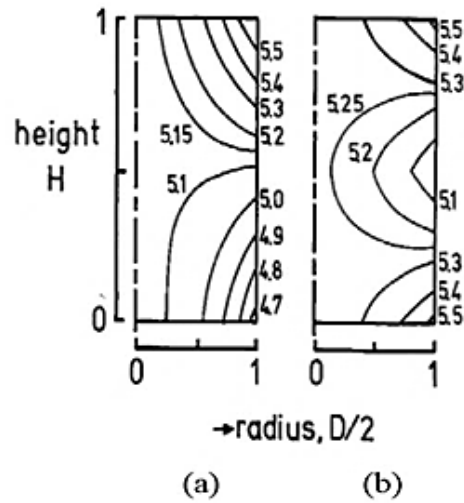


Figure 2.20. Density distribution a) single action pressing b) double action pressing (German, 1984).

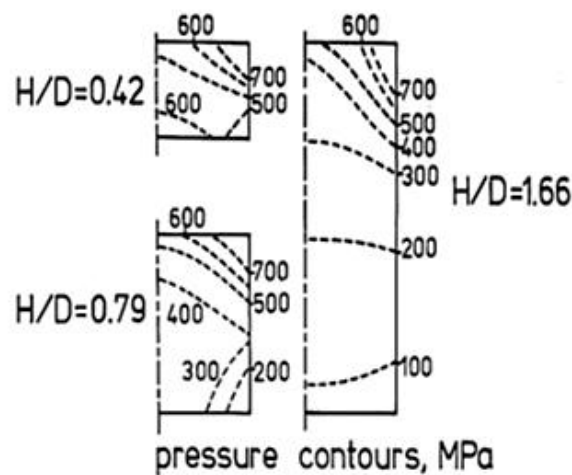


Figure 2.21. Effect of H/D on pressure distributions (German, 1984).

### 2.3.4. Powder metallurgy

Sintering of metal or ceramic powder mixtures is simplest production technique used for fabricating various parts.

Sintering is used to make loose or weakly bonded powders at elevated temperatures, close to the melting temperature with or without additional pressure. Figure 2.22 shows changes of the microstructure during sintering. In the initial stage shown in Figure 2.22 (a) cohesive bonds are formed between particles. When the

sintering process is continued, the necks between particles grow due to mass transport Figure 2.22 (b) (Nosewicz et al., 2013). Porous Ti compacts were successfully produced for biomedical applications by Oh et al. (2003) by controlling sintering conditions and Ti powder sizes, the rate of porosity in the samples are from 5.0 to 37.1 vol%. On the other hand, except lubrication for die wall if necessary, the process does not require a polymeric binder and hence minimize possible contamination associated with binder removal (German, 1984). In this process powders are bonded together when heated before about half of the absolute melting temperature of the powder (Tiwari, 2000). For loose sintered powders, the pore size, volume fraction, shape and distribution throughout the sample thickness and the inter particle neck size have a main influence on the mechanical properties of the sample (German, 1984).

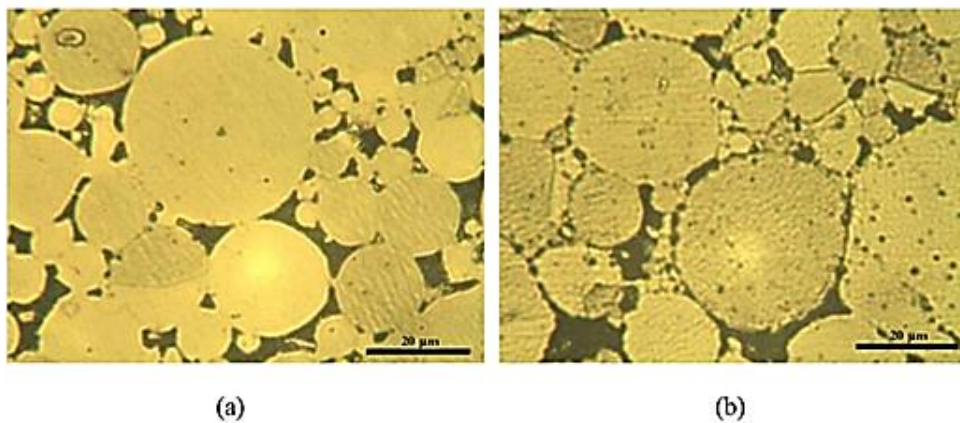


Figure 2.22. Microstructure evolution during sintering of NiAl a) early stage, b) final stage (Nosewicz et al., 2013).

Based on Figure 2.23 it can be concluded that densification is improved with the rise of temperature for all types of sintered materials (Chmielewski et al., 2014). It can be assumed from the observation of density measurements that sintering is a complex process influenced by many factors including temperature, sintering time, pressure and atmosphere which determine the properties of sintered materials (Węglewski et al., 2012). The porosity decreases by the decrease in powder size because smaller particles with high specific surface area have higher energy; this means they could be sintered faster in spite of lower sintering temperature. Figure 2.24 shows that micro-pores in the samples prepared using the fine powder were significantly smaller than those in the samples prepared by coarse powder and the use of fine powder cause many small pores,

while the use of coarse powders produce a small amount of large pores (Čapek et al., 2015).

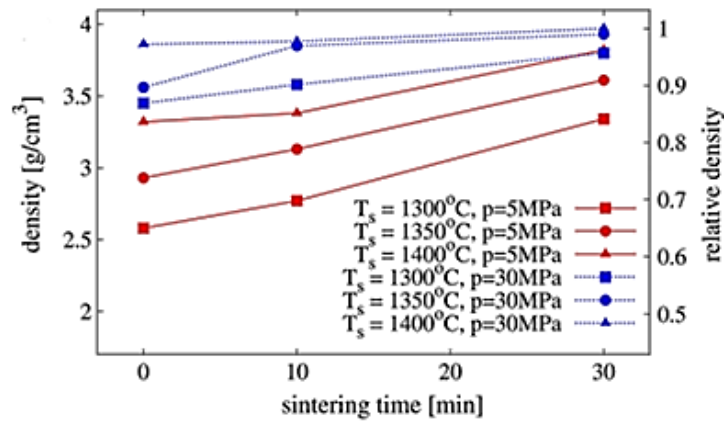


Figure 2.23. Density evolution of pure  $\text{Al}_2\text{O}_3$  (Chmielewski et al., 2014).

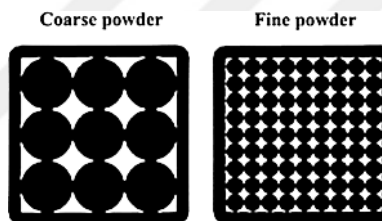


Figure 2.24. A scheme explain the influence of powder size on pore size (Čapek et al., 2015).

Increasing porosity cause the decrease in the elastic modulus, compressive yield strength and bending strength as shown in Figure 2.25.

In the case of space holder method the influence of pore size and shape on mechanical properties is different. For powder sintered with space holders, space holder is used to control porosity amount, pore shape and macropore size by controlling the shape, size and volume fraction of space holder materials. Moreover, space holder materials have a great effect on the mechanical properties. Increasing amounts of spacer in the initial mixture decreases the amount of micropores and increases the total porosity in the structure. The use of finer iron powder as an initial material increased the microporosity. However, this led to smaller micropores and more spherical macropores and significantly enhanced the mechanical properties as a consequence ( Ryan et al., 2006; Maya et al., 2012; Čapek et al., 2015).

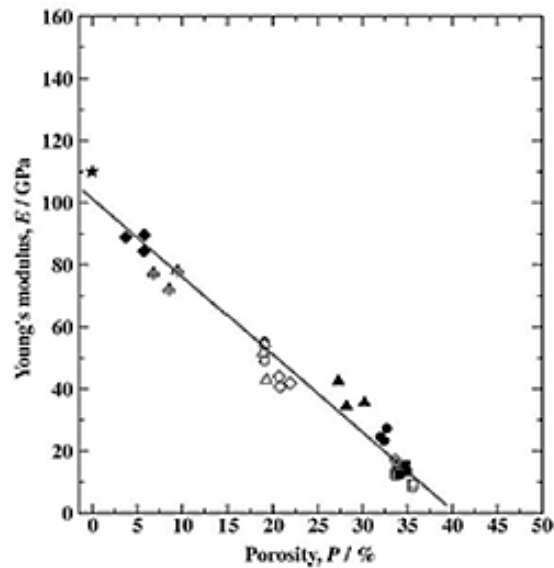


Figure 2.25. Relationship between porosity and Young's modulus in porous titanium (Niinomi, 2008).

It is possible to control the distribution of macropore size by careful sieving of the Mg space holder powders. Total porosity is interconnected if the macropores are interconnected via microporosity channels. The porous samples show nearly spherical shape and homogenous distribution of pores throughout a cross-section. When sample of  $\beta$ -type Ti40Nb prepared with a total porosity range of 50-60% by Zhuravleva et al., (2014) with low stiffness for biomedical applications, NaCl used as a space holder. The samples that produced from Ti-40Nb alloys comprise macropores formed by NaCl space holder and micropores during sintering with size of 100-300  $\mu\text{m}$  and 1-3  $\mu\text{m}$  respectively.

## 2.4. Production Methods

### 2.4.1. General

There are many techniques to manufacture cellular materials. Possibility to produce near net shape porous components, homogenous distribution of pores and different ranges of pore sizes make powder metallurgy processes more popular to use for fabrication of Ti and Ti alloys. Generally, manufacture of porous structures consists of various steps:

- i. Preparation of powder.
- ii. Compaction or molding.
- iii. Binder or spacer material removal.
- iv. Sintering to get sample.

Powder metallurgical process variables, its content and the type of the process have influence on the resultant pore structures and distribution of pores. Figure 2.26 shows the pore types obtained using several of the powder metallurgical processes.

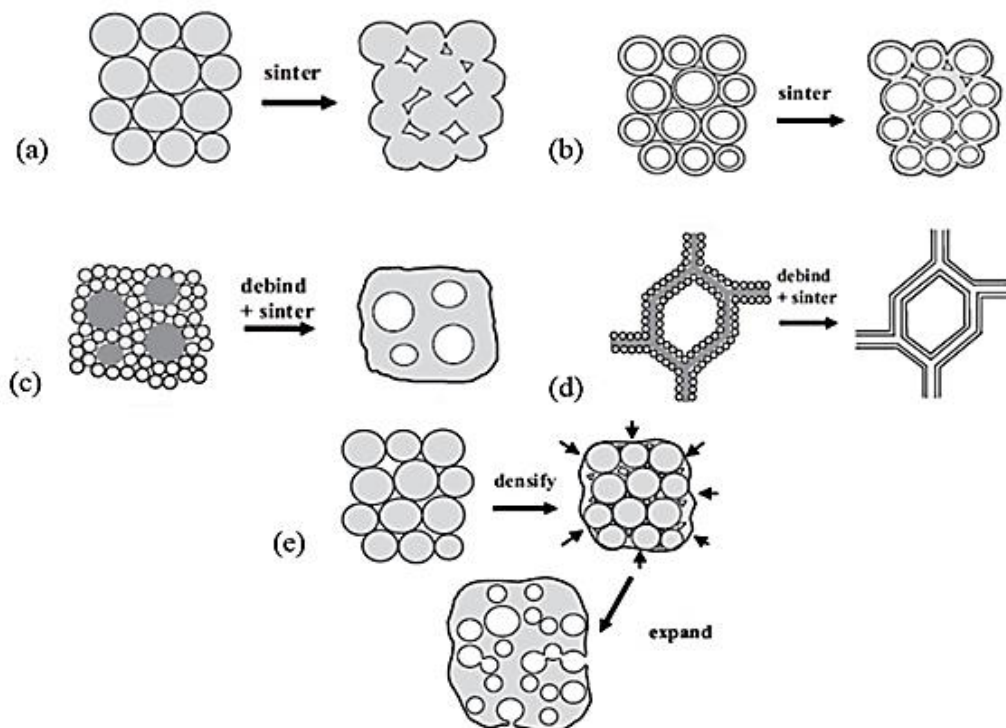


Figure 2.26. Pore morphologies obtained by powder metallurgical processing techniques, a) sintering of powders, b) sintering of hollow spheres, c) space holder technique, d) sintering slurry saturated sponge or replication process, e) gas entrapment technique (Dunand, 2004).

#### 2.4.2. Spark plasma sintering (SPS)

Electric field assisted powder consolidation techniques such as spark plasma sintering (SPS) can be used to fabricate high porosity titanium samples (Zhang et al., 2015b; Ghasali et al., 2016). This technique has other different names; such as field activated sintering technique (Risbud and Han, 2013), field assisted sintering (Manière et al., 2016) and pulse electro-discharge consolidation (Anderson et al., 1999). All



techniques mentioned above have the combination of an electrical discharge with rapid heating and pressure application to reach fast sintering of powders. The SPS studies on porous Ti-based alloys generally used low temperatures and low pressures to decrease the relative density of samples (Ibrahim et al., 2011).

Zhang et al. (2015a) introduced spark plasma sintering of prealloyed powders. As shown in Figure 2.27 after loading powder into a graphite die and (5-25MPa) pressure used to press powders to get desire shape and then a huge on-off pulsed current was encouraged through the die and loaded powder particles. Under the condition of pulsed current heating, neck formation easily occurred where powder particles activated only for 5 minutes to a high energy state and at low temperature around 800°C (Aydoğmuş, 2010).

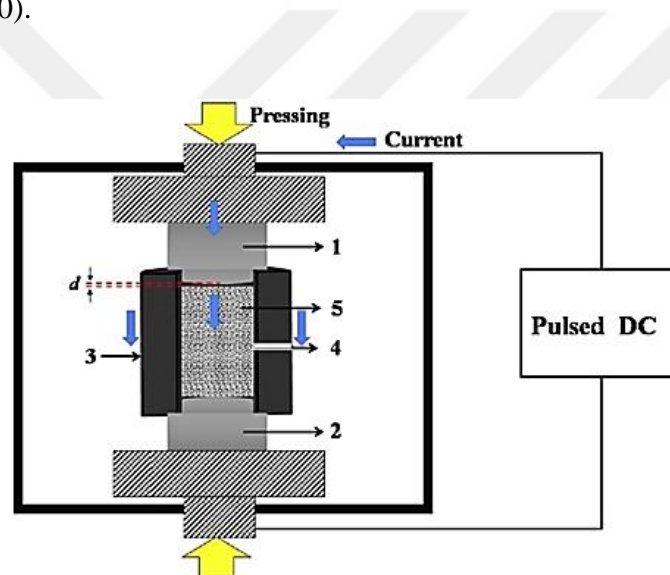


Figure 2.27. Schematic diagram of spark plasma sintering device 1) Top punch, 2) Bottom punch, 3) Die form, 4) Pyrometer measurement hole, 5) Porous sample, and d) Gap  $\geq 0$  mm (Zhang, L. et al, 2015a).

Hussein et al. (2015) used SPS to prepare nearly full density structure at 1200°C nanostructured near- $\beta$  Ti-20Nb-13Zr at % alloy with non-toxic elements. The process like that the temperature during spark plasma sintering was varied between 800 and 1200°C, while the heating rate and holding time were 100K/min, 10 min respectively.

As shown in Figure 2.28 spark plasma sintering (SPS) was used to prepare porous CP titanium with porosities of 30%-70% and pore sizes of 125-800 $\mu$ m with sodium chloride (NaCl) dissolution method. The porous titanium sample sintered under 50MPa for 8min at 700 °C showed single  $\alpha$  phase. All the samples that produced



exhibited highly interconnected structure and uniform pore distribution. The macroporous titanium sample with elastic modulus 6.2-36.1GPa and yield strength 27.2-94.2MPa can be used as bone implants (Zhang et al., 2010).

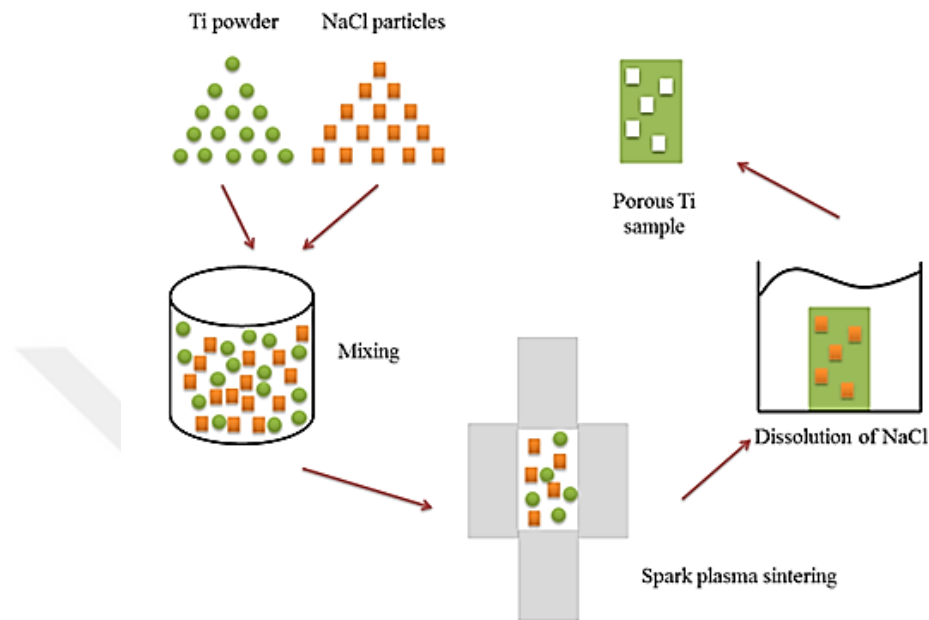


Figure 2.28. Spark plasma sintering process.

Another sample of porous titanium and Ti-5Mn alloy by using SPS technique were successfully prepared at pressureless conditions this time using 250-245 $\mu\text{m}$  particles of ammonium hydrogen carbonate as well as blowing agent  $\text{TiH}_2$  in size  $<44\mu\text{m}$  for 5min at different temperatures. Experimental results showed that the Ti5Mn alloy indicated a good pore distribution, and if sintering temperature increased from 950 $^\circ\text{C}$  to 1100 $^\circ\text{C}$  the porosity decreased from 56% to 21% and Elastic modulus was increased from 35 to 51.83GPa. Pure Ti sample prepared under pressureless condition at 1000 $^\circ\text{C}$  sintering temperature the range of porosity in the sample was 53% and elastic modulus was 40GPa (Ibrahim et al., 2011).

### 2.4.3. Microwave sintering

Microwave processing technique emerged as a new method used for sintering metals, ceramics, semiconductors and composites, in this process the materials couple

with microwaves, absorb the electromagnetic energy volumetrically, heating the green compacts till sintering temperature for densifying and alloying ( Das et al., 2009; Oghbaei and Mirzaee, 2010; Xu *et al.*, 2015). For dental implants microwave processing method has also been suggested to sinter titanium powders, the pore size in the samples that produced was about 30-100 $\mu\text{m}$  and thickness was ranging from 100–200 $\mu\text{m}$ , as determined by the level of microwave power (Wally et al., 2015).

To prevent impurity formation such as oxides, the sintering wants to be performed in either a protective gas atmosphere or in a vacuum because powder metallurgy processing of Ti-based alloys and their composites requires a long sintering time. Although to ensure complete sintering prolonged heating time requires ( Liu et al., 2006; Mendes et al., 2016). The advantage of MW heating is to save energy and time used for the processing of materials such as metals, ceramics and composites decreased processing cost, reduced sintering temperature, achieving faster generate and uniform heating by transfer of microwaves to the materials directly, better production quality, and lower environmental hazards (Oghbaei and Mirzaee, 2010; Benavente et al., 2014).

Gupta and Wong employed the two-directional microwave sintering method with silicon carbide (SiC) as a susceptor material in an experimental arrangement shown in Figure 2.29. Moreover, it was noted that the sintering conducted in that study may also be considered as hybrid sintering with direct heating/sintering of the compacts from microwaves forming one component and the radiative heating/sintering from the SiC susceptor forming the second component of the total heat imparted into the compacts (Gupta and Wong, 2005).

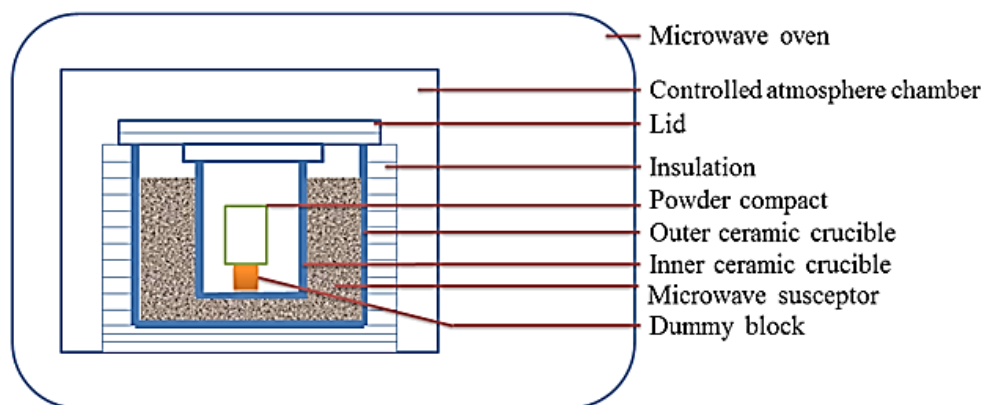


Figure 2.29. Schematic diagram of the two-directional microwave used in Gupta and Wong study (Gupta and Wong, 2005).

#### 2.4.4. Space holder technique

Space holder technique (SHT) employed to produce high porosity TiNb porous as shown schematically in Figure 2.30. Metals, ceramic particles, polymeric grains and salts can be used as space holder materials (or pore formers, space fillers, pore forming reagents etc.), SHT has advantages like adjustable amount of porosity, pore shape, and pore size distribution (Wen et al., 2001; Esen and Bor, 2007; Aydoğmuş and Bor, 2009).

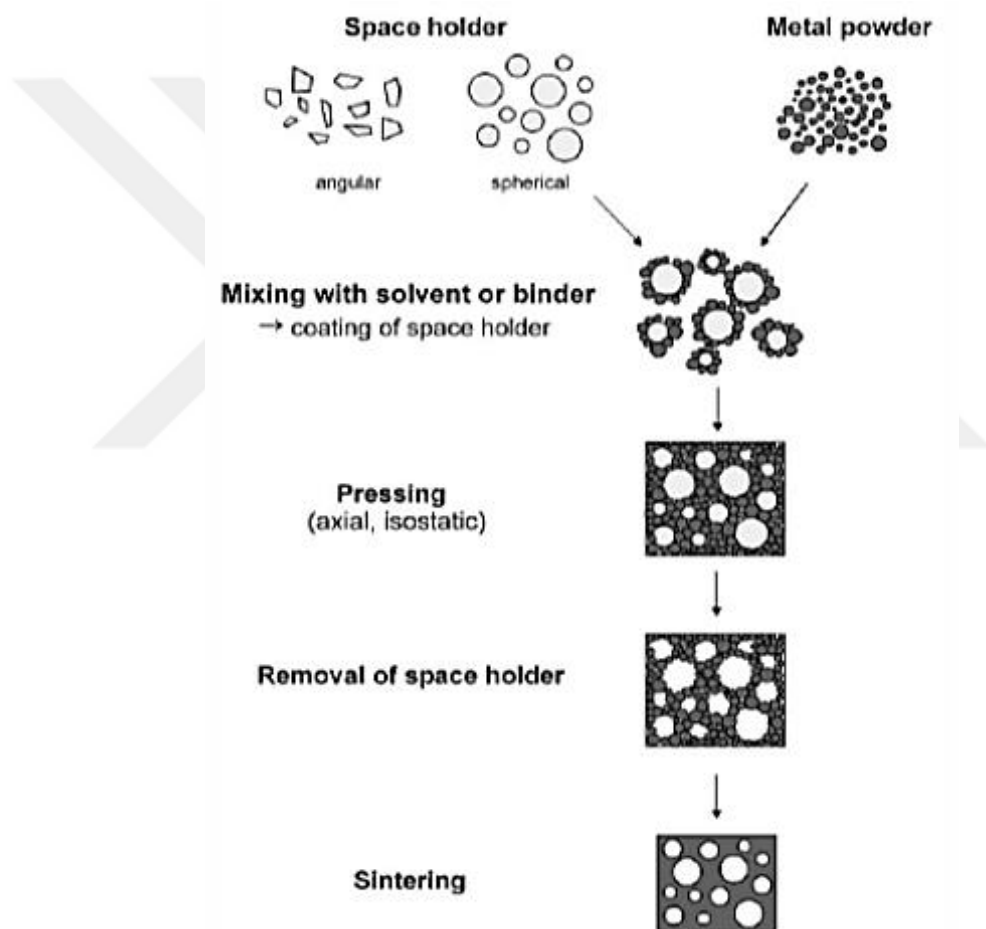


Figure 2.30. Schematic fabrication process for porous titanium alloy by space holder technique (Banhart, 2001).

Generally, in this technique the process consists of these main steps:

- Select the type of powder.
- Mixing: all powders are mixed together by hand or by special machine. They must be mixed completely for homogeneity of the mixture.

- iii. Hot or green compaction: mixed powders are poured into a mold under controlled pressure to produce good sample and make the particles connected.
- iv. Sintering: the sample that formed by hot or cold pressing is heated to the sintering temperature inside of a furnace and held for sufficient time.
- v. Spacer removal: depends on what type of space holder used, it can be removed by heat or water.

The size, shape and quantity of the space holder have effect on the mechanical properties. Moreover, pore diameter, morphology and porosity level of the porous metal can be adjusted under relatively low temperatures with low reactivity (Wen et al, 2001; Li et al., 2009; Niu et al, 2009). It can create porous metal samples with larger porosity Figure 2.31.

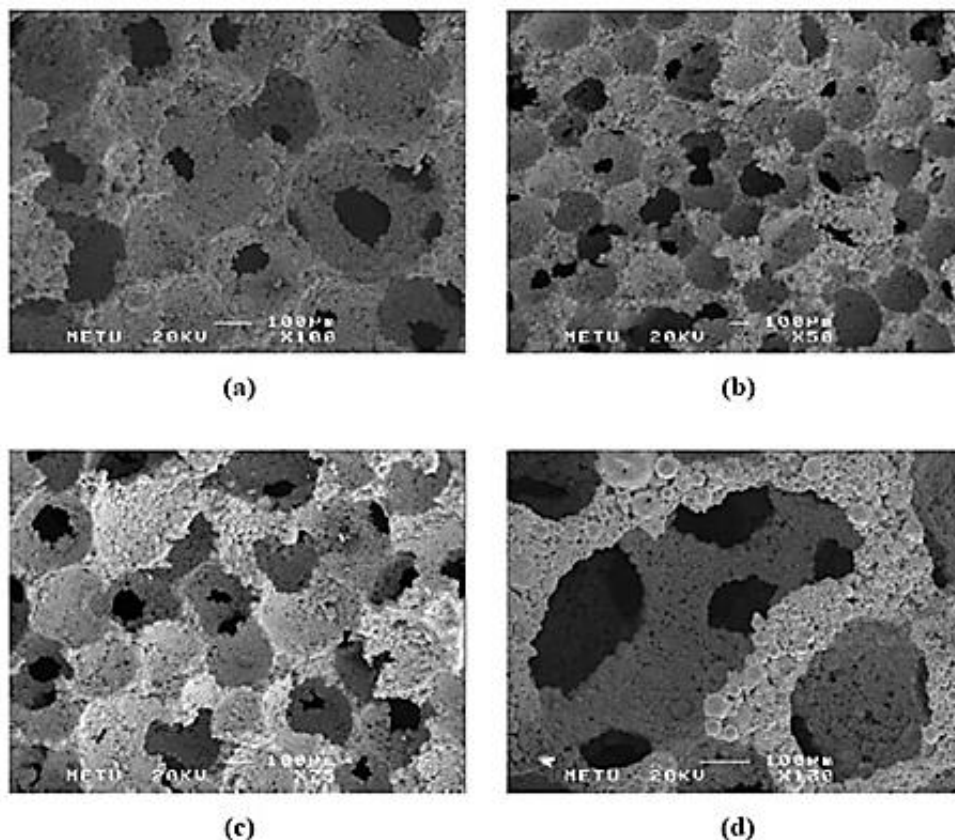


Figure 2.31. SEM images of fractured TiNi foams (1100°C, 1h) showing interconnected pore structure a) 59%, b) 66%, c) 73% and d) side view of interconnected pores in 73% porosity TiNi foam (Aydoğmuş, 2010).

Some conditions should be known before selecting space holder such as:

- i. Space holder that selected must not react with Ti and its alloys.

- ii. After sintering the sample should be clear from any residue.
- iii. The process for producing pores should be easy.

When a space holder material is used a common difficulty is how to remove a large amount of the space holder? Another difficulty in this process is what type of space holder should be selected? Any remains of space holder after sintering left must not be harmful or toxic for biomedical applications because there is a possibility that any remains of space holder absorbed by human body if they are harmful could import unfavorable effects. Actually, the space-holders have low melting points can be removed at low temperatures or many of them can removed by a dissolution in water.

Several materials have been attempted by various investigators as temporary space holders, including urea (Andrade et al., 2015), ammonium hydrogen carbonate (Lin et al., 2010), tapioca starch (Mansourighasri, 2012), sodium chloride (Jha et al., 2013), polymeric materials (Nugroho et al., 2010) and magnesium (Nakas et al., 2011). There are many water soluble spacers such as sodium chloride (Ye and Dunand, 2010) potassium sorbate (Esen and Bor, 2011) and potassium chloride (Esen, and Bor, 2011) all of which have been utilized to fabricate porous titanium and its alloys. In fact, it is possible to remove most of the space holders by dissolution process commonly in water or evaporate at low temperatures. A general difficulty of this technique is the removal of large amounts of space holder material in the sample and what kind of space holder material should be selected. After sintering any residue left should be either bio-inert or bio-compatible, for biomedical applications. It is understood that sodium chloride (NaCl) residue can be easily removed through dissolution in water. So, (NaCl) is a better choice and even is any residue is left it would be not toxic for bio-implants (Ye and Dunand, 2010).

On the other hand, space holders like urea and ammonium hydrogen carbonate if used any residues left import detrimental effect because there is a possibility of absorption of residues left by the bio-implants (Aydoğmuş, 2010). Low cost, much lower toxicity from residual content, fast dissolution in water and reduced etching of metal during dissolution are the main advantages of using sodium chloride as a space holder. Sodium chloride was used as a space holder to prepare porous titanium and its alloys with macro pore size 200-400 $\mu$ m with porosity up to 90% (Zhao et al., 2009).

In latest years, to adjust porosity and pore structures space holders like urea or ammonium hydrogen carbonate have been used (Wan, 2011; Prado, et al., 2015). Wen et al. (2002; 2002) used ammonium hydrogen carbonate with carbamide both together in the manufacture of porous titanium with mechanical properties close to the mechanical properties of human bone to be used as an implant material for biomedical applications (Wen et al., 2001). By space holder technique magnesium powders were used to produce porous Ti-6Al-4V alloys where magnesium powders were employed to generate porosity in the range of 51-65 vol%. The process like that spherical magnesium powders with an average size of  $375\mu\text{m}$  were mixed with spherical Ti-6Al-4V powders with an average size of  $55\mu\text{m}$ . After that 500MPa pressure used to compact the mixtures by using a double-ended steel die. Finally, to evaporate magnesium powder the green compacts were heated to  $1200^{\circ}\text{C}$  and sintered for 2h under high purity argon gas atmosphere (Aşık and Bor, 2015). At the result two types of pores exist as shown in Figure 2.32.:

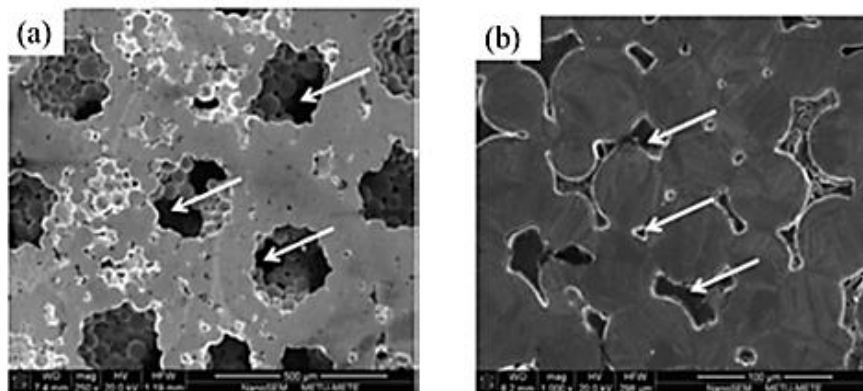


Figure 2.32. Pore characteristics of produced Ti-6Al-4V foams; a) macro-pores and interconnections between them b) micropores existent in the structure due to insufficient sintering (Aşık and Bor, 2015).

- i. Micro pores exist in the structure due to insufficient sintering.
- ii. Macro pores exist due to removal of space holders.

But, rapid decomposition at lower temperature of ammonium hydrogen carbonate cause an inexact control of porosity and pore structures, in addition to an unsatisfactory mechanical properties of porous alloys. Also, the presence of notches and sharp corners of the pores in the alloys, because of shape of the ammonium hydrogen

carbonate space holder particles, they have needle-like or flake shapes. These shapes have negative influence on mechanical properties due to stress concentration (Kopas et al., 2007). Besides, urea and ammonium hydrogen carbonate have relatively low melting temperatures, their removal by thermal treatment may cause oxidation resulting in decrease in mechanical properties. Additionally, they cannot be fully removed and may leave some residue that makes hydrogen carbonate and urea useless for many unblemished requiring applications.

The advantage of magnesium is to prevent contamination when evaporated. Magnesium was used as a space holder to produce 59%-81% homogeneous porous TiNi alloys. Prealloyed powders (TiNi and Mg) were mixed for 30 min in this process with 5 wt% polyvinyl alcohol (PVA) solution (2.5 wt% PVA + water) used as the binder before compaction. 250-600 $\mu$ m particle size of Mg powders were used, averaging at 450 $\mu$ m. After that double ended steel die used to compact the mixture by hydraulic press 10mm for height and diameter at 400MPa. Then, for debinding and removing of magnesium compacts were heated to 1100°C in cleaned argon atmosphere at a rate of 10°C/min. Sintering time at 1100°C was 1h for complete removal of magnesium. The sample that produced showed interconnected open pores near 400 $\mu$ m for an average macro-pore size and spherical in shape as shown in Figure 2.33 (Aydoğmuş, 2010).

Basically, three criteria were taken into account in choosing magnesium as space holder in porous TiNb alloys production in the present study. First, Mg solubility in TiNb is expected to be negligible since magnesium has very limited solid solubility around (% 1 at RT) in titanium as shown in Figure 2.34 and no solid solubility in Nb as shown in Figure 2.35. Second, during sintering Mg provides a reducing atmosphere that prevents oxidation of TiNb alloys. Finally, Mg in small amounts dissolved in the body and forms compounds that are non-toxic, incomplete removal from the foam does not constitute a drawback and it can be removed by the body when implanted.

Zhuravleva et al. (2013) prepared porous  $\beta$  type non-toxic Ti40Nb (wt.%) alloy by compaction. Two different samples were prepared. Firstly, bulk sample of (Ti40Nb (wt.%) was prepared and used as a reference sample. Secondly, Mg powders used as space holders to prepare porous samples. For the bulk samples 700MPa for 2h at room temperature was used to produce green compact then sintered in argon atmosphere at 1273K for 2h and finally water quenched. For the porous samples firstly %50 Mg



powders (vol.%) were mixed with Ti40Nb then 700MPa for 2h at room temperature used to produce green compact, the samples were sealed in argon filled quartz tubes and 1273 K for 2h was used to evaporate Mg powders then water quenched.

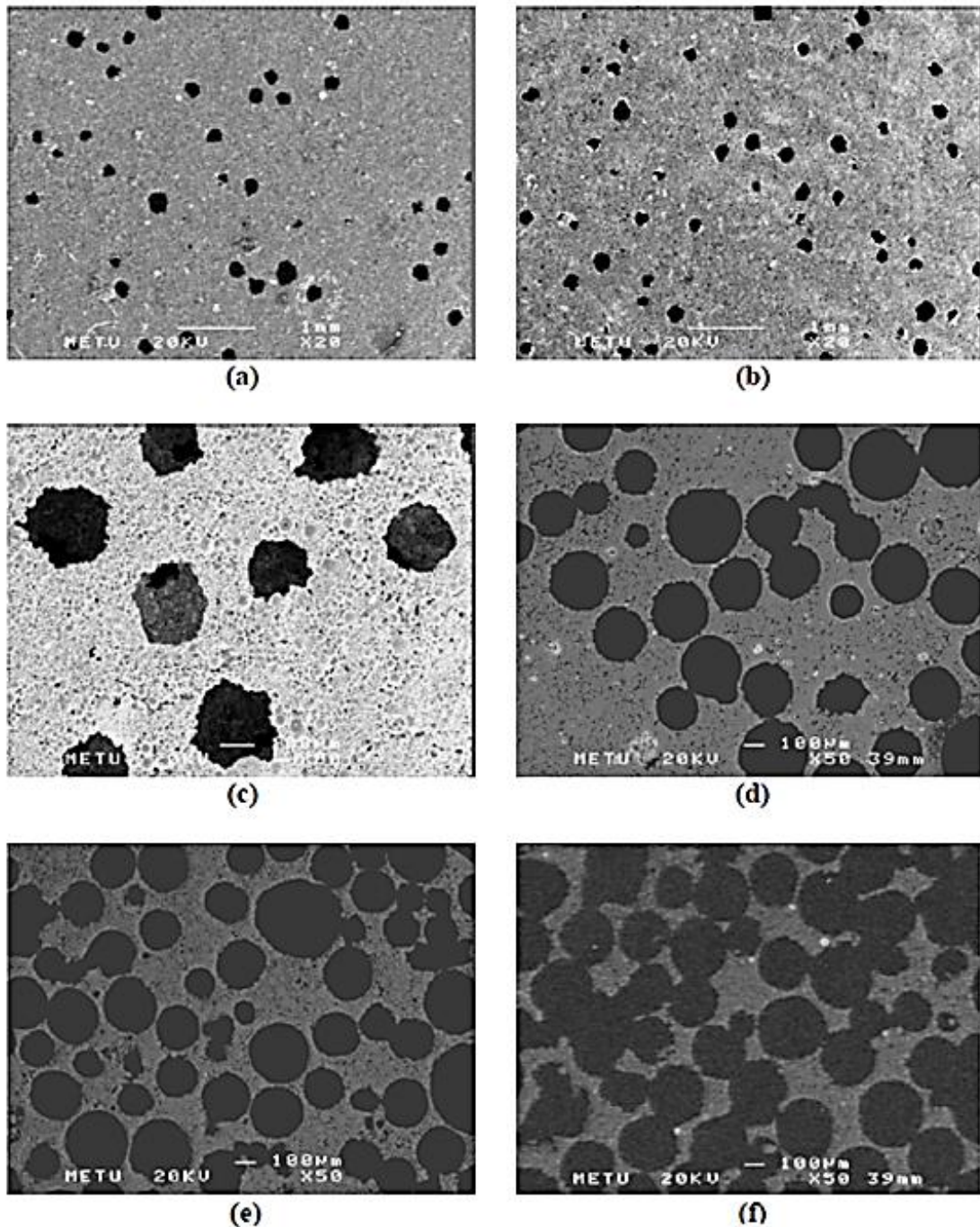


Figure 2.33. SEM micrographs of porous TiNi samples produced with Ti-50.6 at. %Ni powders (1100 °C, 1 h) with the porosity of (a) 37%, (b) 43%, (c) 51%, (d) 59%, (e) 66% and (f) 81% (Aydoğmuş, 2010).





XRD patterns of Ti40Nb and Ti40Nb with 50% porosity samples as shown in Figure 2.36 shows that the diffraction peaks of sintered samples displayed  $\alpha'$ Ti and  $\beta$ Ti.

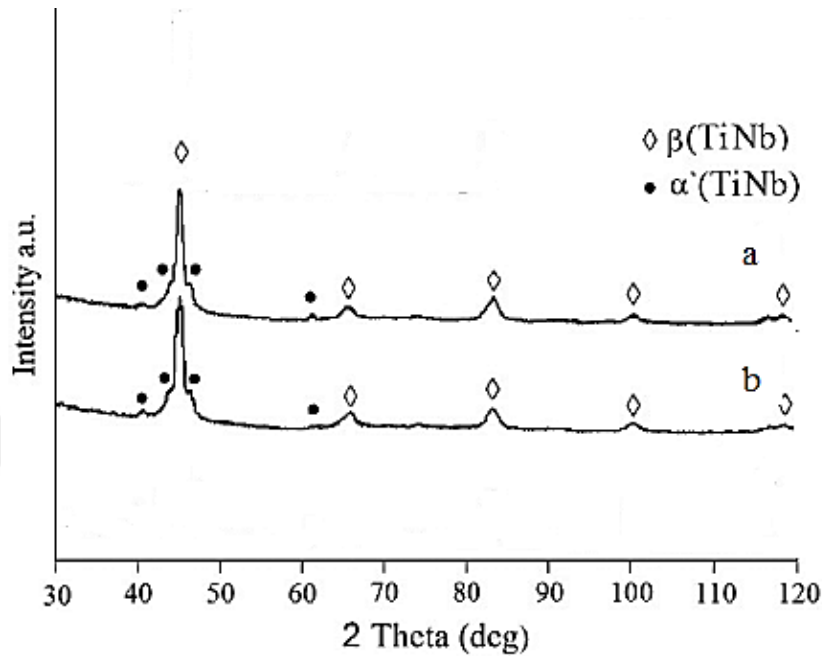


Figure 2.36. XRD patterns of as-quenched sintered Ti40Nb samples a) reference sample without space-holder b) 50% porous sample prepared using Mg as space holder (Zhuravleva et al., 2013).

Space holder technique was used to prepare porous Ti-65 wt.% and Nb-35 wt.% (Oliveira, et al., 2015). Ammonium bicarbonate (355-425 $\mu\text{m}$ ) was used as space holder and the particle size of both Ti and Nb powders were (50-149 $\mu\text{m}$ ) and (31-500 $\mu\text{m}$ ), respectively. Two types of samples were prepared, TiNb with macropores were pressed by uniaxial compaction at 400MPa followed by isostatic compaction at 250MPa another samples TiNb with micropores were pressed by uniaxial compaction at 800MPa. For TiNb with macropores samples, the pore former additive elimination was conducted at 170 $^{\circ}\text{C}$  for 2h in a chamber furnace in air. Then, the green samples were sintered in a vacuum furnace (better than  $10^{-5}$  Torr) for 2h at 1200 $^{\circ}\text{C}$  or 1300 $^{\circ}\text{C}$ . The samples were slowly cooled to room temperature in the furnace. TiNb micropore samples, the same sintering parameters were used, were sintered only at 1300 $^{\circ}\text{C}$ . SEM micrographs of Ti35Nb samples sintered at 1200 $^{\circ}\text{C}$  and 1300 $^{\circ}\text{C}$  after chemical etching presented closed and homogeneously dispersed micropores; while Ti35Nb with macropores samples showed a structure consisting of closed micropores and large interconnected

macropores. However, only the samples sintered at 1300°C presented a predominance of  $\beta$  Ti phase. XRD patterns of Ti35Nb samples sintered at 1200°C and 1300°C show that the diffraction peaks of sintered samples displayed  $\alpha$  Ti,  $\beta$  Ti and Nb phases. Further, NbO, TiO and Ti<sub>3</sub>O peaks can also be observed.

Porous Ti-35Nb (mass fraction) prepared by space holder technique (Lin et al., 2010). Ammonium bicarbonate particles with the size in the range of 300-500 $\mu$ m as space holder used. Ti-35Nb powders mixed with ammonium bicarbonate and compacted under a pressure of 750MPa inside cylindrical bars. The green compacts were sintered in a vacuum furnace under a pressure of about 1KPa. The sintered condition was 175°C,4h + 1200°C, 2h. XRD used to investigate the microstructure of sintered porous Ti-35Nb at 1200°C for 2h. XRD pattern of Ti35Nb foam with a porosity of 66% as shown in Figure 2.37 show both  $\beta$ -Ti and Ti<sub>3</sub>O.

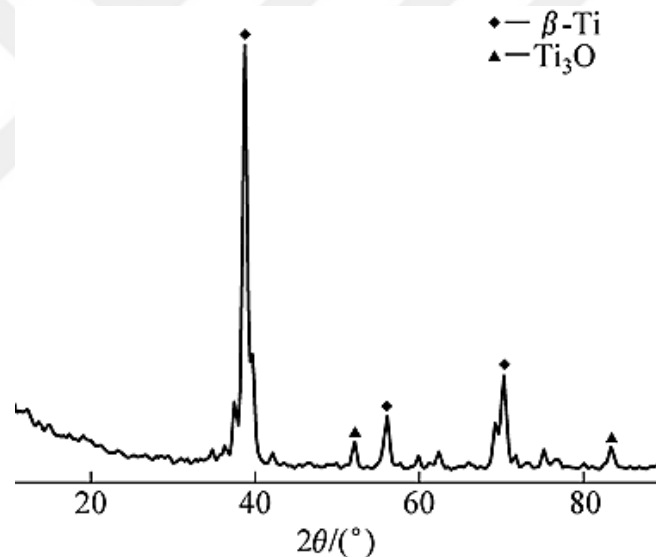


Figure 2.37. XRD pattern of porous Ti35Nb sintered at 1200°C for 2h (Lin et al., 2010).

Porous Ti for the application in clinic orthopedics field was fabricated by space holder technique using polymethyl methacrylate (PMMA) as the space holder under different sintering conditions. The results show that improvement of grain size of porous Ti can be achieved by increasing of sintering temperature and time and decreased pore size, resulted in with a concomitant increase of tensile strength and elastic modulus. The sintering temperature and time have more influence on the microstructure and mechanical properties than those of porous Ti (Li et al., 2015).

### 2.4.5. Metal injection molding (MIM)

The net-shape fabrication of small, complex, and precise metallic and ceramic parts and components are achieved by a manufacturing technology called metal injection molding (MIM). The MIM process includes mixing of powders with one or more polymers or binders to produce a feedstock; followed by injection molding to form shape parts by making the feedstock flow into and fill a mold under pressure; removing polymer or binder, and finally sintering to near full density as shown in Figure 2.38 (Chen et al., 2009).

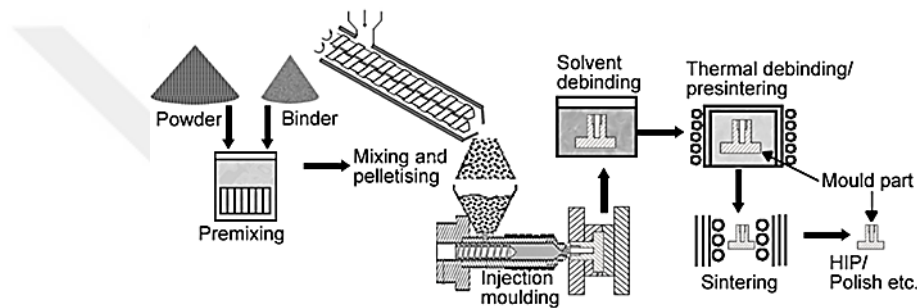


Figure 2.38. Flow diagram of metal injection molding (Sidambe, 2014).

German and Bose stated that during the sintering to prepare sample by MIM there are three stages (Zhao et al., 2015):

- i. Starts of the shrinkage of the powder compact when neck growth takes place and this is the initial stage.
- ii. The intermediate stage the rate of the shrinkage is higher than other stages and determines the densification of the final compact during the sintering process.
- iii. At the final stage shrinkage becomes very low due to the formation of the closed spherical pores.

Zhao et al., (2013) used metal injection molding to manufacture a series of Ti–Nb binary alloys with niobium content. Samples made from CP Ti, Ti–10Nb, Ti–16Nb and Ti–22Nb (all wt.%). It was found that the range of porosity in the samples increased from about 1.6% to 5.8% with increasing niobium content from 0% to 22%, also the carbide area fraction increased from 0% to about 1.8% in the as-sintered samples. All samples after mixing were sintered at 1500°C for 4h after that hot isostatic pressing

(HIP) at 915°C for 2h under a pressure of 100MPa was used to treated CP-Ti, Ti-10Nb, Ti-16Nb and Ti-22Nb samples. XRD spectra for all samples shown in Figure 2.39 show both  $\alpha$  Phase and  $\beta$  phase.

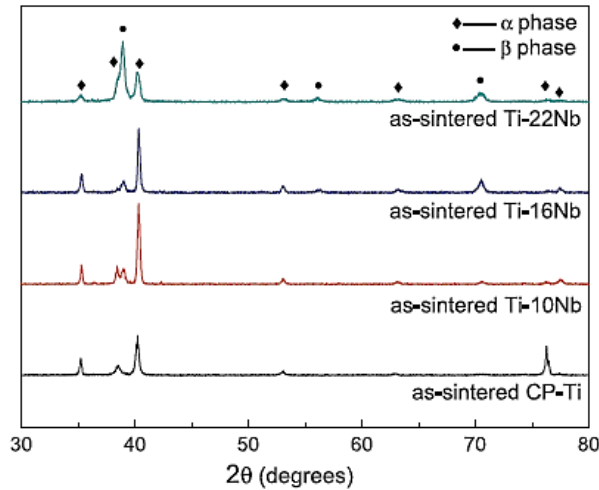


Figure 2.39. XRD pattern for as-sintered CP Ti, Ti-10Nb, Ti-16Nb and Ti-22Nb (Zhao, et al., 2013).

However, due to the high reactivity of titanium with atmospheric components such as oxygen, nitrogen and carbon, MIM of Ti alloys are still not standard (Sidambe et al., 2012; German, 2013). On the other hand, in all the porous samples contamination occur by polymer decomposition during sintering. The MIM process has found very small application with reactive metals, such as titanium, zirconium, niobium, and molybdenum, primarily because of problems with carbon, nitrogen, hydrogen and oxygen impurities. Even at low concentration, these interstitials can severely reduce the mechanical properties of titanium and its alloys ( Shibo, et al., 2009; Aydoğmuş, 2010).

#### 2.4.6. Conventional sintering (CS)

In conventional sintering of Ti and Ti alloys mixed elemental or prealloyed powders requires compaction and sintering under high vacuum or Ar gas atmosphere at elevated temperatures around (1200-1400°C) for long times usually varying in the range of 2-72 hours (Aydoğmuş, 2010). On the other hand, porous alloys fabricated through conventional sintering methods have coarse grains. It is hard to obtain single equiaxed  $\beta$  phase. For example, by using blended elemental powders together with space holder

method, porous Ti-10Nb-10Zr alloys obtained at a sintering temperature of 1200°C for 10h under a high vacuum condition ( $10^{-4}$ - $10^{-5}$  Torr) consist of lamellar  $\alpha$  and  $\beta$  phases with grain size above 10 $\mu$ m (Li et al., 2014). Detrimental changes in the microstructure and mechanical properties occur when the high temperatures involved in these processes.

#### **2.4.7. Additive manufacturing (3D printing)**

Additive manufacturing or 3D printing is a novel method in which digital model is directly used for fabricating parts layer by layer material build-up approach. In another words 3D printing is a method for joining materials to produce objects from 3D model data (Duda and Raghavan, 2016). RP (rapid prototyping) involving solid free form fabrication as shown in Figure 2.40 (a) and (b) which uses metal wire feedstock melted by laser or electron beams or similar schemes using powder feed delivery nozzles forming layer-by-layer solid objects began to developing in the late 1980. As shown in Figure 2.40 (b) laser sintering of powders were developed as direct metal laser sintering (DMLS) or selective laser sintering (SLS), and both wire and powder feed processes have been referred to as direct energy deposition (DED) processes. In Figure 2.40 (c) CAD-driven laser beam is used in the process like that powder from a reservoir is rolled into a layer which is selectively melted, under an inert gas (Ar or N) environment. Electron beam melting is on the other hand carried out in vacuum. Figure 2.40 (d) shows that a suitable binder from an ink-jet printer head directed by a CAD program to create a metal/binder product which is sintered at high temperature to remove the binder and sinter (solidify) the metal powder (Murr and Johnson, 2017).

### **2.5. Compression Behavior of Porous Metallic Materials**

#### **2.5.1. General**

Generally, pore types (closed, open and partially open), porosity content and the structure of the cell walls have influence on the corresponding mechanical properties of porous samples and the forms of the stress-strain curves.

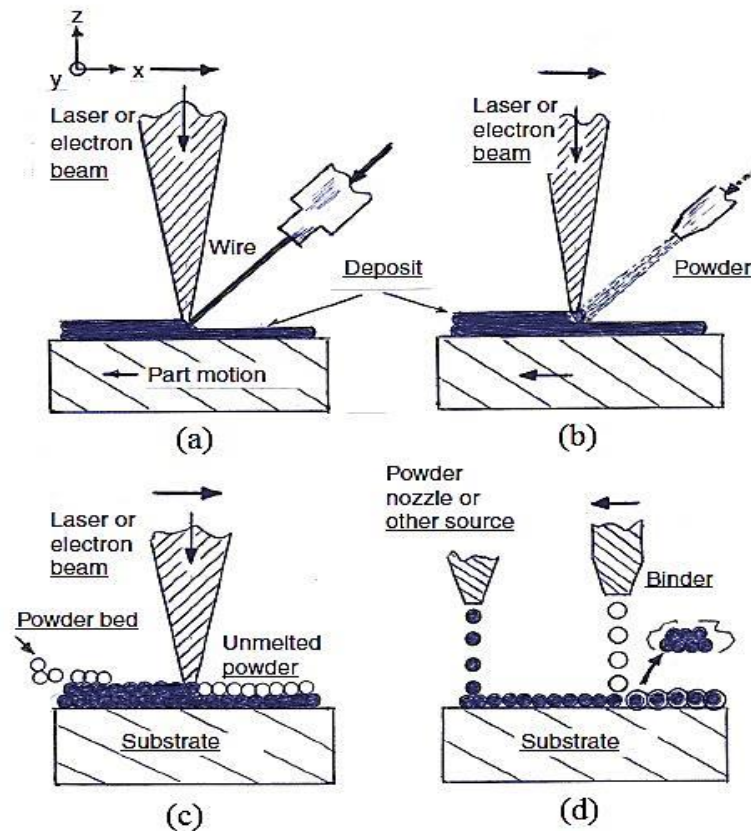


Figure 2.40. Schematic comparisons of metal AM processes and systems a) Laser or electron beam cladding using wire feed process b) Laser or electron beam sintering based systems. System can incorporate multiple powder feeders c) Powder bed fusion processes using electron or laser beam selective melting. Powder is rolled or raked from supply container or cassettes d) Binder jet powder process which requires post sintering to permanently bind metal powder and expel binder. Unbound powder is recovered (Murr and Johnson, 2017).

### 2.5.2. Compression response

Porous metallic materials can be divided into three main groups according to the deformation behavior they exhibit; elastomeric, elastic-plastic and elastic-brittle, as shown in Figure 2.41:

- i. **Elastomeric:** in this type linear elasticity has a very small strain; it's around %5 or less. In this structure cell face stretching if the cells are closed or cell wall bonding controls the linear elasticity. Figure 2.41 (a) shows this type of deformation. Elastic collapse in pores occurs due to the elastic buckling of the cell walls. Either open or closed pore have

different influence on elastic collapse stress. Compression for the close pores with the gas inside the pores gives the stress-strain curves, which rises with the strain, while open pores gives a long flat plateau.

- ii. Elastic-plastic collapse and densification: Figure 2.41 (b) shows this behavior of deformation. Polymers and metallic foams that have plastic yield point collapse plastically when loaded beyond the linear-elastic regime. Long horizontal plateau to the stress-strain curve achieved by plastic collapse. When the plastic deformation take place completely densification starts in which the stress raises steeply.
- iii. Elastic-brittle: Figure 2.41 (c) this type of compression behavior is observed generally in ceramics foams and in brittle porous materials.

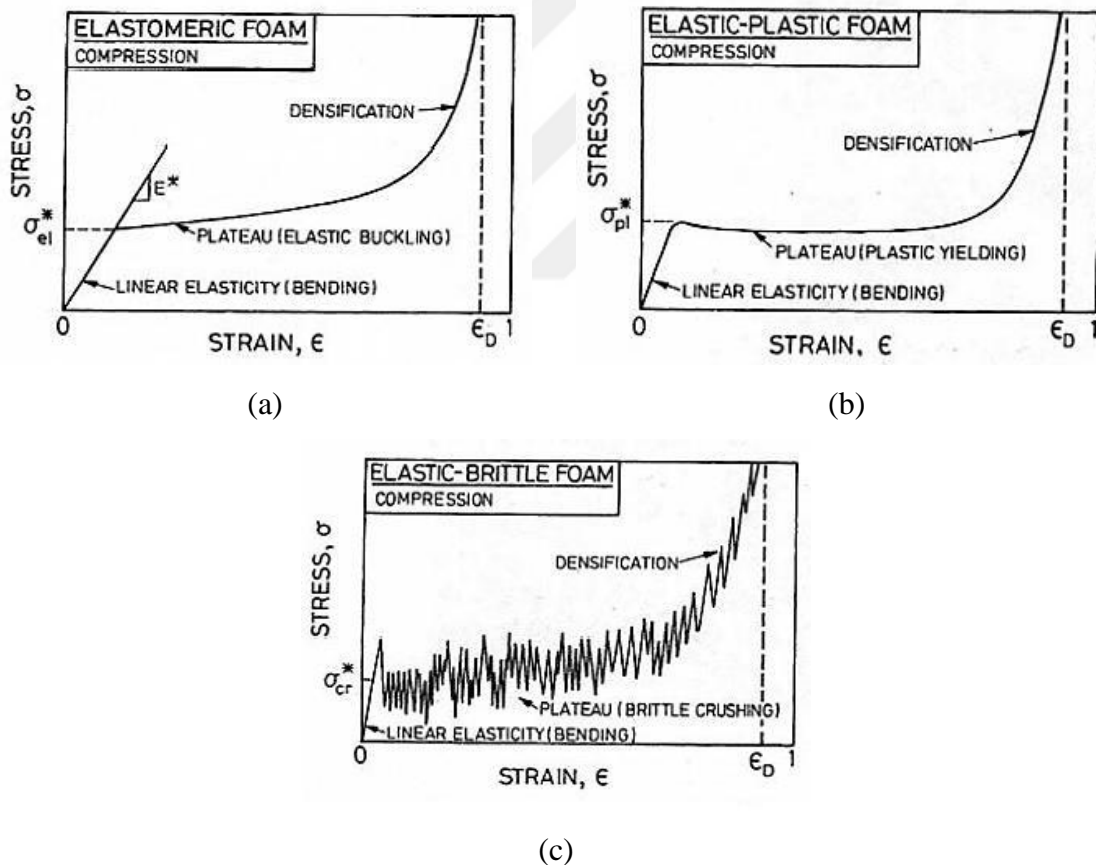


Figure 2.41. Schematic stress-strain curves of porous materials (Esen, 2007).

Ti40Nb (wt.%) mixed with 60 (vol.%) NaCl was compacted under 700MPa for 2h. Then the green samples were sintered at 1273K for 2h and water quenched. For



removing the NaCl particles, the samples were then immersed in purified water kept at 353K for 4h. To determine compression strength and Young's modulus compression tests were carried out. Figure 2.42 shows the effect of porosity on the Young's modulus and compression strength. It's clearly visible, with increasing porosity from 62 to 80% the compression strength of samples decreased from 34.6 to 9.6MPa (Zhuravleva et al., 2013).

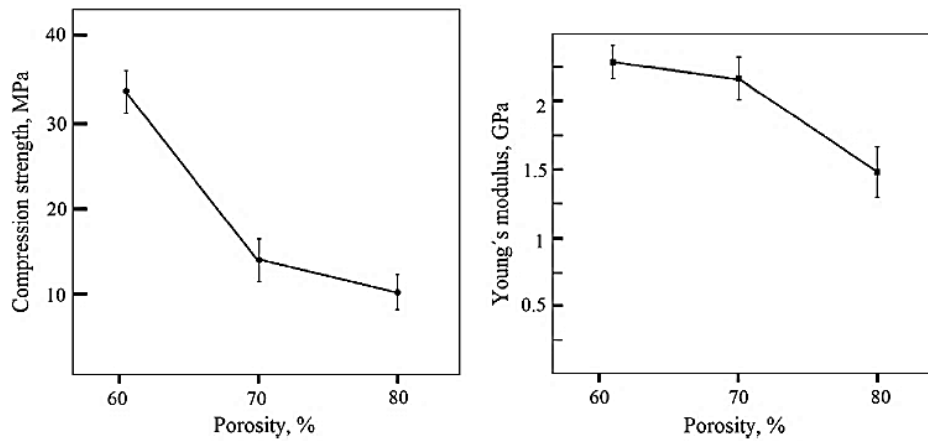


Figure 2.42. Porosity versus Young's modulus and compression strength for samples produced with NaCl space-holder (Zhuravleva et al., 2013).

SHT was used to produce porous TiNi alloys having porosities in the range 59–81% and magnesium powders were used as pore forming agent (Aydoğmuş and Bor, 2009). Mechanical properties of the porous samples, as obtained from compression tests with the mechanical properties of cancellous bone are summarized in Table 2.2.

Table 2.2. Mechanical properties of TiNi foams tested in compression, where E is Young's modulus,  $\sigma_0$  is yield strength,  $\sigma_{max}$  is compressive strength. The values given together with the standard deviations are average of four or more tests (Aydoğmuş and Bor, 2009)

Porosity (%)	E (GPa)	$\sigma_0$ (MPa)	$\sigma_{max}$ (MPa)
59	$6.8 \pm 2.68$	$22.85 \pm 8.5$	$88.83 \pm 4.21$
66	$3.04 \pm 0.6$	$13.87 \pm 3.11$	$44.91 \pm 10.37$
73	$2.6 \pm 0.88$	$8.2 \pm 3.03$	$21.41 \pm 2.4$
81	$1 \pm 0.44$	$4.91 \pm 1.81$	$7.58 \pm 1.32$
Cancellous bone	$1.08 \pm 0.86$	$15.2 \pm 8$	$25 \pm 8.1$

SPS technique was used to produce porous Ti and  $\text{NH}_4\text{HCO}_3$  was used as pore formation agent. Ti was mixed with 20 (wt.%)  $\text{NH}_4\text{HCO}_3$ . These mixtures were green compacted and compaction pressure was 300MPa. Then sintering was applied at 1000°C, 1050°C, 1100°C, 1150°C and 1200°C. Figure 2.43 shows the static compressive stress-strain ( $s$ - $\epsilon$ ) curves of the porous Ti with different SPS sintering temperatures. Elastic deformation stage (a), long plateau stage (b) and densification stage (c) for all of the samples were observed. The elastic modulus and the compressive strength were 11.2GPa and 287MPa respectively (Zhang et al., 2015).

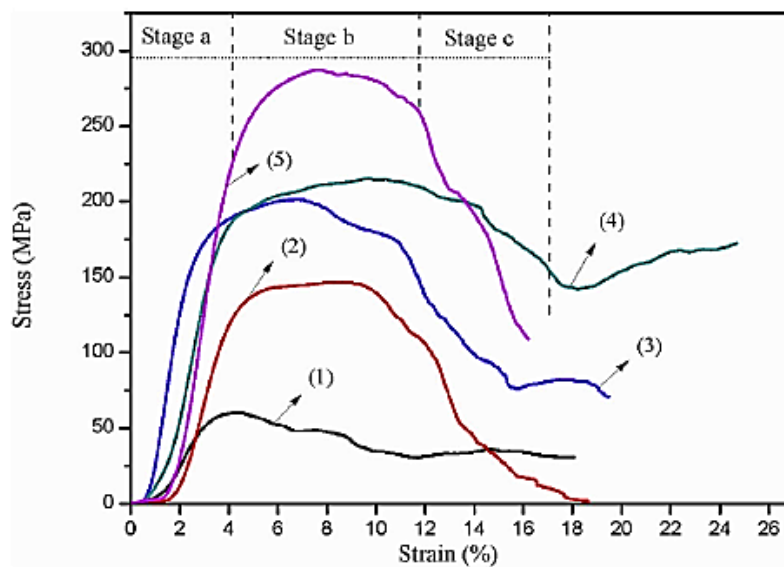


Figure 2.43. Static compressive stress-strain ( $s$ - $\epsilon$ ) curves of the porous Ti at different SPS sintering temperatures 1) 1000°C 2) 1050°C 3) 1100°C 4) 1150°C and 5) 1200°C (Zhang et al., 2015).

### 3. MATERIALS AND METHODS

#### 3.1. Powders Used

In the present study pure Ti powders, Nb powders and Mg powders were used to produce porous TiNb alloys. Atomic percentage of the alloy was chosen as  $Ti_{74}Nb_{26}$  which has the minimum elastic modulus among the binary Ti-Nb alloys and accordingly suitable for use in biomedical applications. Particle size of pure titanium (99.5 mass% in purity) and pure niobium (99.8 mass% in purity) was -325 mesh, less than  $45\mu m$ , and both of them were supplied by Alfa Aesar, Germany. To obtain spherical pores inside the samples spherical magnesium powders (supplied by TangShan WeiHao Magnesium Powder Co., Ltd., China) were used as space holder material, and particle size of magnesium (99.8% pure) powders was adjusted by screening in the range of  $100-600\mu m$  which is the optimum pore size range for bone ingrowth (Aydođmuş, 2010).

Figure 3.1 shows SEM images of as-received Ti, Nb and Mg powders and Figure 3.2 displays XRD patterns of all these starting powders. Ti and Nb powders were produced applying hydrogenation-milling-dehydrogenation processes and Mg powders were produced via inert gas atomization method. XRD results stated that microstructures of pure starting powders Ti, Nb and Mg were consisting of only single  $\alpha$ -Ti with hexagonal close packed (HCP) crystal structure, body centered cubic (BCC) Nb and HCP Mg, respectively. None of the powders did not include any contamination products such as oxides or carbides. As a result of atomization process, Mg powders were almost completely spherical in shape. On the other hand, Ti and Nb powders were irregular due to the heavy plastic deformation they experienced during milling.

#### 3.2. Experimental Method

In the scope of the present study, hot pressing and space holder technique (SHT), two well-known powder metallurgy processing methods, were combined to produce porous TiNb alloys.

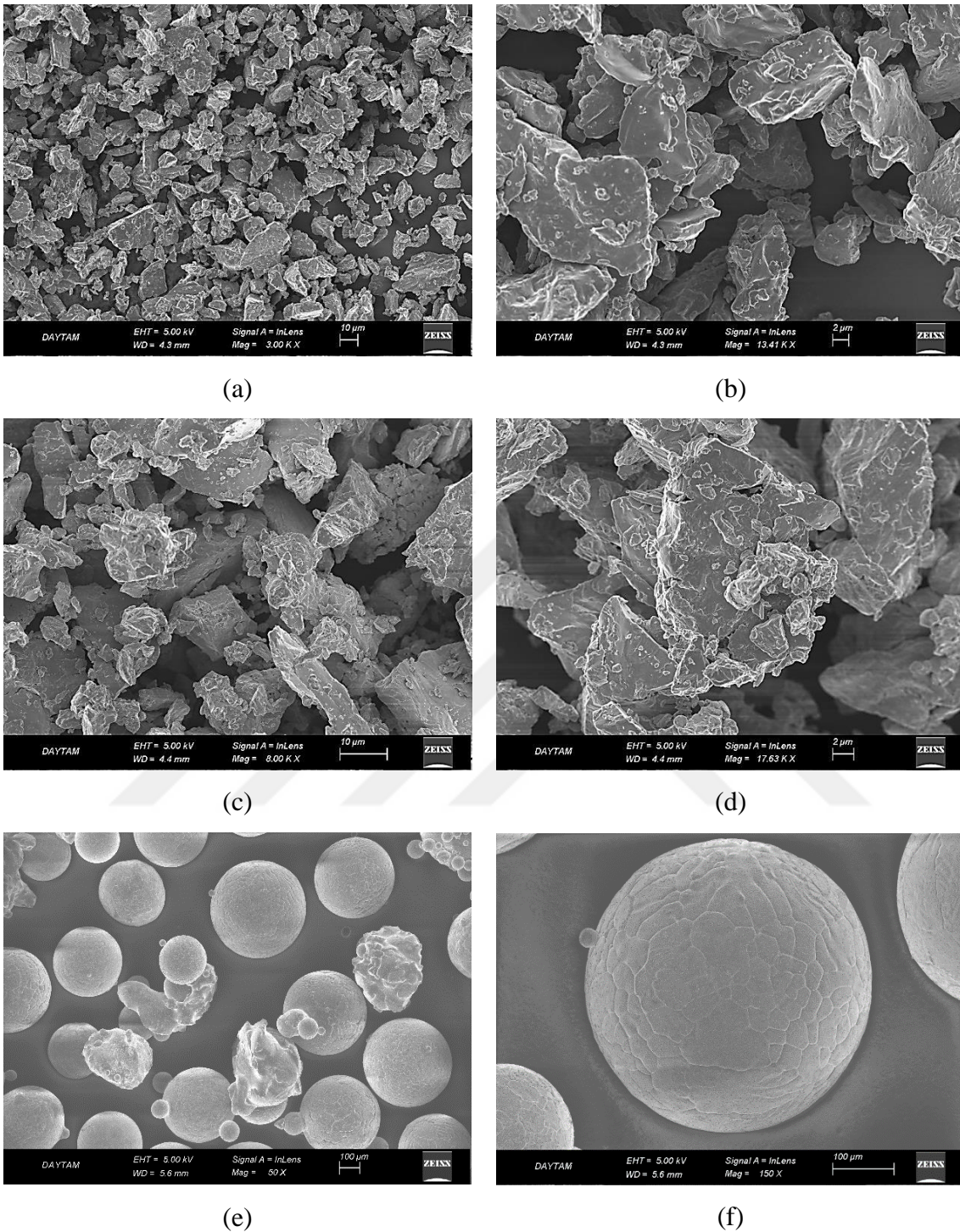


Figure 3.1. SEM micrographs showing morphology of a) and b) Ti powders c) and d) Nb powders, and e) and f) Mg powders.

A recent approach (cold pressing + sintering with Mg spacer particles) proposed by Aydogmus and Bor (2009) for the production of porous titanium nickel alloy using magnesium as space holder was adapted and enhanced for the fabrication of porous

TiNb samples with suitable pore characteristics and mechanical properties. Instead of cold pressing, hot pressing was used in the present study to improve the green and final strength.

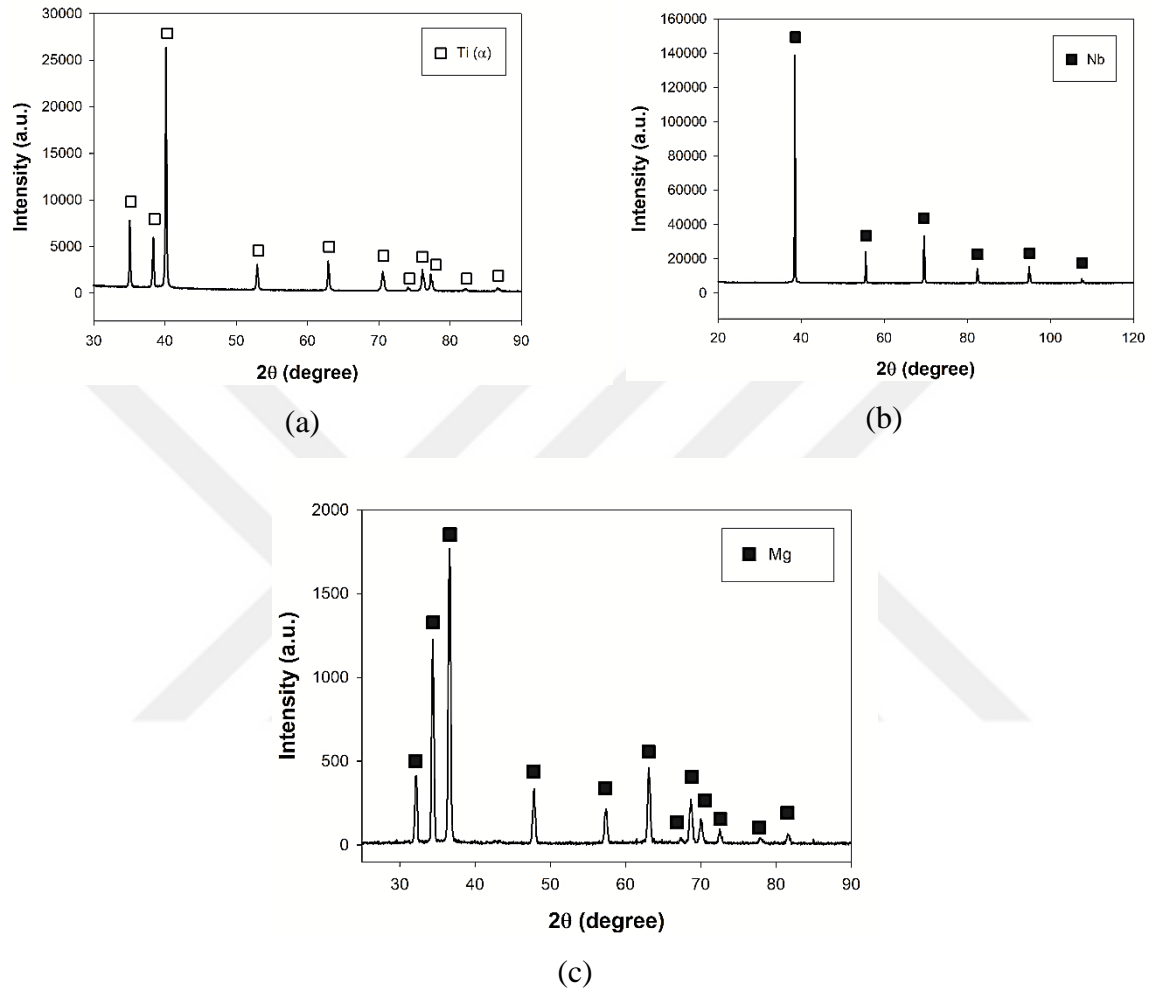


Figure 3.2. XRD patterns for a) Pure Ti b) Pure Nb and c) Pure Mg.

This basic space holder technique, utilizes pure magnesium spacer particles for pore formation. Mg is found to be so suitable to maintain a protective atmosphere during sintering. Mainly, two criteria were taken into account in choosing magnesium as space holder in TiNb alloy foam production:

1. Magnesium solubility in TiNb is expected to be negligible since magnesium is not soluble in any appreciable amount neither in Ti nor in Nb.

- Dissolved Mg in the body and compounds that may form in small quantities during processing are non-toxic.

It provides a reducing atmosphere that prevents oxidation of TiNb during sintering.

### 3.3. Space Holder Technique

Porous TiNb alloys with high porosity were produced by hot pressing + space holder technique as shown schematically in Figure 3.3. Ti powder, Nb powder and Mg powder in various ratios (40%, 50%, 60% and 70% Mg by volume, Table 3.1 shows weights of powders for each volume % of Mg) as shown in Figure 3.4 were mixed by hand using a small amount of ethanol (a few droplets) as the binder prior to hot compaction. Ethanol was necessary for the uniform coating of coarse Mg particles with fine Ti and Nb powders. Mixing time was kept as 15min to ensure a homogeneous distribution.

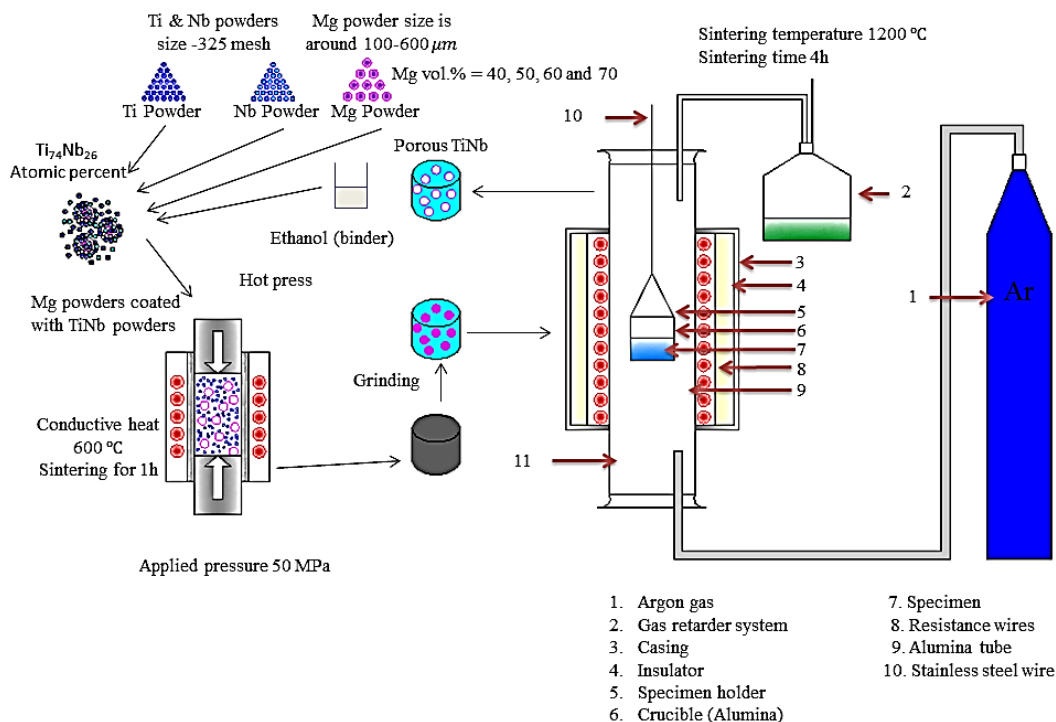


Figure 3.3. Schematic process of hot pressing and space holder technique.



Table 3.1. Amount of powders used to produce samples

Volume of Mg (%)	Weight of Ti (g)	Weight of Nb (g)	Weight of Mg (g)
40	3.51	2.39	1.22
50	2.92	1.99	1.53
60	2.34	1.59	1.84
70	1.75	1.19	2.14

Then the mixture of powders were compacted in a double ended graphite die as shown in Figure 3.5 using a hot press furnace under 50MPa pressure and at 600°C temperature for 1 hour as shown in Figure 3.6. The reasons for choosing 600°C as the hot pressing temperatures are summarized below:

1. It is lower than the melting temperature of magnesium (650°C).
2. To minimize plastic deformation of spherical magnesium powders that may occur during hot pressing.

At 600°C and under 50MPa, consolidation of the powders was not enough for effective sintering because of the micro pores present inside the samples. Figure 3.7 shows a sample produced by hot pressing at 600°C with 50MPa pressure for 1h and then cooled slowly to room temperature.



Figure 3.4. Ti, Nb and 70% Mg before mixing.

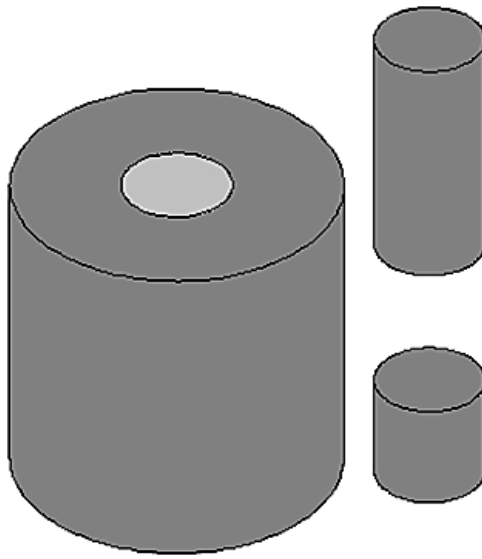


Figure 3.5. Graphite die.



Figure 3.6. Powders in a graphite die under pressure inside the hot press furnace.



Figure 3.7. Sample hot pressed at 600°C under a pressure of 50MPa for 1h.



After hot pressing grinding were required for cleaning surface of the samples. Grinding is an abrasive material removal, in another mean surface generation process used to clean or finish components made from metals and other materials. Typically, grinding abrasive paper starts with 240 grit SiC paper in belt or disk form and continues to 1200 grit SiC.

In our samples after hot pressing there was a graphite deposited layer on the surface of the samples. To clean the surface of the samples we used Struers LaboPol5 grinding wheel rotating machine with 240 and 320 grit SiC paper in disk form as shown in Figure 3.8. Ethanol was used as a lubricant to flush away removed material and keep fresh abrasive exposed.

To remove any deformation introduced after grinding polishing is required. Polishing has many more variables to consider compared to grinding while the procedure is similar to grinding. For polishing there are many types of abrasives, suspension mediums, and polishing clothes available. The choice of polishing abrasive type is a personal preference. Figure 3.9. shows samples before and after grinding.

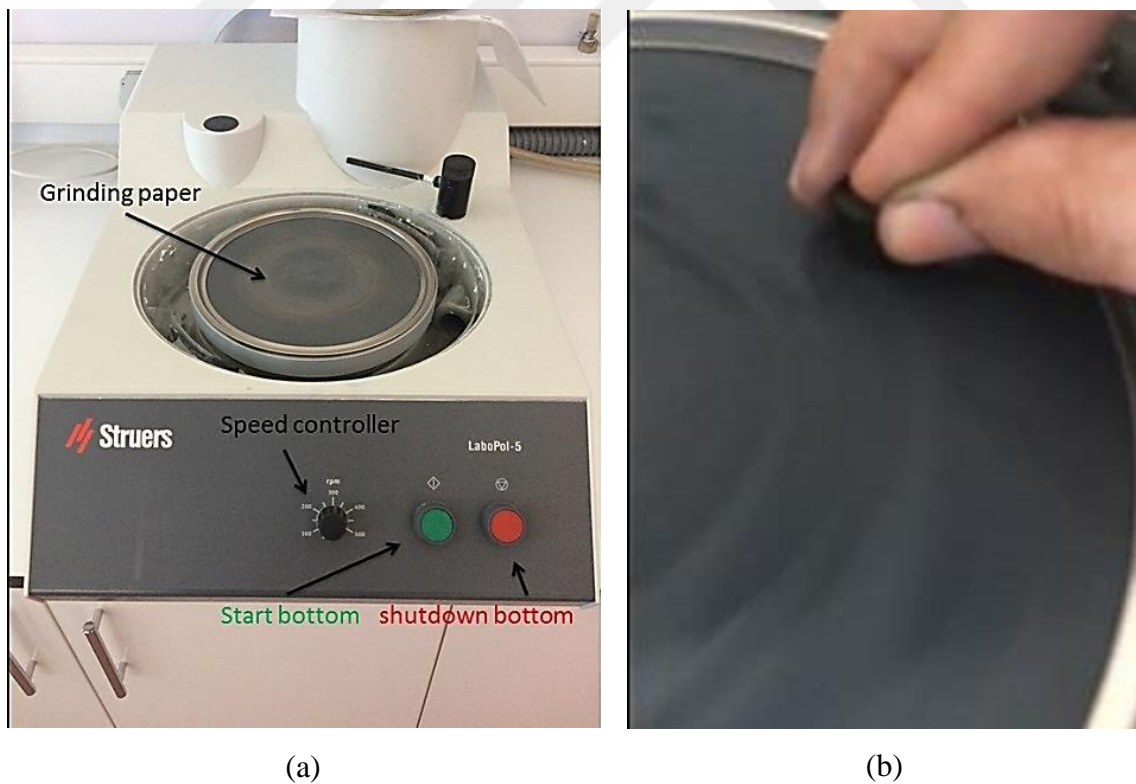


Figure 3.8. a) Grinding machine b) Grinding a sample.



Figure 3.9. a) Sample before grinding b) Sample after grinding.

After grinding all samples containing  $Ti_{74}Nb_{26}$  (atomic percent) with different amount of Mg (40%, 50%, 60% and 70% vol.%) added are shown in Figure 3.10.



Figure 3.10.  $Ti_{74}Nb_{26}$  with different amount of Mg spacers (vol.%).

A Protherm PTF 14/50/450 model vertical furnace was used for sintering and samples without pressure after hot pressing and grinding steps. Schematic drawing and a picture of vertical furnace and its equipment's used are shown in Figure 3.11.

Mg was removed and pores were formed during sintering simultaneously. Melting point of Mg is  $650^{\circ}C$  as shown in Figure 2.35 and evaporation (boiling) of Mg occurs at  $1090^{\circ}C$  according to the same figure. Sintering temperature was  $1200^{\circ}C$  and sintering time was 4h. All the sintering and Mg removal experiments were carried out under flowing high purity argon atmosphere. Argon flow rate was kept at a minimum adequate inside the vertical furnace to avoid possible leakage of air into the furnace and prevent oxidation during heating, sintering and cooling steps.

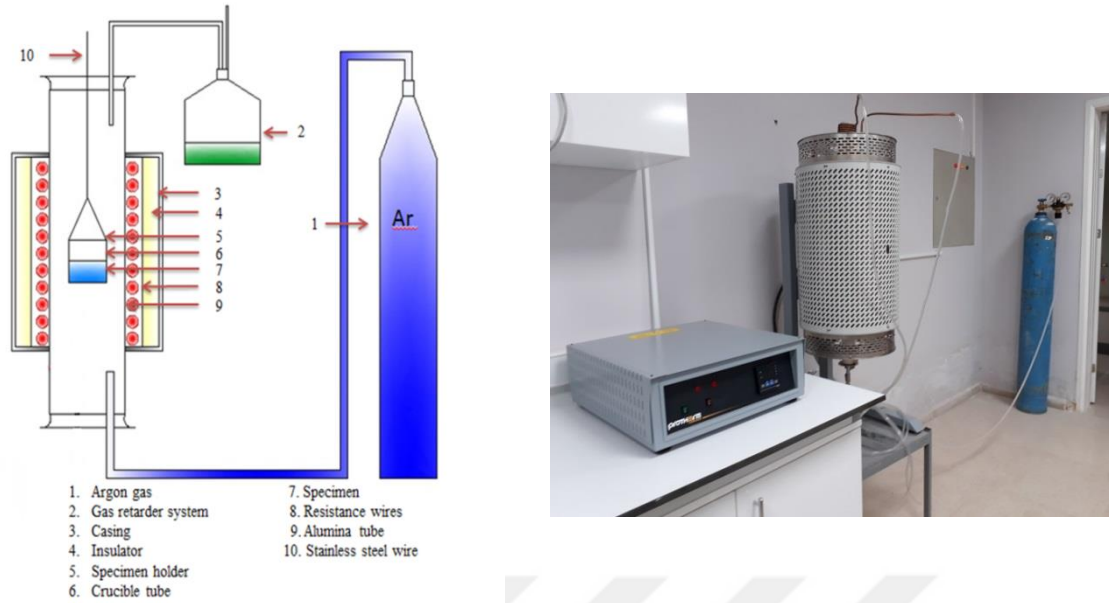


Figure 3.11. Schematic drawing and picture of the vertical furnace and its equipment's.



Figure 3.12.  $\text{Ti}_{74}\text{Nb}_{26}$  porous sample with 40% porosity cooled in the hot zone of the furnace after having been sintered for 4h at  $1200^{\circ}\text{C}$ .

Sintered porous  $\text{Ti}_{74}\text{Nb}_{26}$  samples were slowly cooled inside the hot zone of the vertical furnace. Cooling from  $1200^{\circ}\text{C}$  to  $150^{\circ}\text{C}$  lasted around 8 hours. Pure Ti getters were used to minimize oxidation during sintering. Nevertheless, some oxidation on the surface of the samples Figure 3.12 occurred, because the argon gas used was not stoichiometric. Heating, holding and cooling steps during hot pressing and sintering experiments are presented in Figure 3.13. Heating rate for hot pressing was  $10^{\circ}\text{C}/\text{min}$  and for sintering it was  $8^{\circ}\text{C}/\text{min}$ .

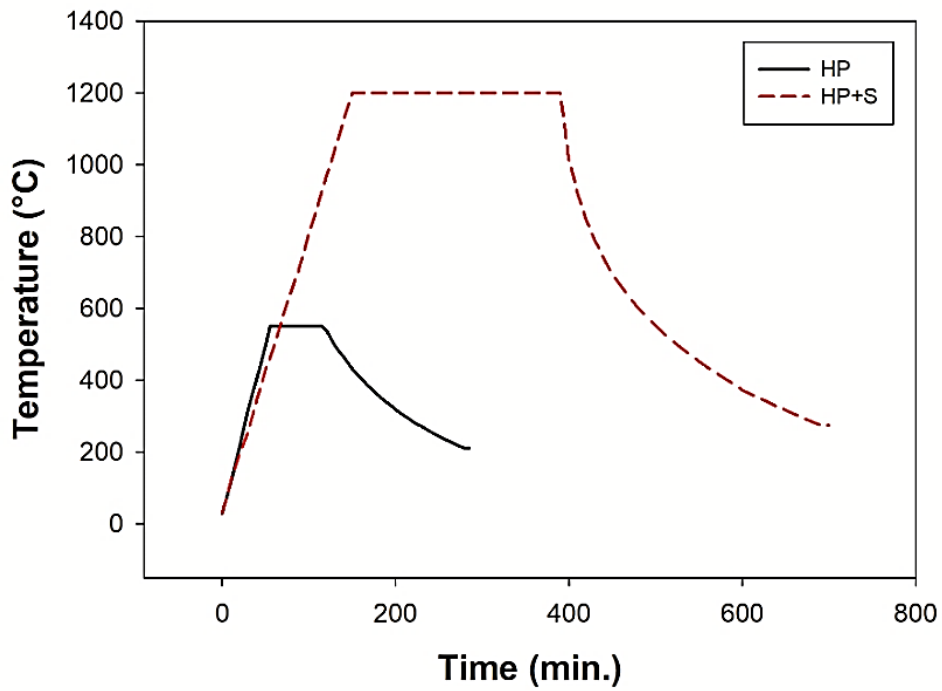


Figure 3.13. Temperature-time curves for hot pressing (HP) and sintering (HP+S).

To prevent oxidation inside the porous samples pure titanium sponges with diameter around 3mm, were used as getter just above the sample as shown in Figure 3.14.

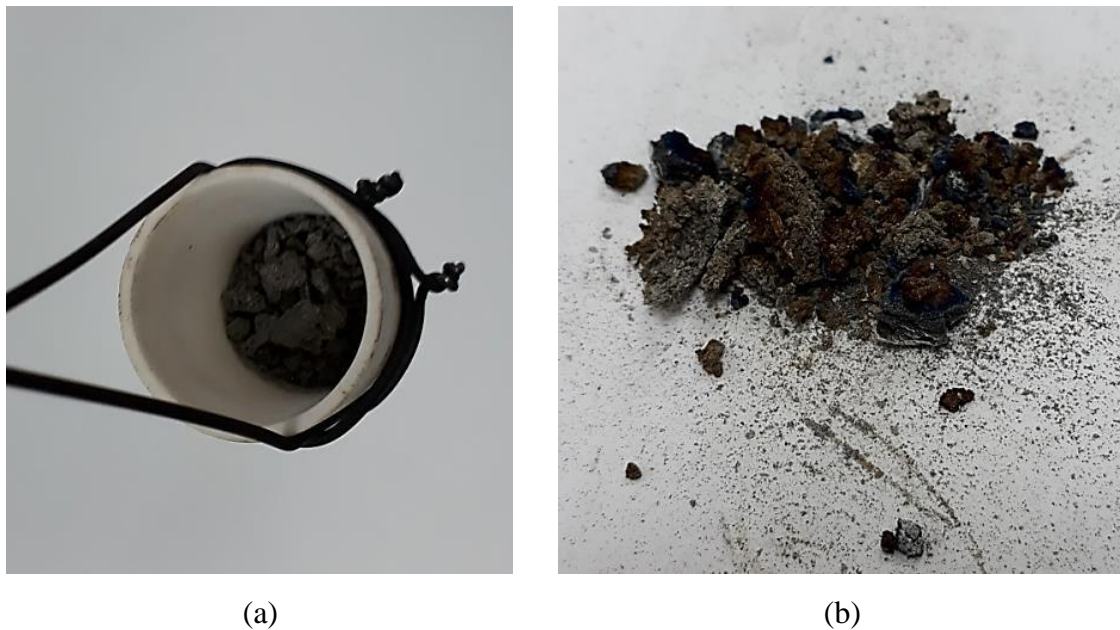


Figure 3.14. Pure Ti sponge particles used as getter during sintering, a) before sintering, b) after 4h sintering at 1200°C.

Wire electrical discharge machining EDM as shown in Figure 3.15 was employed to cut all the porous samples produced in the dimensions of 5x5x10mm as shown in Figure 3.16.



Figure 3.15. An electrical discharge machine (EDM)



Figure 3.16.  $Ti_{74}Nb_{26}$  with 68% porosity sample after cutting by wire EDM with 5x5x10mm in dimension.



For characterization the samples cut were subjected to a number of surfaces cleaning processing by using both grinding and polishing. The cleaning processes are as follows:

- 240, 320, 400, 600, 800, 1000 and 1200 grit SiC papers in disk form were used for grinding samples and ethanol used during grinding to clean the surface of the grit SiC papers.
- Samples were washed and cleaned by ethanol after grinding then dried by a drier.
- Polishing cloth pad in disk form as shown in Figure 3.17 was used with polycrystalline diamond suspension (3 micron) for polishing the surface of porous samples after grinding.
- After polishing residues coming from polishing cloth pad filled the inside of the pores, for removing polishing cloth pad residues ultrasonic cleaning was used as shown in Figure 3.18 for 3 minutes.
- After cleaning samples were washed by ethanol and dried with the drier.



Figure 3.17. Polishing cloth pad (disk form).

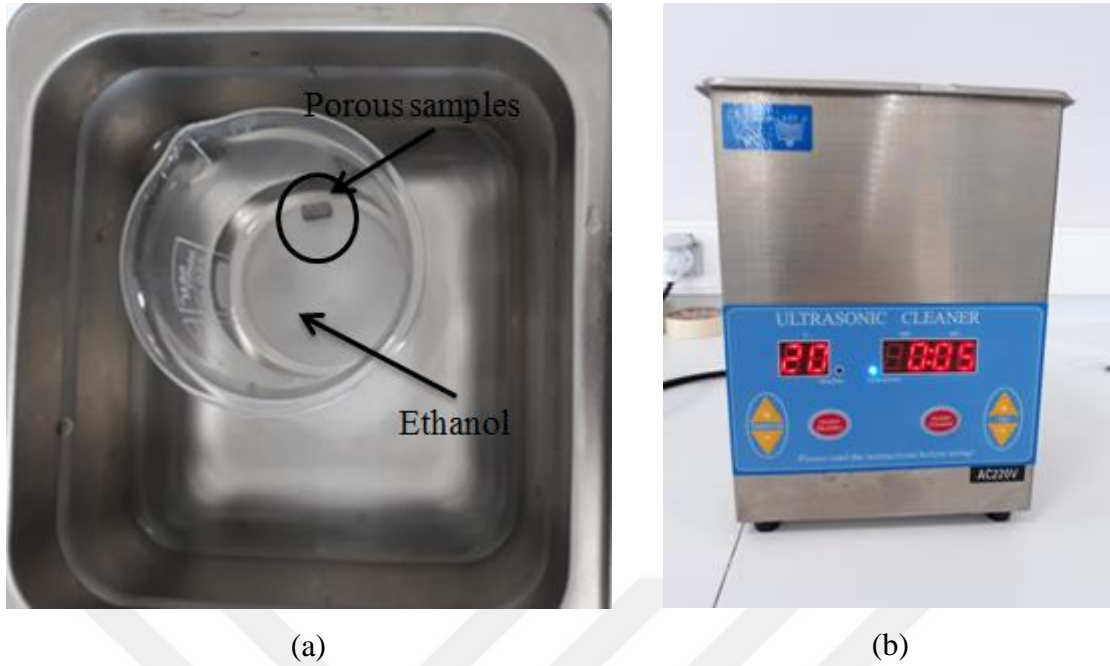


Figure 3.18. Cleaning samples by ultrasonic cleaner a) sample inside ethanol b) ultrasonic cleaning machine.

### 3.4. Sample Characterization

#### 3.4.1. SEM

Scanning Electron Microscopy (SEM) was used to scan and analysis the surface of the samples, the process like that first electrons are produced at the top of the column, to hit the surface of the sample electrons accelerated down and passed through a combination of lenses and apertures to produce a focused beam of electrons. SEM contains a chamber and the sample is fixed on a stage in the chamber area. In order to characterize the internal structure, both macro and micro pores and morphology of the powders and samples produced at the beginning, SEM analyzes were carried out with a Zeiss brand Sigma 300 model device in Eastern Anatolian High Technology Application and Research Center, Erzurum as shown in Figure 3.19.

After installing  $Ti_{74}Nb_{26}$  porous samples inside the vacuum chamber as shown in Figure 3.20 the electron beam hits the samples, two types of electrons reflected one of them is secondary electrons (SE) and the other one is backscattered electrons (BS). For the first type energy of electrons from the electron beam absorbed by the atoms and the secondary electrons come from those atoms. After reflecting the detector picks up those

electrons to show the property of the sample surfaces. For the backscattered electrons reflected electrons came from deeper inside the sample as shown in Figure 3.21.



Figure 3.19. Scanning electron microscopy.

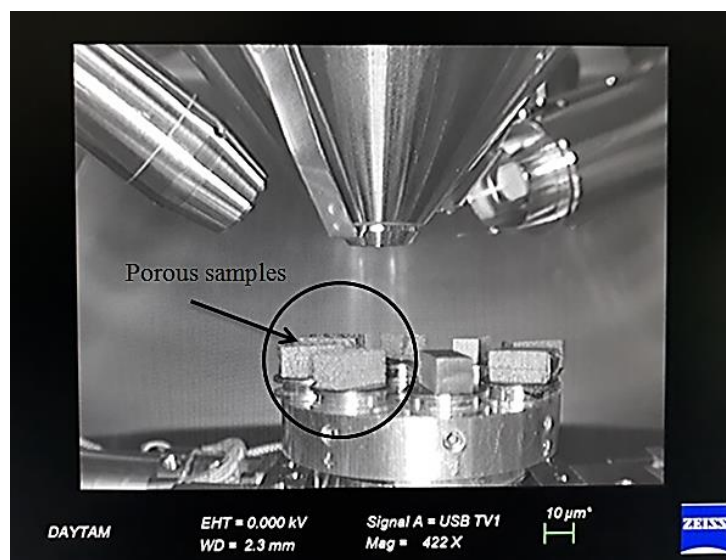


Figure 3.20.  $\text{Ti}_{74}\text{Nb}_{26}$  porous samples inside vacuum chamber.



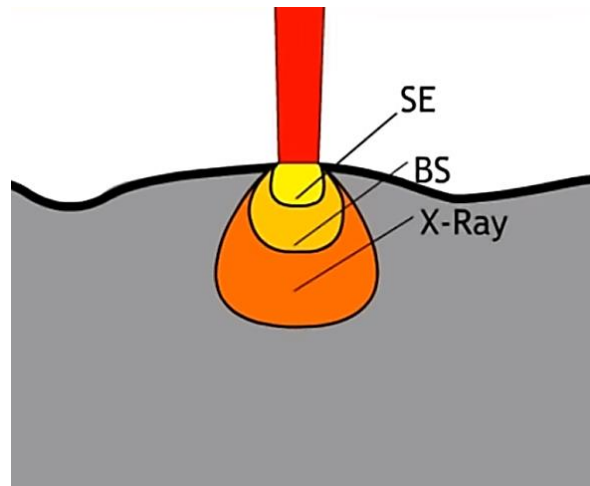


Figure 3.21. Types of reflected electrons according to surface of the sample.

### 3.4.2. XRD

XRD technique was used to analyze the microstructure of the samples, it have a form of electromagnetic radiation when electrons have high energies and short wavelengths. When a beam of x-rays impacts on a sample, a portion of this electron beam that comes from the source will be scattered in all directions by the electrons associated with each atom or ion that lies within the beam's path. A PANalytical Empyrean model X-ray diffractometer with  $\text{CuK}\alpha$  radiation ( $\lambda=1.540598 \text{ \AA}$ ) at 45 kV, 40 mA was used within a range of diffraction angles  $2\theta$  from  $20^\circ$  to  $90^\circ$  at a scan speed of 2 degree/min to identify the phases present in the starting pure powders and in the porous samples produced.

### 3.4.3. Density and porosity measurements

Density is the most important factor that has influence on the mechanical properties. It affects the elastic modulus, compressive strength and yield strength as well as ductility of the porous metals. Archimedes' principle was employed to measure the density of the porous samples, Precisa balance (model LS 220A) equipped with a density determination kit was used as shown in Figure 3.22.

The sample preparation procedure for density and porosity measurements is explained below:

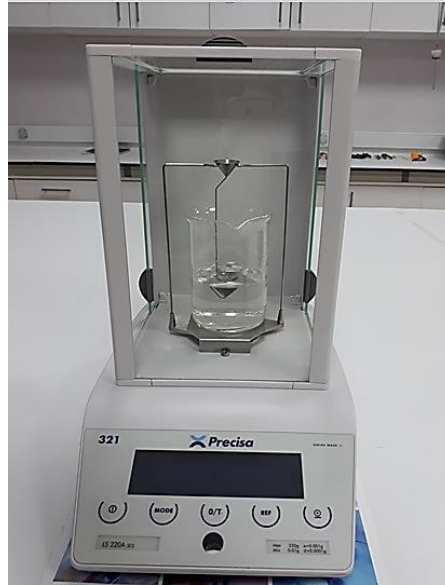


Figure 3.22. Precisa balance (model LS 220A) equipped with a density determination kit.

- Each sample was ultrasonically cleaned further for 3min in ethanol to remove any residue left from polishing as shown in Figure 3.18.
- The wet samples were dried inside glasses by using an electrical oven. 40°C for 1h was used to dry wet samples as shown in Figure 3.23.
- Samples were left at room temperature inside a glass for 24h to assure drying of pores completely as shown in Figure 3.24.
- Firstly, samples were weighted dry ( $W_{dry}$ ) and the weight of each samples are shown in Table 3.2.  $W_{dry}$  for each sample



(a)



(b)

Figure 3.23. a) drying oven b) samples inside drying oven.

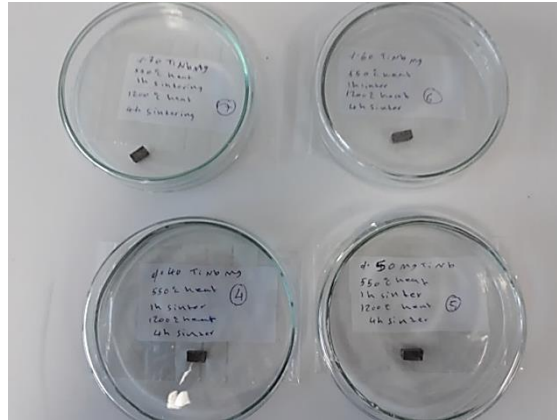


Figure 3.24. Samples left at room temperature for 24h.

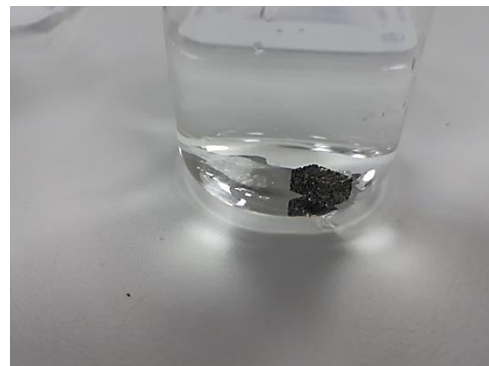
Table 3.2.  $W_{dry}$  for each sample

$Ti_{74}Nb_{26}$ with %porosity	$W_{dry}$ (g)
43% porosity	0.8048
54% porosity	0.5911
59% porosity	0.4998
68% porosity	0.3744

- Then the samples were immersed in purified water for 3 days to get complete impregnation of water into both macro and micro open pores as shown in Figure 3.25 (a). On the surface of the samples during impregnation bubbles formation occurred, that means there were air inside the pores and formed the bubbles as clearly seen in Figure 3.25 (b).



(a)



(b)

Figure 3.25 a) samples impregnated inside pure water b) bubbles on the surface of the porous sample.

- Afterwards impregnated samples suspended in purified water were weighted ( $W_{\text{susp.}}$ ) and the weight of each sample is shown in Table 3.3.

Table 3.3.  $W_{\text{susp.}}$  for each sample

Ti <sub>74</sub> Nb <sub>26</sub> with %porosity	$W_{\text{susp.}}$ (g)
43% porosity	0.6267
54% porosity	0.4687
59% porosity	0.3975
68%porosity	0.2985

- Finally, samples were removed from the purified water bath, wiped immediately to remove the purified water over the surface and the last weight measurement was carried out in air ( $W_{\text{sat.}}$ ) and the weights of each sample are shown in Table 3.4.  $W_{\text{sat.}}$  for each sample

Table 3.4.  $W_{\text{sat.}}$  for each sample

Ti <sub>74</sub> Nb <sub>26</sub> with %porosity	$W_{\text{sat.}}$ (g)
43% porosity	0.8772
54% porosity	0.6983
59% porosity	0.6176
68%porosity	0.5057

- Bulk density of the porous samples was calculated as,

$$\rho_{\text{porous}} = \frac{W_{\text{dry}} * \rho_{\text{purified water}}}{W_{\text{sat.}} - W_{\text{susp.}}} \quad (3.1)$$

where

$\rho_{\text{bulk}}$  : Bulk density of the sample.

$W_{\text{dry}}$  : Dry weight of the sample.

$\rho_{\text{purified water}}$ : Density of purified water, 0.998205 g/cm<sup>3</sup>.

$W_{\text{sat.}}$  : Weight of the sample saturated with purified water.

$W_{\text{susp}}$  : Weight of the purified water impregnated sample suspended in purified water.

Total porosity of the samples was calculated as,

$$P_{\text{total}} = 1 - \frac{\rho_{\text{porous}}}{\rho_{\text{TiNb}}} \quad (3.2)$$

where

$P_{\text{total}}$  : Total porosity of the sample.

$\rho_{\text{TiNb}}$  : Theoretical density of  $\text{Ti}_{74}\text{Nb}_{26}$  alloy:  $5.578 \text{ g/cm}^3$ .

To calculate open porosity ( $P_{\text{open}}$ ) and closed porosity ( $P_{\text{closed}}$ ) of the samples the equations (3.3) and (3.4) were used, respectively, where  $V_{\text{sample}}$  represents volume of the sample.

$$P_{\text{open}} = \frac{\text{volume of water in pores}}{V_{\text{sample}}} = \frac{\frac{W_{\text{sat}} - W_{\text{dry}}}{\rho_{\text{purified water}}}}{\frac{W_{\text{sat}} - W_{\text{susp}}}{\rho_{\text{purified water}}}} = \frac{W_{\text{sat}} - W_{\text{dry}}}{W_{\text{sat}} - W_{\text{susp}}} \quad (3.3)$$

$$P_{\text{closed}} = P_{\text{total}} - P_{\text{open}} \quad (3.4)$$

#### 3.4.4. Compression behavior

To obtain the mechanical properties of brittle nonmetallic, porous metals and other materials that have very low strength in tension compression test is used. Compression tests were carried out on porous samples produced with space-holder method. In the present study the compression test samples had a shape of rectangular prism with dimensions of  $5 \times 5 \times 10 \text{ mm}$ . Only one porous sample of the same type (40%, 50%, 60% and 70% porous in volume) was taken for each test. The samples were loaded continuously to failure at room temperature. The Young's modulus was calculated from the linear part of the stress-strain curve in the elastic region according to:

$$E = \frac{\sigma}{\varepsilon} = \frac{\frac{F}{A_0}}{\frac{\Delta L}{L_0}} \quad (3.5)$$

Where

$\sigma$  : stress.

$\varepsilon$  : strain.

F : compression force.

$A_0$ : initial cross sectional area of the sample.

$L_0$  : initial length.

$\Delta L$ : length change of the sample during compression.

Yield strength was determined applying 0.2% offset method whereas compression strength was the maximum stress observed during compression test. As a measure of ductility, the strains at which the samples fractured (fracture strains) were used.

## 4. RESULTS AND DISCUSSION

### 4.1. Density and Porosity

According to the previous researches to allow bone ingrowth inside the porous structures the optimal size of pores should be around 100-600 $\mu\text{m}$  (Aydoğmuş, 2010). With increasing open porosity ratio to the total porosity, the interconnectivity between macro-pores also increases. When the amount of porosity in the sample is equal to 68% or more nearly all the pores inside the porous sample are interconnected.

Increasing the amount of porosities causes reduction in the thickness of the cell walls, in other words when the amount of porosity increases the density of samples decrease.

Equation 3.1 was used to calculate bulk density of porous samples and the results are shown in Table 4.1. Figure 4.1 shows the relation between density and the porosity. Density and porosity are inversely proportional to each other. When the density increases the porosity decreases or vice versa.

Table 4.1. Bulk density of each sample

Ti <sub>74</sub> Nb <sub>26</sub> alloy	Bulk density (g/cm <sup>3</sup> )
43% porosity	3.2070
54% porosity	2.5698
59% porosity	2.2667
68%porosity	1.8037

To calculate the percentage of closed pores inside the samples firstly we must find total porosity and open porosity of each sample by using equation (3.2) and (3.3) as shown in Table 4.2. Finally closed porosity can be calculated by using equation 3.4 as shown in Table 4.3 and Figure 4.2 shows how increase in the rate of porosity percent decreases the rate of closed pores. Macro-pores formed as a result of Mg vaporization and these pores are the desired pores. These pores are suitable for bone ingrowth and body fluid transportations. Micro-pores formed due to insufficient sintering are not

desired in the microstructure since they affect mechanical properties negatively. Although their sizes are suitable for body fluid transportation, bone cannot grow inside the micro-pores due to their small size.

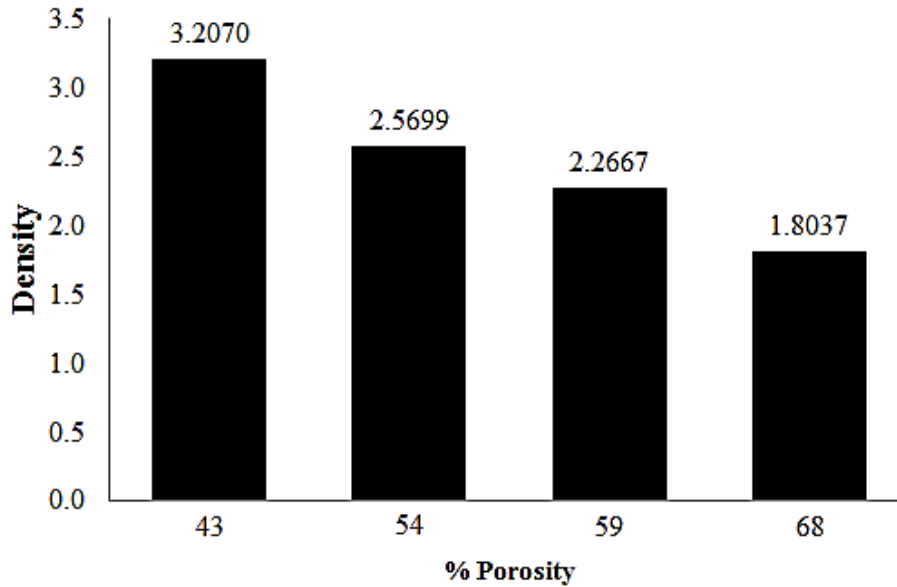


Figure 4.1. Relation between density and porosity.

Table 4.2. Percentages of both total porosity and open porosity as a function of Mg addition

Mg added	%Total porosity (Ptotal)	%Open porosity (Popen)
40%	42.5061	28.9021
50%	53.9287	46.6898
60%	59.3633	53.5211
70%	67.6639	63.3687

Table 4.3. Percent of closed porosity

Ti <sub>74</sub> Nb <sub>26</sub> sample	%Closed porosity (Pclosed)
43% porosity	13.6039
54% porosity	7.2388
59% porosity	5.8422
68% porosity	4.2951

40 and 50% Mg addition resulted in 43 and 54% total porosity respectively. 60 and 70% Mg addition gave final porosities of 59 and 68%. For lower Mg additions total



porosities were higher than the Mg added initially. Because in addition to macro-pores micro-pores also formed and these micro-pores increased the total porosity. On the other hand, higher Mg additions resulted in porosities lower than the Mg added. During heating for sintering melting of Mg at 650°C occurred and some pores were collapsed as a result of insufficient sintering of Ti and Nb powders during prior hot pressing process. Pore shrinkage during sintering may be another reason for lower porosity.

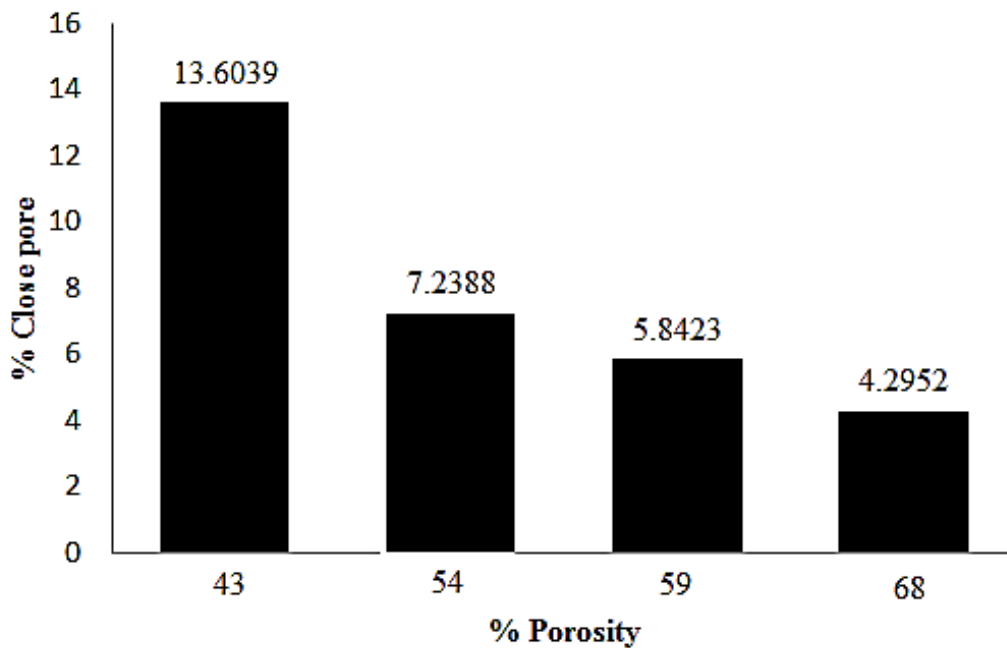


Figure 4.2. Closed porosity total porosity relation.

#### 4.2. Microstructure of Porous $\text{Ti}_{74}\text{Nb}_{26}$ Alloys

XRD patterns of as-sintered (1200°C, 4h) porous  $\text{Ti}_{74}\text{Nb}_{26}$  alloys are shown in Figure 4.3 to Figure 4.6. As it can be seen from these figures a little amount of  $\alpha$  phase remained in all the samples with varying porosity, but no contamination products such as oxides, carbides, and Mg/MgO were detected. XRD results were in good agreement with SEM results. Since amount of pure Nb undissolved was very low XRD could not detect it.

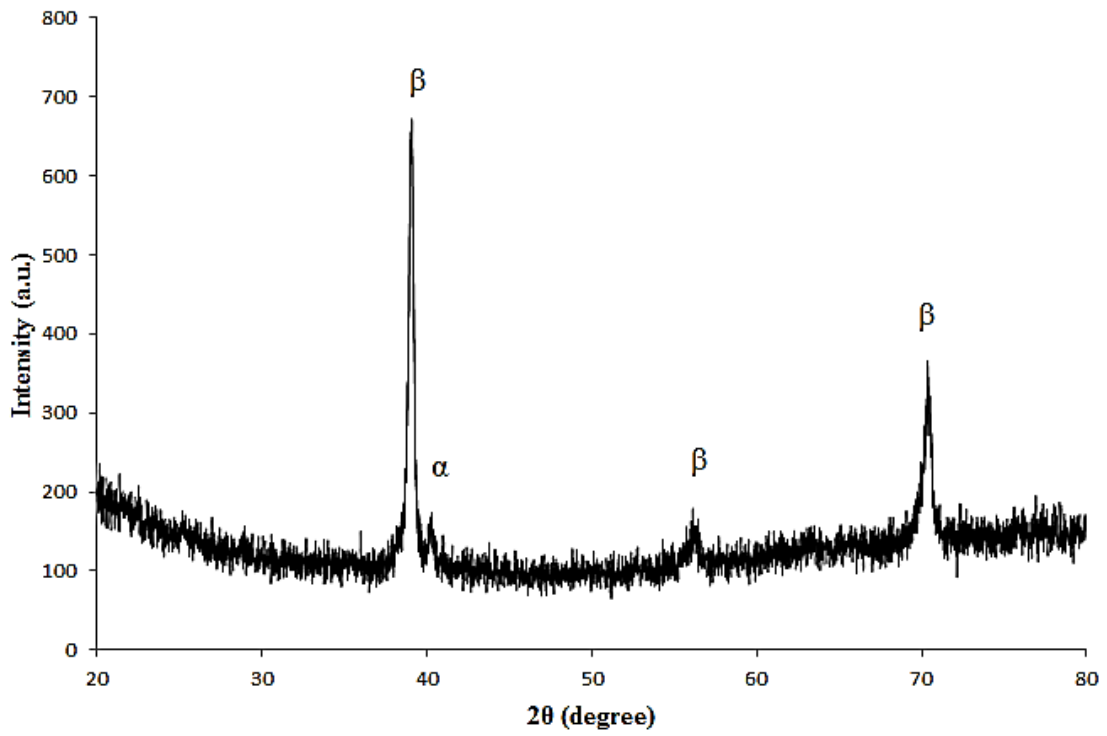


Figure 4.3. XRD spectra of sintered porous  $\text{Ti}_{74}\text{Nb}_{26}$  with 43% porosity.

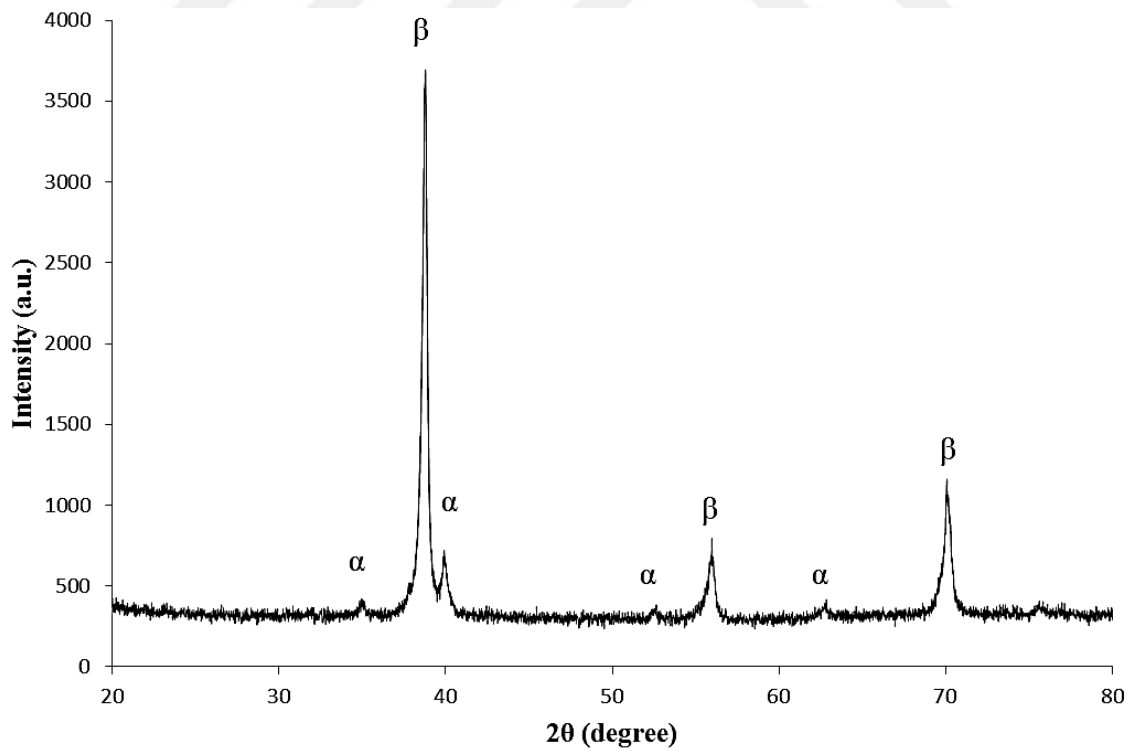


Figure 4.4. XRD spectra of sintered porous  $\text{Ti}_{74}\text{Nb}_{26}$  alloy with 54% porosity.

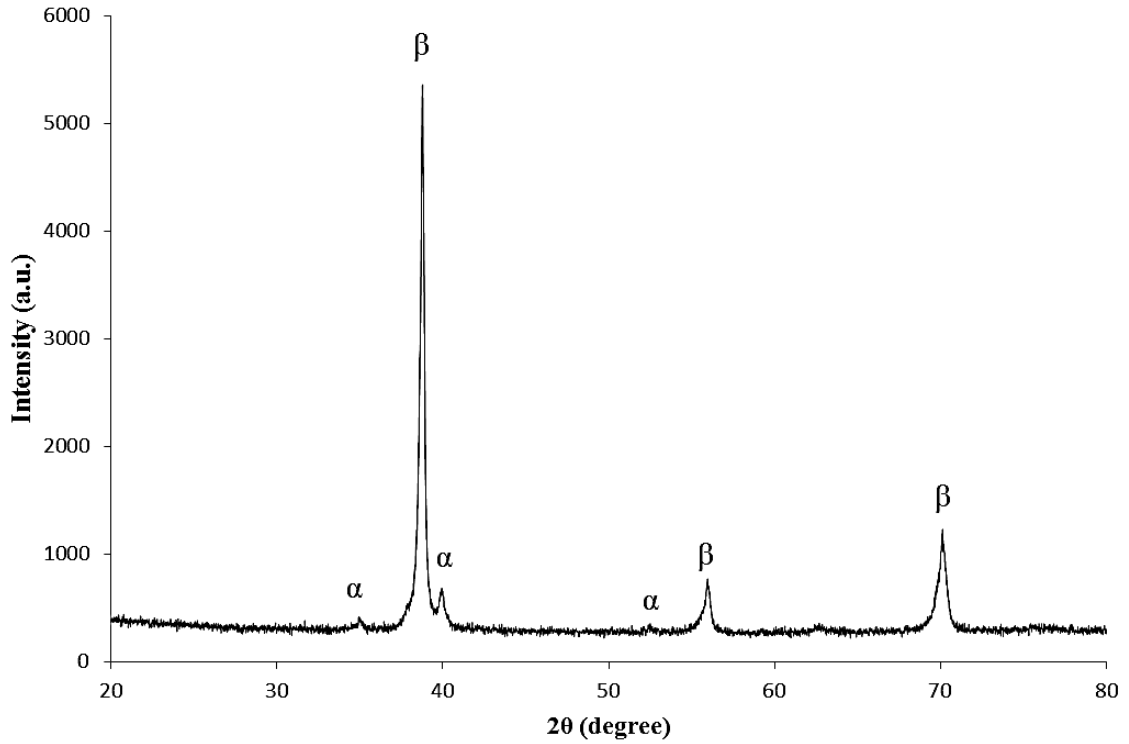


Figure 4.5. XRD spectra of sintered porous  $Ti_{74}Nb_{26}$  with 59% porosity content.

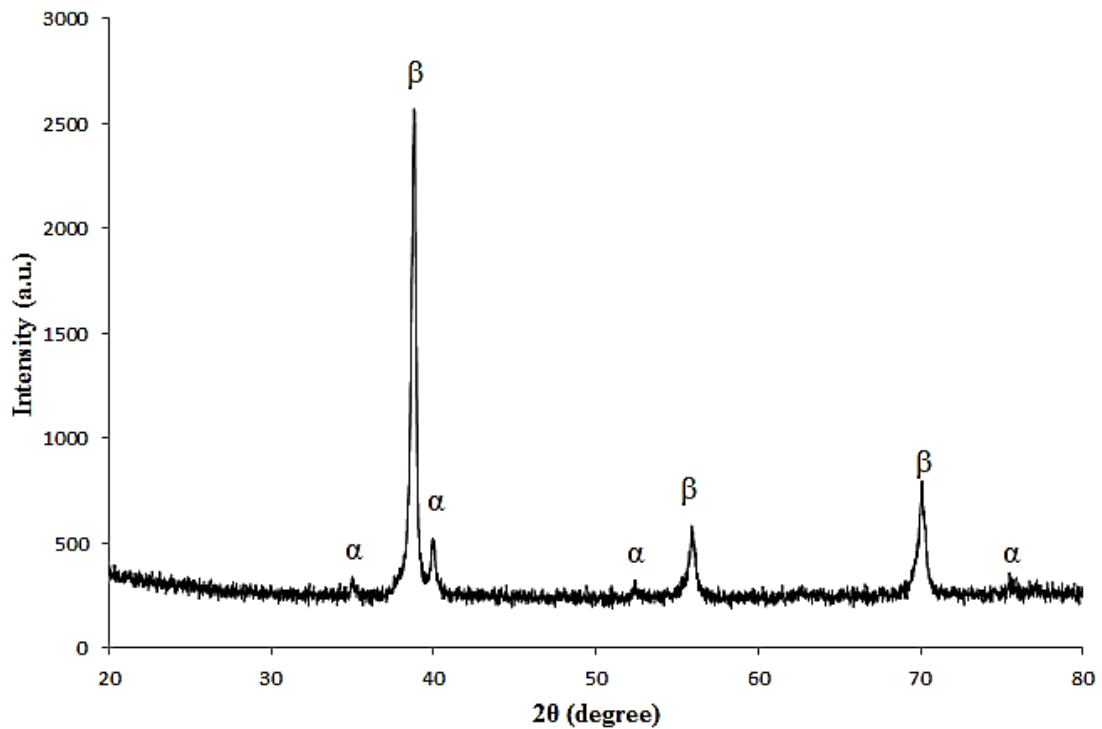


Figure 4.6. XRD spectra of sintered porous  $Ti_{74}Nb_{26}$  alloy with 68% porosity ratio.

The morphological characteristics of the porous samples were examined with the scanning electron microscope (SEM). The microstructures of porous  $\text{Ti}_{74}\text{Nb}_{26}$  alloys with different porosity contents are presented in Figure 4.7 to Figure 4.10. Two types of pores have been observed in all the samples, macro-pores and micro-pores. Macro-pores formed due to evaporation of space holder Mg powders and their size was similar to the particle size of starting Mg powders. Micro-pores with generally a few  $\mu\text{m}$  (up to  $20\mu\text{m}$ ) in size on the other hand, formed as a result of insufficient hot pressing temperature and inadequate sintering. Hot pressing temperature was chosen as  $600^\circ\text{C}$  since the melting temperature of Mg is  $650^\circ\text{C}$ . That temperature was not enough to eliminate all the micro-pores present between elemental Ti and Nb powders. Preliminary experiments showed that hot pressing of Ti and Nb powder mixture at  $600^\circ\text{C}$  for 1h resulted in 18% porosity. Increasing the hot pressing temperature to  $800^\circ\text{C}$  decreased the porosity ratio to 0.8% and almost full density was achieved. As a consequence, the minimum temperature for an efficient hot pressing operation is  $800^\circ\text{C}$  for Ti-Nb alloys. However,  $800^\circ\text{C}$  could not be applied since hot pressing temperature is limited by melting temperature of Mg. The longer hot pressing time would not solve the problem at a low pressing temperature used because melting points of Ti and Nb are extremely high  $1668$  and  $2477^\circ\text{C}$  respectively, since they belong to refractory materials family. Sintering (after hot pressing) at  $1200^\circ\text{C}$  for 4 hours also could not eliminate the micro-pores because diffusion distances were too high as a result of inefficient hot pressing. Sintering temperature applied was also quite low compared to melting temperatures of pure Ti and Nb. The vertical furnace used for sintering has a maximum continuous working temperature of  $1250^\circ\text{C}$  and to be on the safe side  $1200^\circ\text{C}$  was chosen to be sintering temperature. Preliminary experiments resulted that there were not considerable changes for sintering times of 1-4 hours. Sintering is a diffusion phenomenon and depends on time linearly and temperature exponentially. Therefore, longer sintering times would not eliminate the micro-pores probably. Only remaining solution to get rid of or at least to minimize micro-pores seems to be sintering at higher temperatures such as,  $1300$ - $1500^\circ\text{C}$ .

Mg was removed efficiently and any remaining pure Mg or magnesium oxide ( $\text{MgO}$ ) residues inside the macro or micro-pores and on pore walls were not observed.

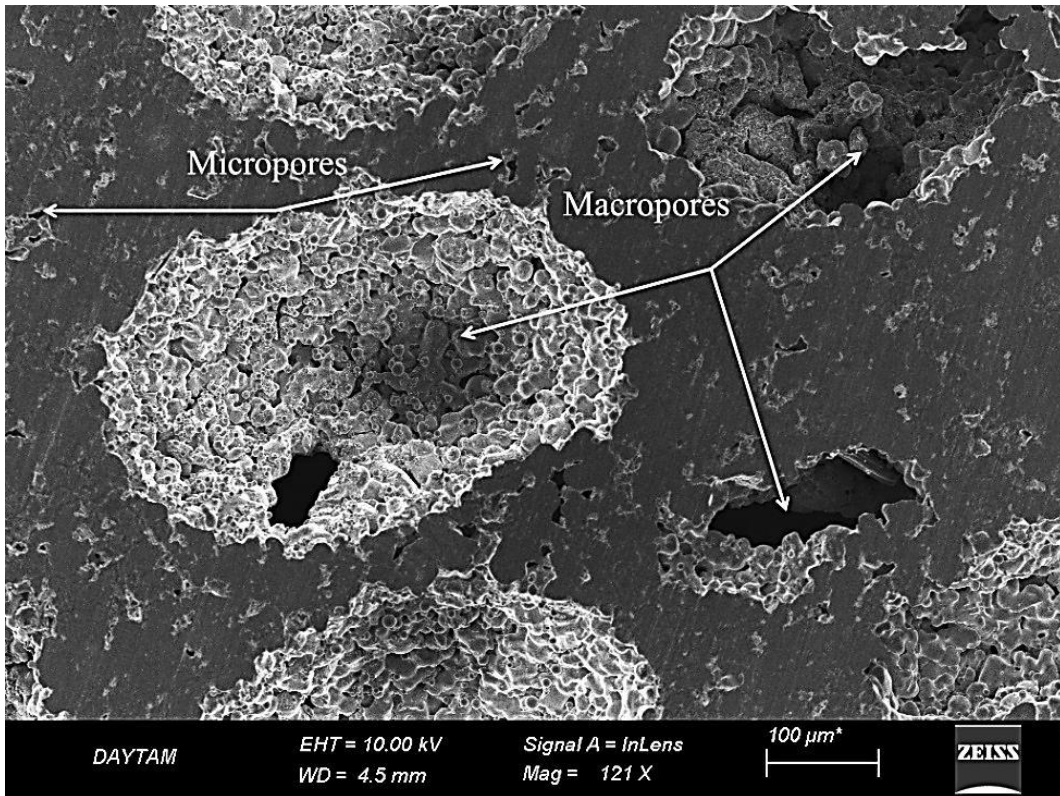


Figure 4.7. SEM micrograph of porous  $Ti_{74}Nb_{26}$  with 43% porosity.

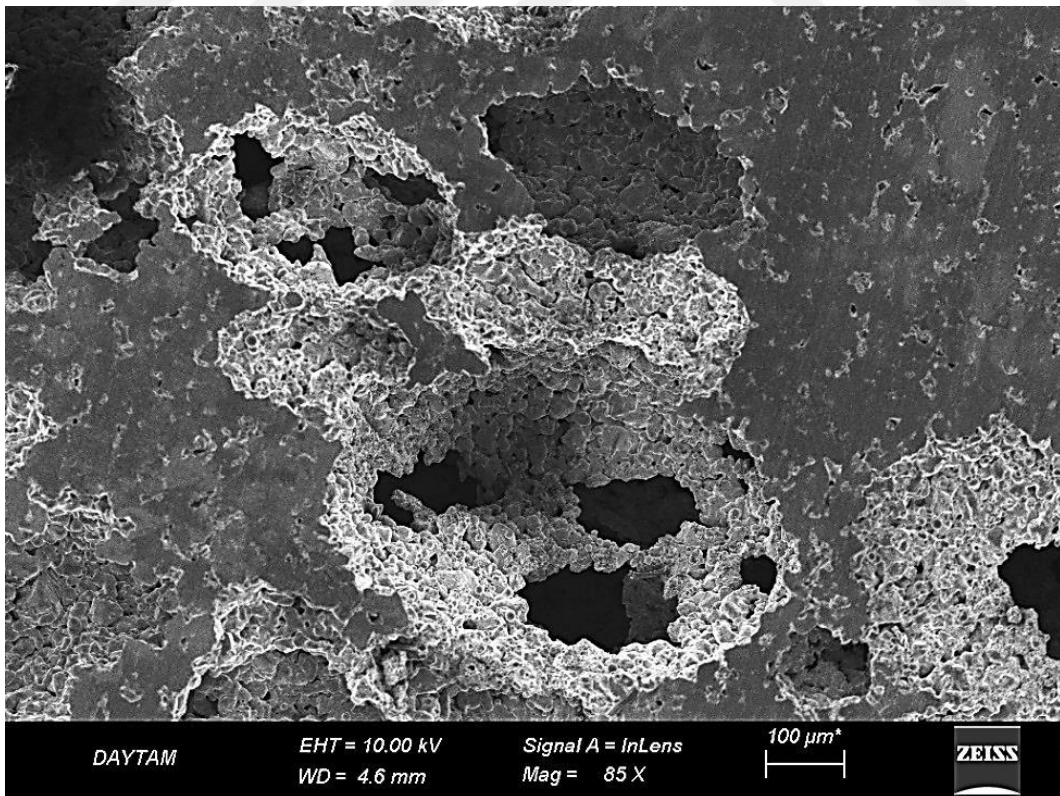


Figure 4.8. SEM micrograph of porous  $Ti_{74}Nb_{26}$  alloy with 54% porosity.

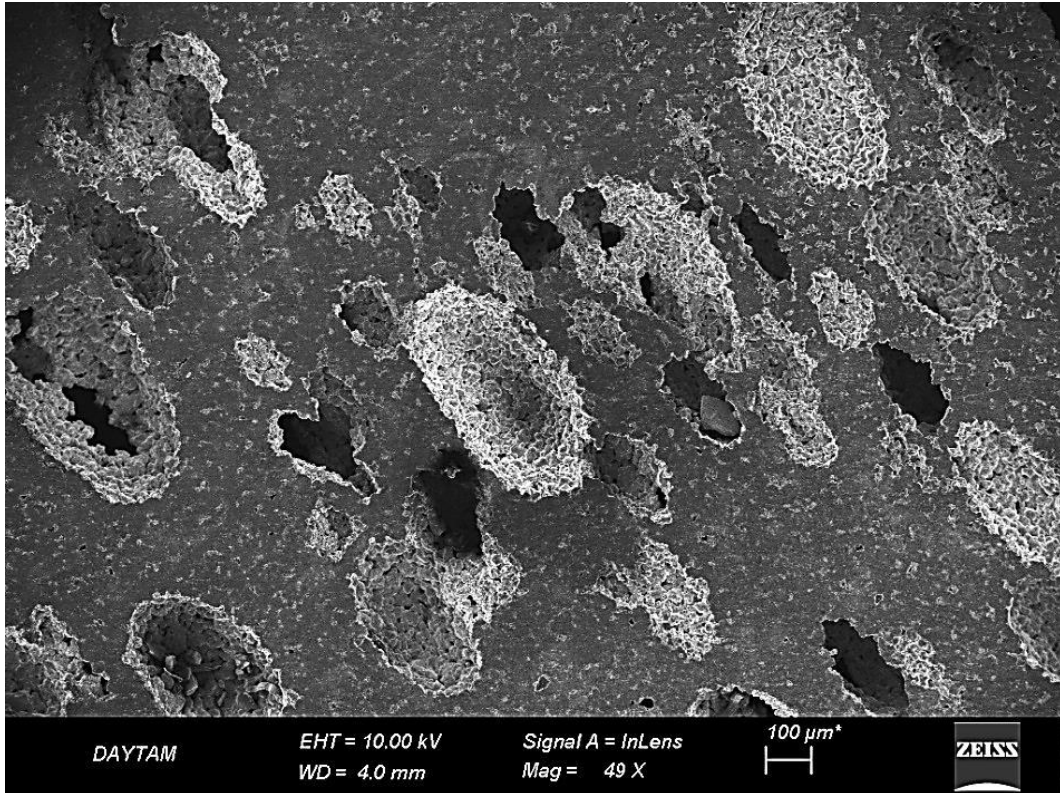


Figure 4.9. SEM image of porous Ti<sub>74</sub>Nb<sub>26</sub> with 59% porosity.

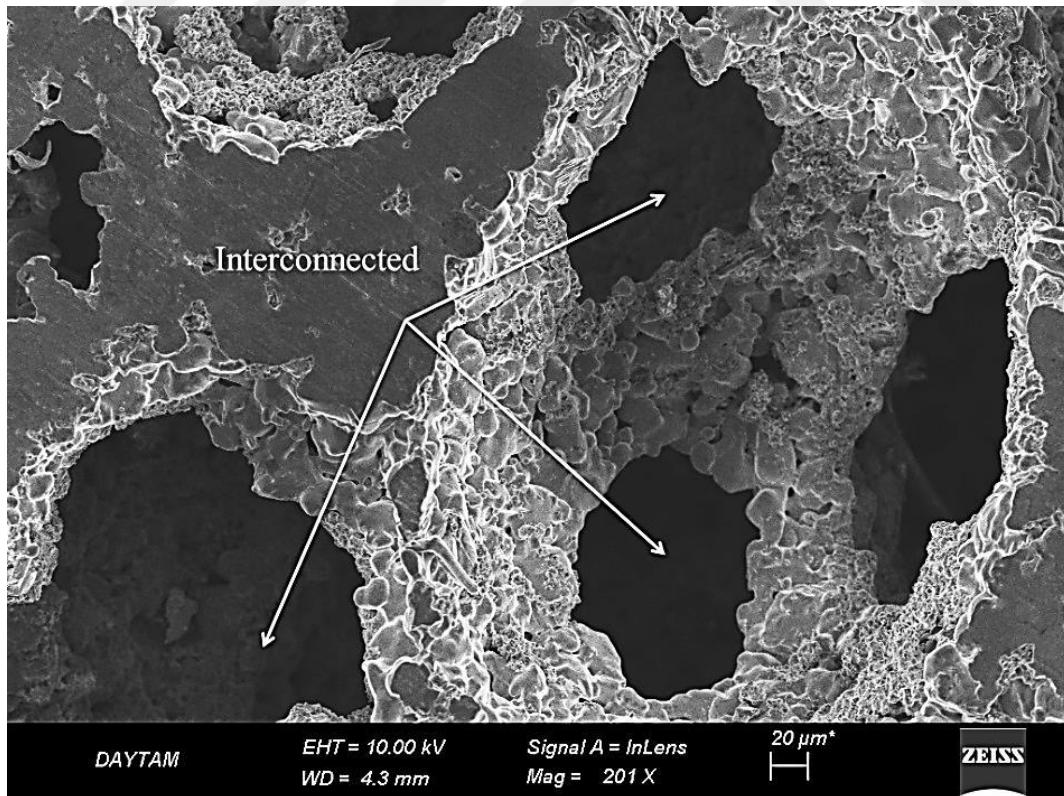


Figure 4.10. SEM micrograph of porous Ti<sub>74</sub>Nb<sub>26</sub> with 68% porosity content.

BSE micrographs of porous  $Ti_{74}Nb_{26}$  alloys are given in Figure 4.11 to Figure 4.14. The micrographs are similar and the microstructures consist of the same phases. In addition to main phase  $\beta$  small amount of  $\alpha$  phase and a little undissolved pure Nb were observed. Unlike  $\alpha$  phase pure Nb was not observed in secondary electron mode. XRD results also did not show any peaks belonging to pure Nb. Only BSE mode could detect the existence of undissolved Nb regions. In order to produce full  $\beta$  phase and provide complete dissolution of Nb in Ti, sintering temperature should be higher than  $1200^{\circ}C$ .

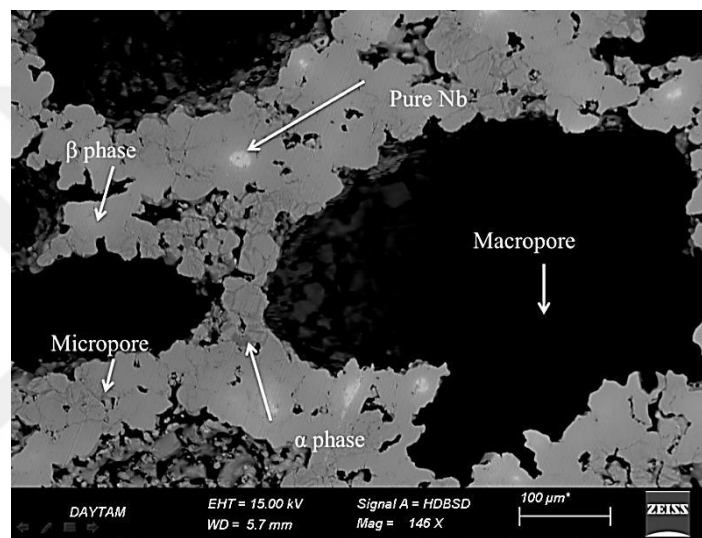


Figure 4.11. BSE micrograph of 43% porous  $Ti_{74}Nb_{26}$ .

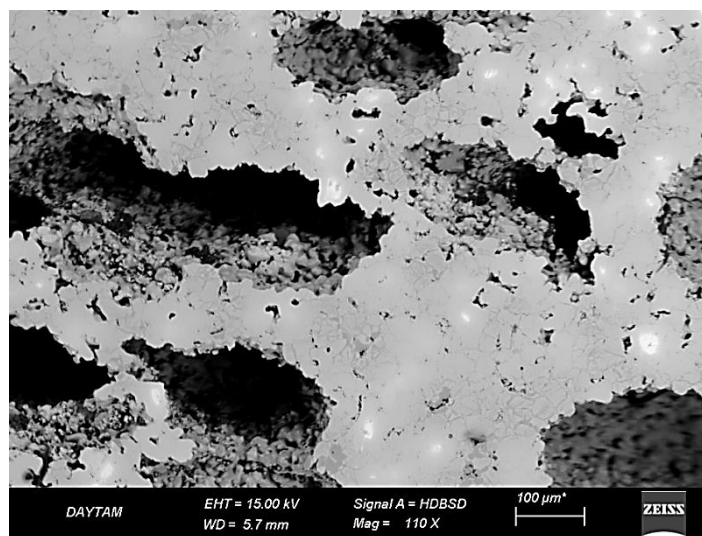


Figure 4.12. BSE micrograph of 54% porous  $Ti_{74}Nb_{26}$ .



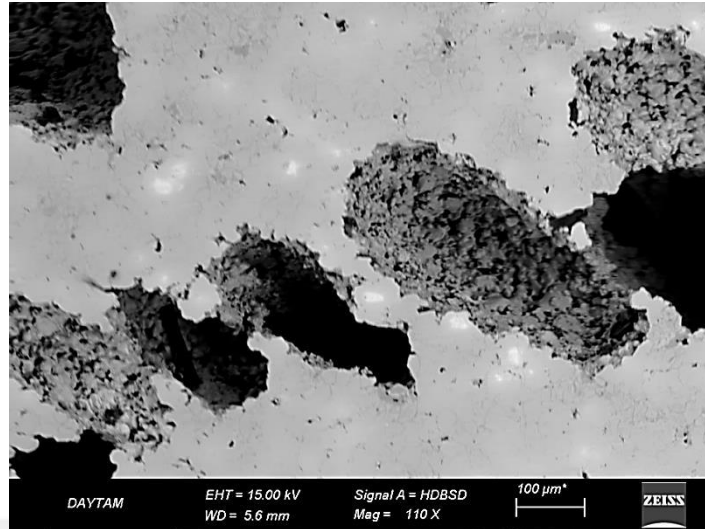


Figure 4.13. BSE micrograph of 59% porous  $Ti_{74}Nb_{26}$ .

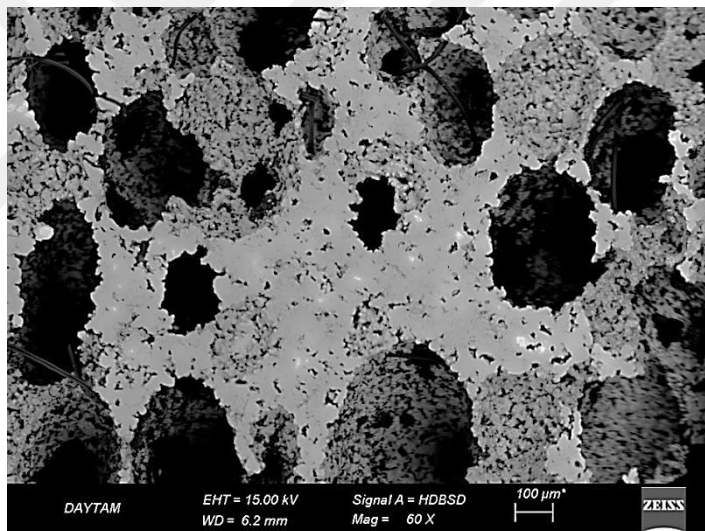
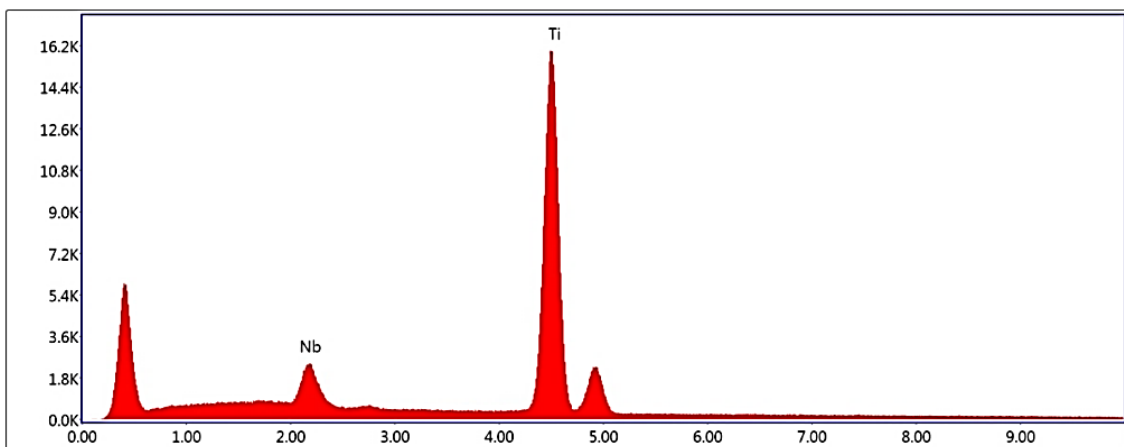
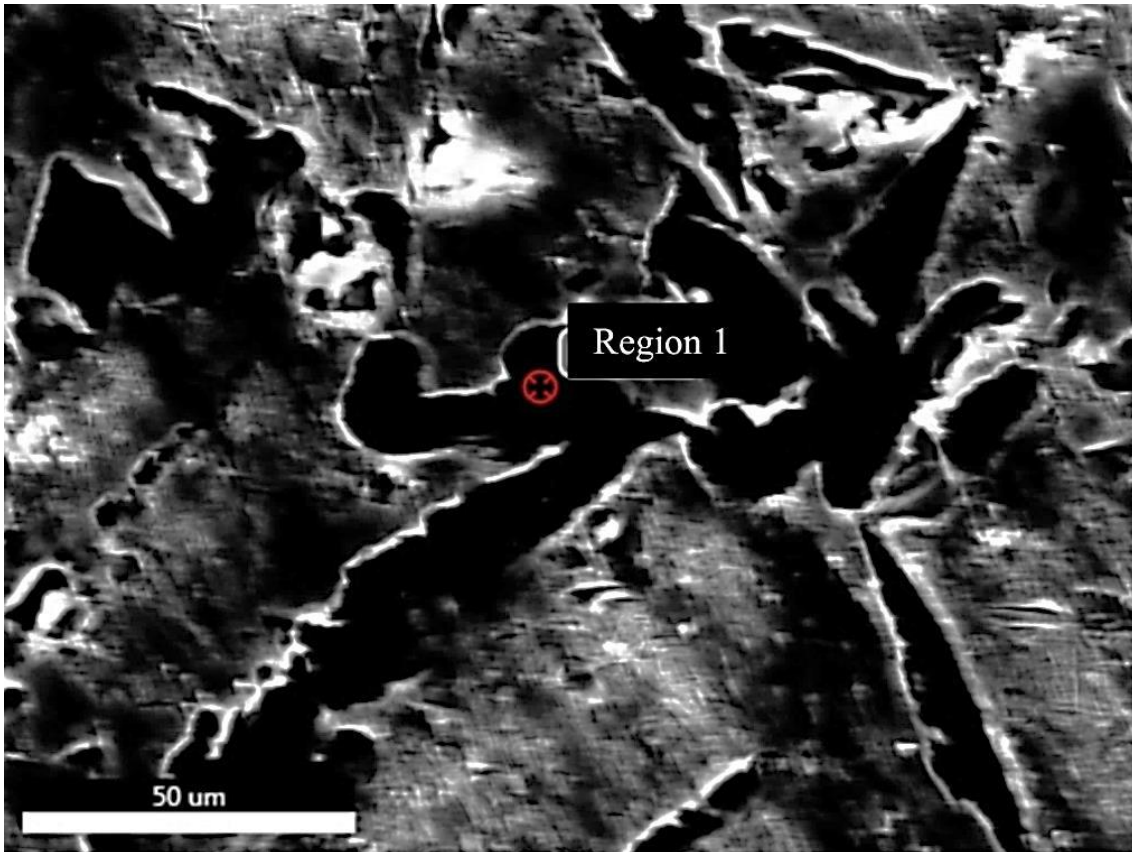


Figure 4.14. BSE micrograph of 68% porous  $Ti_{74}Nb_{26}$ .

EDS point analysis technique was used to determine the phase constituent elements. EDS point analyses taken from four different regions of porous samples are shown in Figure 4.15 to Figure 4.18. The atomic percentage of Ti in the region 1 ( $\alpha$  phase), region 2 ( $\beta$  phase), region 3 ( $\beta$  phase) and region 4 (undissolved pure Nb) was 96.2, 79.1, 70.2 and 0%, respectively. Increasing Nb content provides  $\alpha$  to  $\beta$  phase transformation since Nb is a  $\beta$  stabilizing element. As expected  $\alpha$  phase includes less amount of Nb (3.8%), on the other hand Nb amount of  $\beta$  phase was 20.9 and 29.8% for



region 2 and region 3, respectively. Nb content of  $\beta$  phase should be 26% in terms of atomic percentage for complete dissolution and homogeneous distribution of Nb. Region 4 belongs to pure undissolved Nb (100%). All these results state that, sintering temperature of 1200°C was insufficient to obtain single homogeneous  $\beta$  phase.



Lsec: 49.3 0 Cnts 0.000 keV Det: Element-C2 Det

Figure 4.15. EDS analysis result for region 1 ( $\alpha$  phase), Ti% (atomic) = 96.2 and Nb% (atomic) = 3.8.

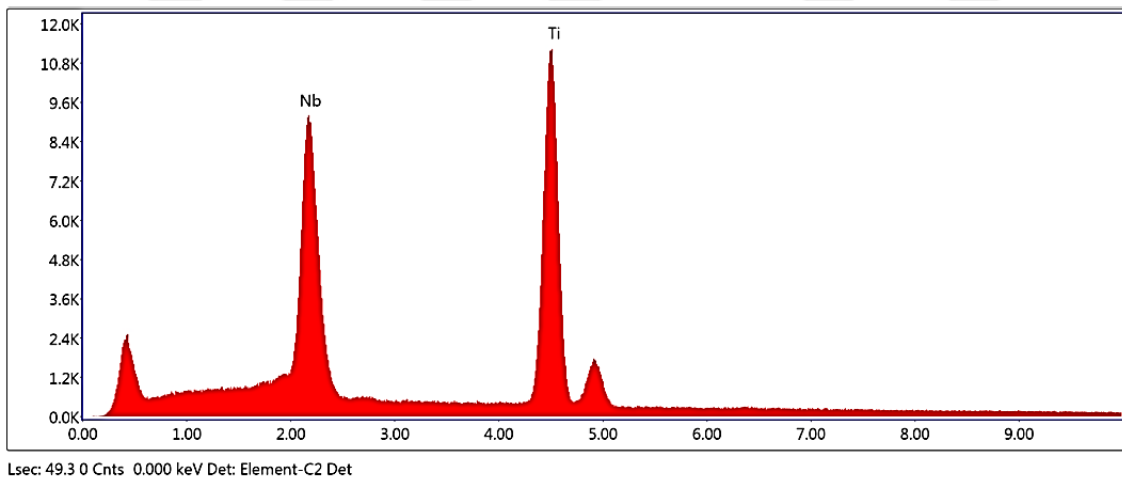
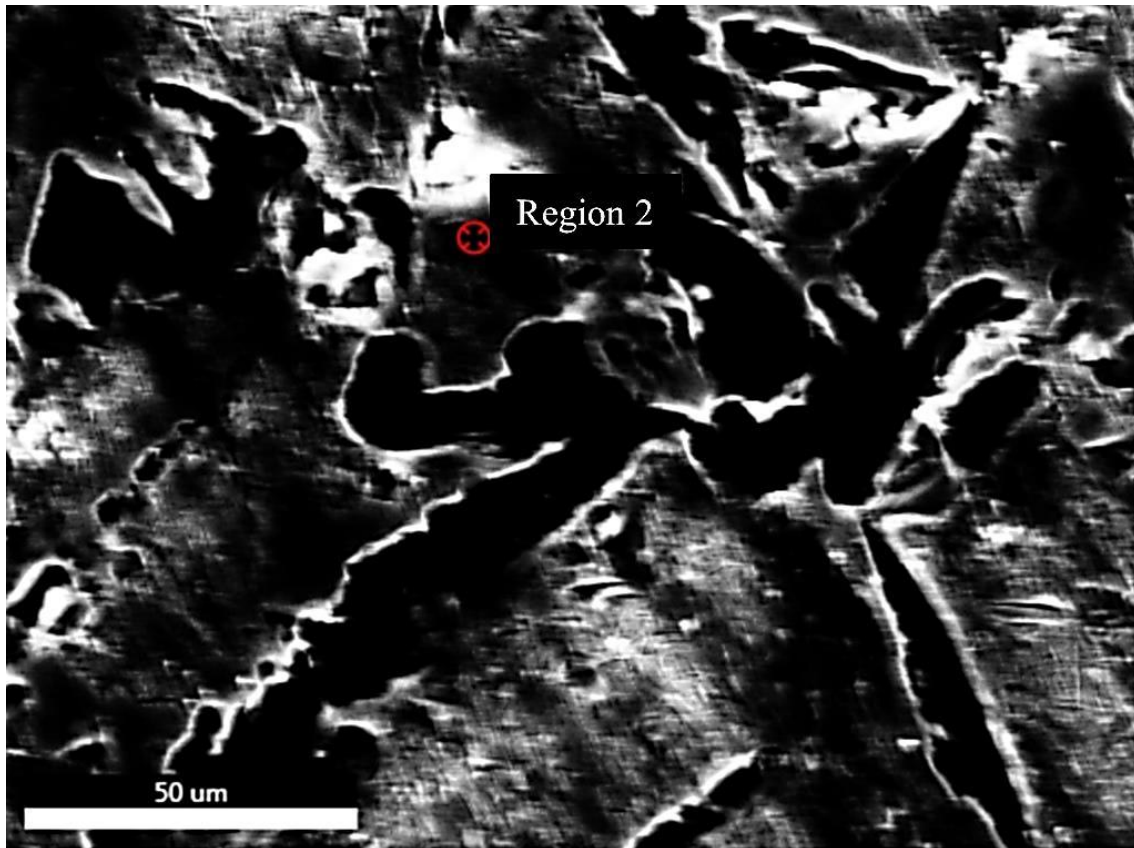


Figure 4.16. EDS micrograph for region 2, Ti% = 79.1 and Nb% = 20.9.

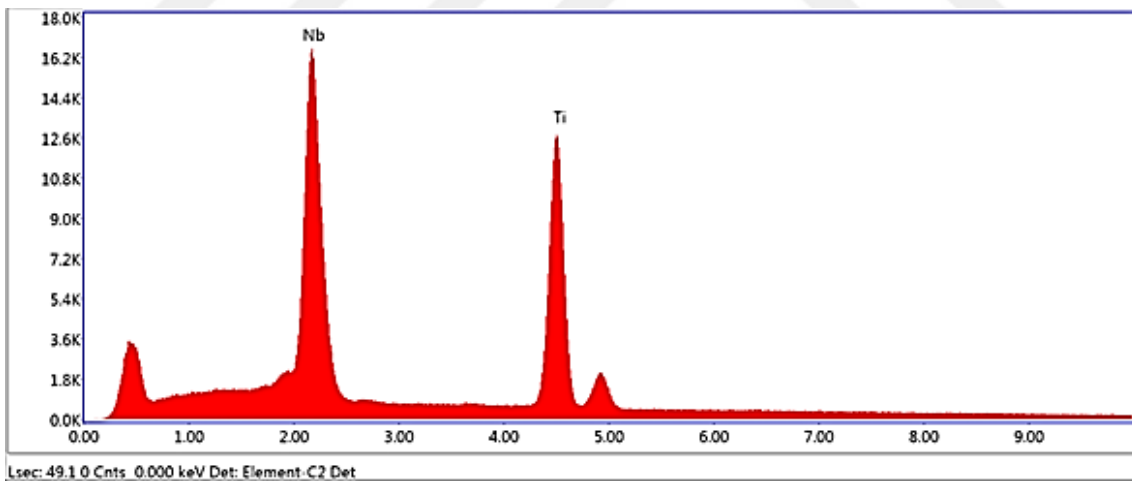
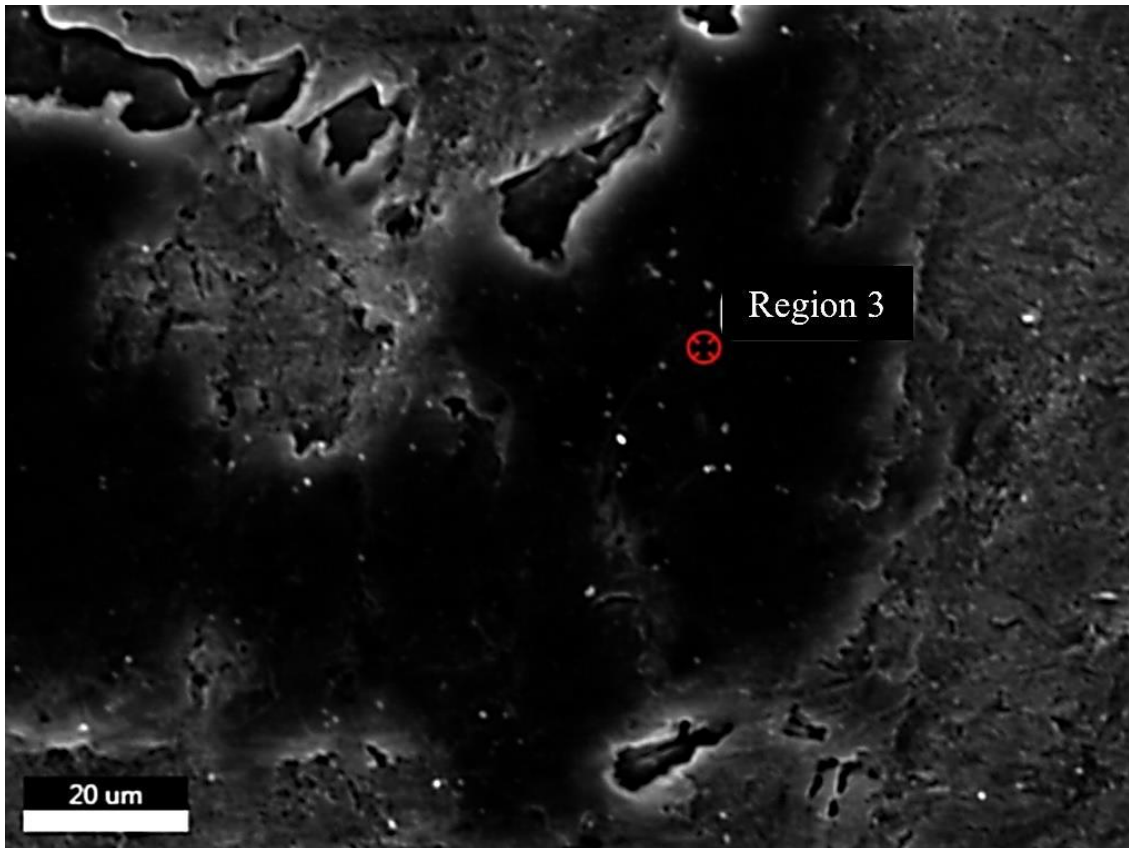


Figure 4.17. EDS micrograph for region 3, Ti% = 70.2 and Nb% = 29.8.

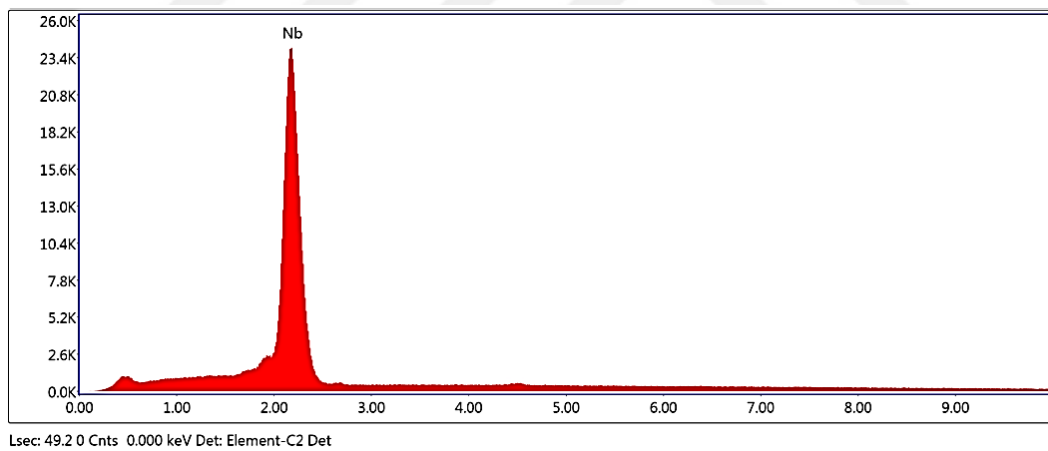
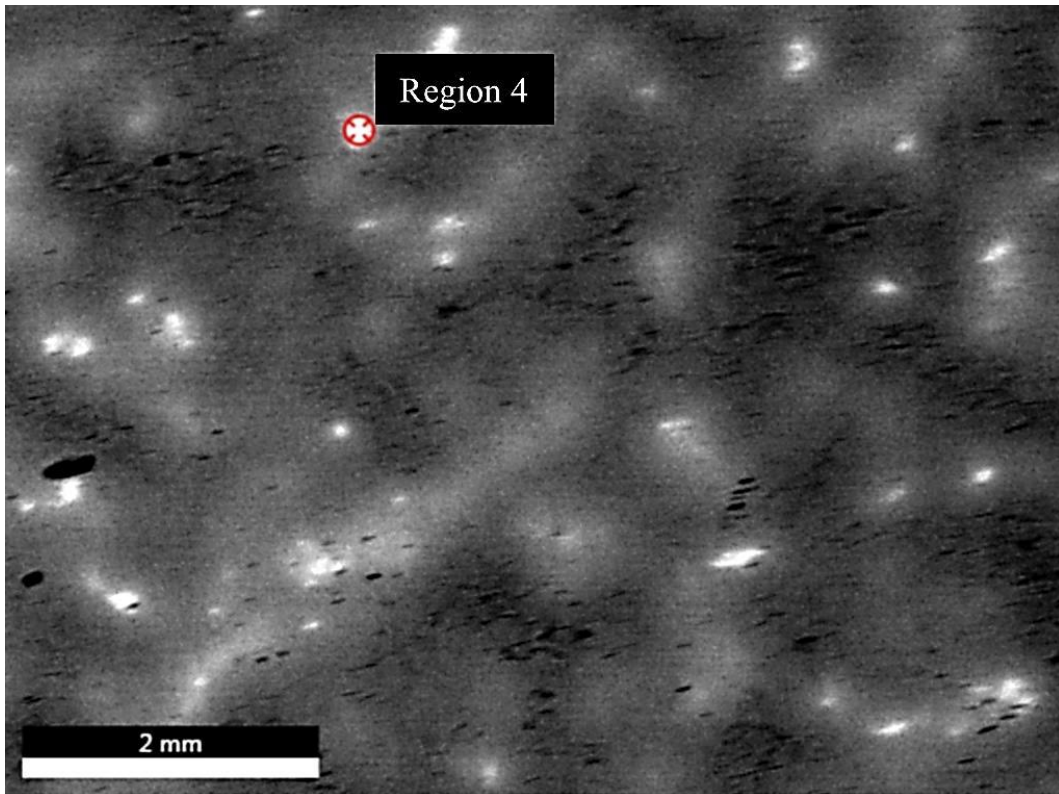


Figure 4.18. EDS micrograph for region 4, Ti% = 0 and Nb% = 100.

### 4.3. Effect of Hot Pressing on Spherical Pore Structure

The effects of hot pressing pressure on final pore shapes are presented in Figure 4.19 (a) to (d). For 43% porous sample shape of pores remains almost spherical. When the amount of Mg added increased from 40% to 70% by volume, the shape of pores changed from spherical to elliptical because the Mg powders were plastically



deformed during hot pressing. In 40% volume Mg containing sample the amount of both Ti and Nb is higher compared to 50, 60 and 70% Mg added samples. The strengths of Ti and Nb is higher than that of Mg so that the larger the Ti and Nb content, the more resistance to plastic deformation. In other words, Ti and Nb minimize plastic deformation of Mg just like in the composites. When their amount is less and Mg amount is high Ti and Nb cannot prevent plastic deformation of soft Mg powders.

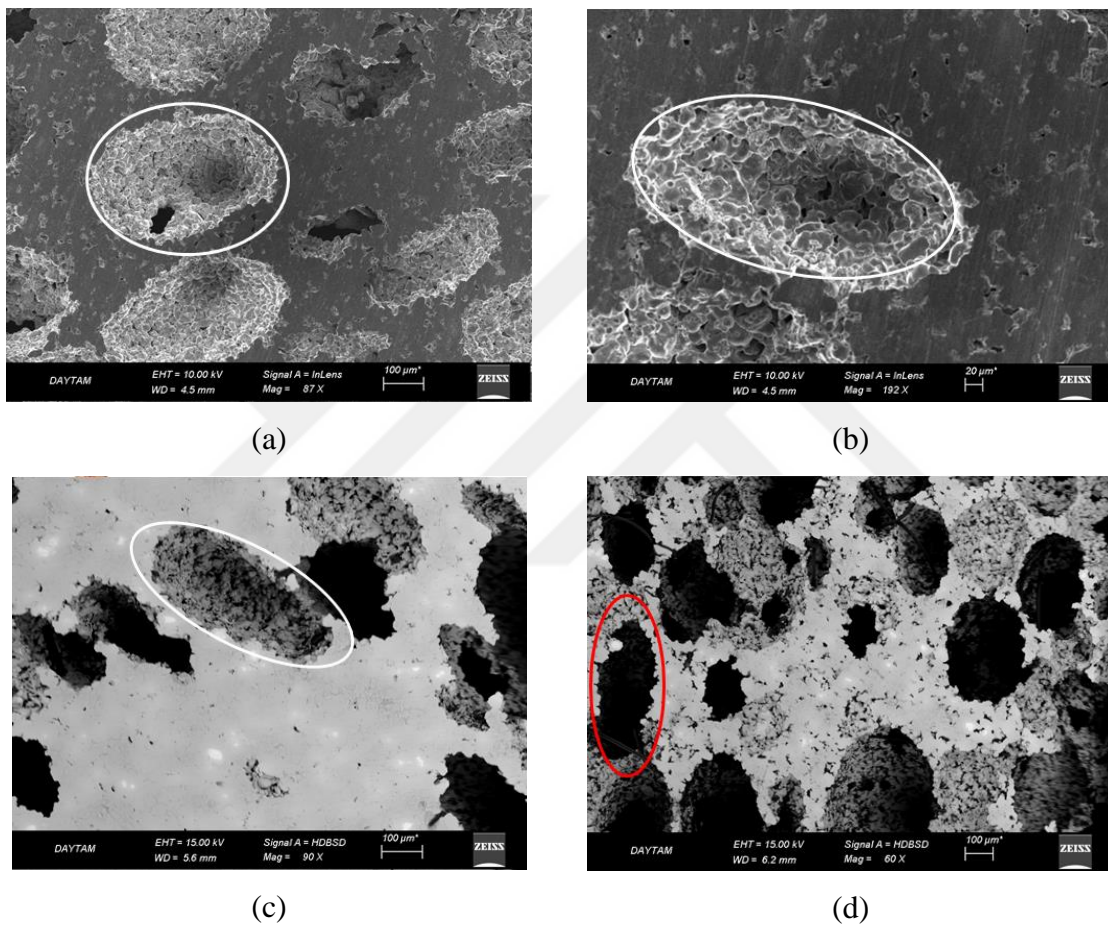


Figure 4.19. Effect of hot pressing on pore structure resulting from yielding of Mg powders for, a) 43%, b) 54%, c) 59%, and d) 68% porous samples.

#### 4.4. Mechanical Behavior of Porous $Ti_{74}Nb_{26}$

##### 4.4.1. Compression behavior

Figure 4.20 shows the compressive stress-strain curves of porous  $Ti_{74}Nb_{26}$  with various porosity contents and sintered at the same temperature and time. Generally,

according to Gibson and Ashby suggestion the typical elastic-plastic metallic foams display a linear elastic deformation stage followed by a horizontal plateau stage and finally a densification stage. But it's clear that, in the present study compressive stress-strain curves of porous  $Ti_{74}Nb_{26}$  produced by (SHT) differ from that proposed by Gibson and Ashby. Plastic collapse or buckling of the pores occur due to open cells pores those have a well-defined plateau stress because the cell edges and walls yield in bending. Plastic collapse occurs, when the moment exerted on the cell walls exceeds the fully plastic moment creating plastic hinges. On another hand, closed cell pores exhibit more complicated behavior which can cause the stress to rise with increasing strain because the cell faces are exposed to tensile stresses. According to the Figure 4.20 and 4.21 (a) in the present study, the horizontal plateau stage has been observed for highly porous (54% and more) specimens. The horizontal plateau region on the other hand has not been observed for 43% porous sample. Instead, a yielding region with linearly increasing stress is ended by a maximum stress and followed by the collapse of the pore structure has been observed. 54% porous sample also fractured however, 59% sample did not fracture up to 55% strain applied. The third stage that corresponding to densification was not observed for 59 and 68% porous samples because the compression experiments were not continued up to very high strains.

Table 4.4 shows the mechanical properties of the porous  $Ti_{74}Nb_{26}$  samples with different porosity obtained from compression tests.  $Ti_{74}Nb_{26}$  porous samples with 43% porosity, 54% porosity and 59% porosity seem to be suitable for cancellous bone replacement applications even with the somewhat higher elastic moduli. Because the elastic modulus, yield strength and the compressive strength of the cancellous bone are reported to be  $1\pm 0.8$  GPa,  $15\pm 8$  MPa and  $25\pm 8$  MPa (Ontanon et al., 2000), respectively.  $Ti_{74}Nb_{26}$  porous sample with 68% porosity, do not appear suitable for load bearing biomedical applications due to its insufficient strength. On the other hand, elastic modulus, yield and compression strength of cortical bone are reported to be 12-17 GPa, 105-121 MPa and 156-212 MPa (Ontanon et al., 2000), so that none of the porous  $Ti_{74}Nb_{26}$  alloys meet these requirements. However, if the sintering temperature is increased to around  $1300^{\circ}C$  or more, some of the micro-pores present in the cell walls may be eliminated and strength of porous samples may be improved.

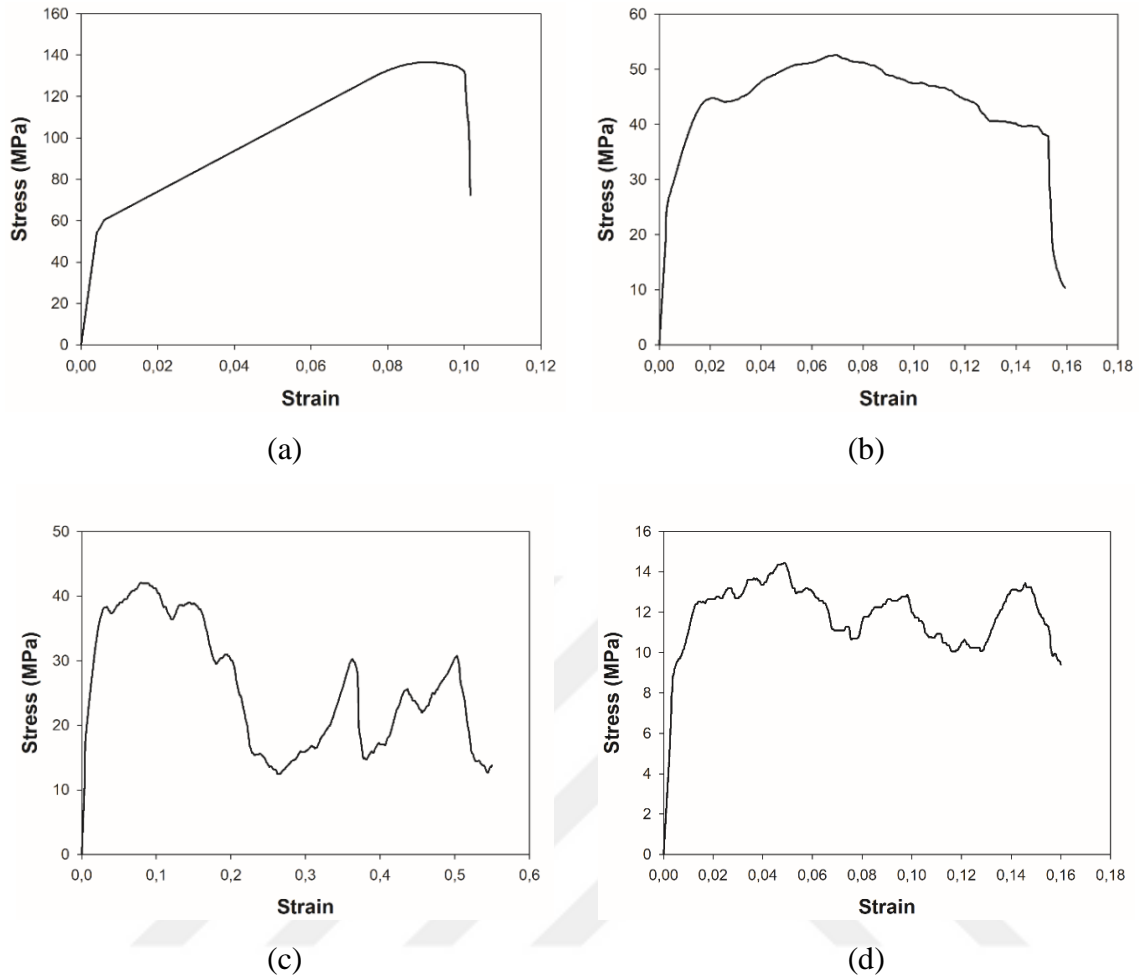


Figure 4.20. Stress-strain curves for porous samples with different amount of porosity, a) 43%, b) 54%, c) 59% and d) 68%.

Powder metallurgy process was used to prepare porous Ti-35Nb (wt.%) samples and 30 (wt.%) ammonium bicarbonate was used as a space holder material (Oliveira et al., 2015). Mixtures were pressed by uniaxial compaction at 400 MPa followed by isostatic compaction at 250 MPa. To remove ammonium bicarbonate the green samples were held at 170 °C for 2h in a chamber furnace in air. Then, the green samples were sintered in a vacuum furnace (better than  $10^{-5}$  Torr) for 2h at 1300 °C then the samples were naturally cooled down to room temperature in the furnace. Mechanical properties for porous samples are shown in Table 4.5. Higher yield strength with lower elastic modulus and lower compression strength can be observed compared to those of 59% porous  $Ti_{74}Nb_{26}$  sample in the present study, in Table 4.4. These differences formed due to different production method and different rate of both micro and macro-pores. Nevertheless, results of the two studies were found to be quite similar.

Table 4.4. Mechanical properties of porous Ti<sub>74</sub>Nb<sub>26</sub> alloys tested in compression

Porosity (%)	Elastic modulus (GPa)	Yield strength (MPa)	Compression strength (MPa)	Fracture strain (%)
43	14.3	61	136	10.1
54	8.2	30	52	15.9
59	5.8	23	42	-
68	1.6	9	14	-
0	44	894	1178	19.9

Table 4.5. Mechanical properties of macroporous Ti-35Nb (wt.%) alloy (Lin et al., 2010)

Porosity (%)	Elastic modulus (GPa)	Yield strength (MPa)	Compression strength (MPa)	Fracture strain (%)
59-63	2.6±0.2	28.95±2.37	33.12±1.63	-

Table 4.6. shows mechanical properties of porous Ti-40Nb (wt.%) alloy prepared by Zhuravleva et al. (2013). NaCl was used as the space holder material. They used conventional cold pressing (700 MPa for 2h) and sintering (1000 °C for 2h) technique. Their elastic modulus and compressive strength results for the 62% porous sample were lower than the results of the sample with 59% porosity in the present study.

Table 4.6. Mechanical properties of macroporous Ti40Nb alloy (Zhuravleva et al., 2013)

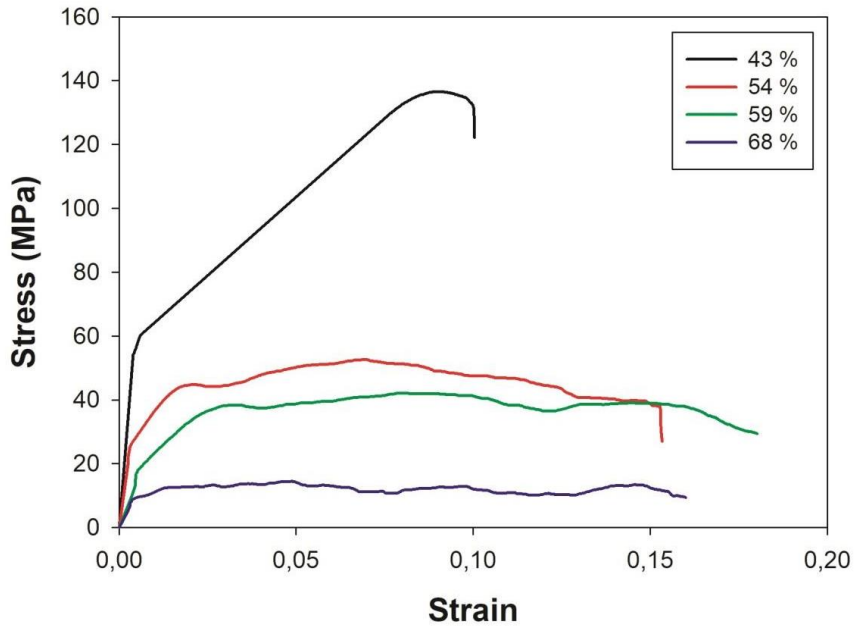
Porosity (%)	Elastic modulus (GPa)	Compression strength (MPa)
62	2.25	34.6
70	2.12	14
80	1.5	9.6

#### 4.4.2. Effect of porosity on the mechanical properties

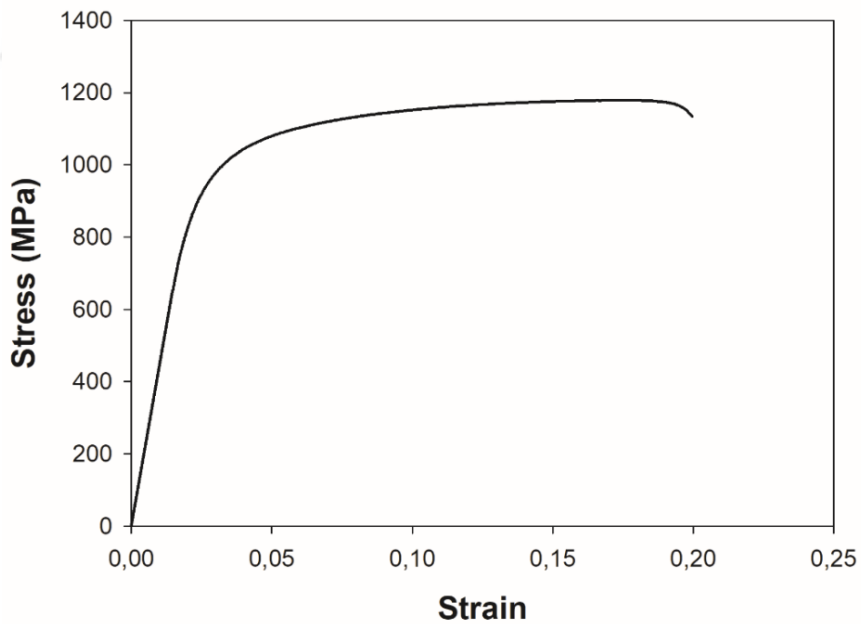
Figure 4.22 exhibits the elastic modulus of porous Ti<sub>74</sub>Nb<sub>26</sub> alloys versus rate of porosity in the samples. As expected, with increasing the rate in porosity elastic modulus of the alloys decreases. Yield and compression strengths also decrease with



increasing porosity as shown in Figure 4.23 and both strengths become close to each other.



(a)



(b)

Figure 4.21. Compressive stress-strain curves of a) porous  $\text{Ti}_{74}\text{Nb}_{26}$  alloys with different porosity and b) full density  $\text{Ti}_{74}\text{Nb}_{26}$  produced by hot pressing at 800°C for 1h following sintering at 1200°C for 4h.

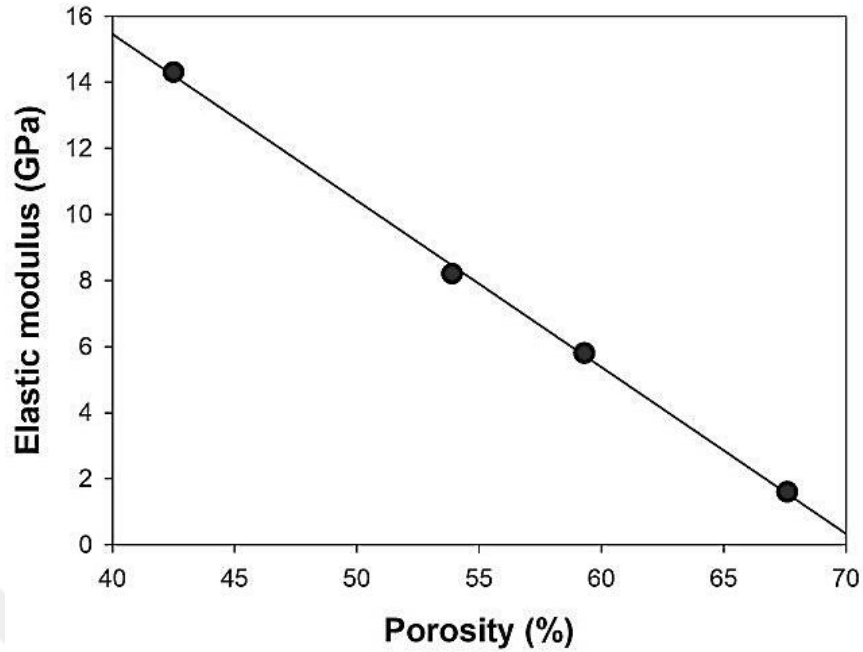


Figure 4.22. Effect of porosity on elastic moduli in porous  $Ti_{74}Nb_{26}$  porous samples with different porosity (43%, 54%, 59% and 68% porosity) sintered at  $1200^{\circ}C$  for 4h.

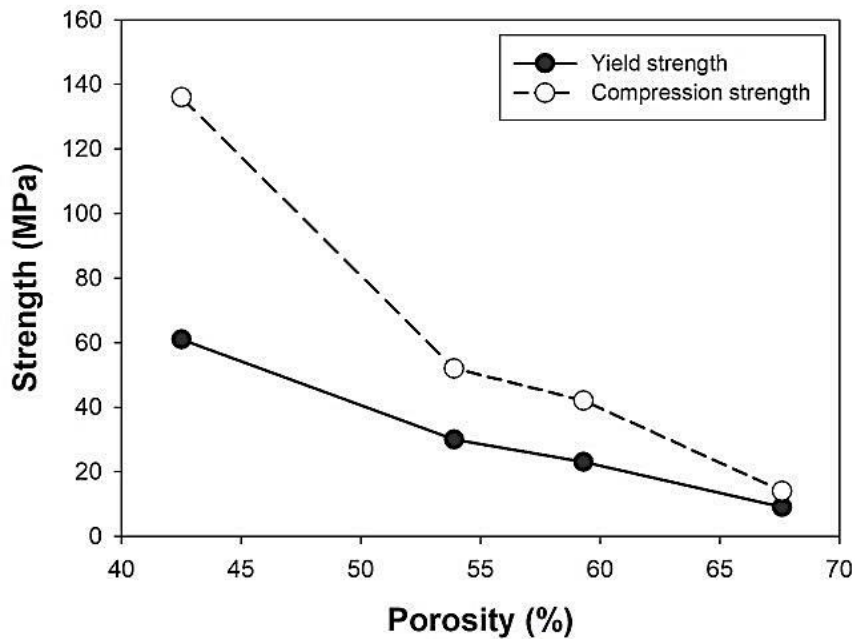


Figure 4.23. Effect of porosity on strength in porous  $Ti_{74}Nb_{26}$  porous samples with different porosity (43%, 54%, 59% and 68% porosity) sintered at  $1200^{\circ}C$  for 4h.

## 5. CONCLUSION

In this study, porous  $Ti_{74}Nb_{26}$  alloys were produced for the first time combining hot pressing and space holder technique. Conclusions obtained from the present study are given below.

- Macro and micro-pores formed in all the samples produced. Macro-pores formed as a result of Mg evaporation and micro-pores formed due to inefficient hot pressing and sintering. Hot pressing temperature is limited by melting point of pure Mg ( $650^{\circ}C$ ).  $600^{\circ}C$  used as hot pressing temperature was not enough to get rid of all the micro-pores. Sintering temperature of  $1200^{\circ}C$  was also not adequate to eliminate undesired micro-pores.
- Microstructures of all the porous samples were consisting of main phase  $\beta$ , and a small amount of  $\alpha$  and pure Nb undissolved.  $1200^{\circ}C$  sintering temperature was not high enough for complete dissolution of Nb. Nb distribution in the microstructure was also not homogeneous. EDS point analysis taken from different regions in  $\beta$  phase resulted in different Nb contents.
- It was not observed any type of contamination products such as oxides, carbides or Mg residues left in the microstructure of porous samples and all the magnesium powders were removed during sintering successfully. Mg and Ti getters were quite efficient to prevent oxidation of porous samples during processing.
- Density test results showed that an increase in porosity from 43% to 68% decreases the density of the samples. Also interconnection between pores increased with increasing total porosity since open porosity ratio increased with increasing total porosity.
- Elastic modulus, yield and compressive strength of porous  $Ti_{74}Nb_{26}$  alloys decreased with increasing porosity. 43, 54, 59% porous samples were suitable for cancellous bone replacement applications while 68% porous sample was not due to its low strength. On the other hand, none of the samples could not meet the cortical bone replacement applications requirements in terms of mechanical properties.

- In order to eliminate or at least minimize micro-pore content and to provide complete and homogeneous dissolution of Nb, sintering temperature should be higher than 1200°C.



## REFERENCES

- Aguilar, C., Guerra, C., Lascano, S., Guzman, D., Rojas, P. A., Thirumurugan, M., Bejar, L., Medina, A., 2016. Synthesis and characterization of Ti-Ta-Nb-Mn foams. *Materials Science and Engineering C*, **58**: 420–431.
- Aherwar, A., Singh, A. K., Patnaik, A., 2015. Current and future biocompatibility aspects of biomaterials for hip prosthesis. *Bioengineering*, **3**: 23–43.
- Aleksanyan, A. G., Dolukhanyan, S. K., Shekhtman, V. Sh., Khasanov, S. S., Ter-Galstyan, O. P., Martirosyan, M. V., 2012. Formation of alloys in the Ti-Nb system by hydride cycle method and synthesis of their hydrides in self-propagating high-temperature synthesis. *International Journal of Hydrogen Energy*, **37**: 14234–14239.
- Anderson, K. R., Groza, J. R., Fendorf, M., Echer, C. J., 1999. Surface oxide debonding in field assisted powder sintering. *Materials Science and Engineering A*, **270**: 278–282.
- Andrade, D. P. D., Vasconcellos, L. M. R. D., Carvalho, I. C. S., Forte, L. F. D. B. P., Santos, E. L. D. S., Prado, R. F. D., Santos, D. R. D., Cairo, C. A. A., Carvalho, Y. R., 2015. Titanium-35niobium alloy as a potential material for biomedical implants: In vitro study. *Materials Science and Engineering C*, **56**: 538–544.
- Aryanpour, G., Farzaneh, M. 2015. Application of a piston equation to describe die compaction of powders. *Powder Technology*, **277**: 120–125.
- Arzt, E., Ashby, M. F., Easterling, K. E., 1983. Practical applications of hot-isostatic pressing diagrams : four case studies. *Metallurgical Transactions A*, **14A**: 211–221.
- Ashby, M. F., Evans, A. G., Fleck, N. A., Gibson, L. J., Hutchinson, J. W., Wadley, H. N. G., 2000. Metal foams: A design guide. *In Typeset by Laser Words, Madras, India Printed in the United States of America*. Butterworth-Heinemann.
- Aşik, E. E., Bor, Ş., 2015. Fatigue behavior of Ti-6Al-4V foams processed by magnesium space holder technique. *Materials Science and Engineering A*, **621**: 157–165.
- Aydoğmuş, T., Bor, Ş., 2009. Processing of porous TiNi alloys using magnesium as space holder. *Journal of Alloys and Compounds*, **478**: 705–710.
- Aydoğmuş, T., 2010. *Processing and Characterization of Porous Titanium Nickel Shape Memory Alloys* (Ph.D thesis). Middle East University, Ankara.
- Banhart, J., 2001. Manufacture, characterisation and application of cellular metals and metal foams. *Progress in Materials Science*, **46**: 559–632.
- Benavente, R., Salvador, M. D., Borrell, A., García-Moreno, O., Peñaranda-Foix, F. L., Catalá-Civera, J. M., 2014. Microwave, Spark Plasma and Conventional Sintering to Obtain Controlled Thermal Expansion  $\beta$ -Eucryptite Materials. *International Journal of Applied Ceramic Technology*, 1–7.
- Biesiekierski, A., Wang, J., Gepreel, M. A-H, Wena, C., 2012. A new look at biomedical Ti -based shape memory alloys. *Acta Biomaterialia*, **8**: 1661–1669.
- Bolzoni, L., Ruiz-Navas, E. M., Neubauer, E., Gordo, E., 2012a. Inductive hot-pressing of titanium and titanium alloy powders. *Materials Chemistry and Physics*, **131**: 672–679.
- Bolzoni, L., Ruiz-Navas, E. M., Neubauer, E., Gordo, E., 2012b. Mechanical properties

- and microstructural evolution of vacuum hot-pressed titanium and Ti-6Al-7Nb alloy. *Journal of the Mechanical Behavior of Biomedical Materials*, **9**: 91–99.
- Calin, M., Gebert, A., Ghinea, A. C., Gostin, P. F., Abdi, S., Mickel, C., Eckert, J., 2013. Designing biocompatible Ti-based metallic glasses for implant applications Mariana. *Materials Science and Engineering C*, **33**: 875–883.
- Čapek, J., Vojtěch, D., Oborná, A., 2015. Microstructural and mechanical properties of biodegradable iron foam prepared by powder metallurgy. *Materials and Design*, **83**: 468–482.
- Chandler, H. W., Sands, C. M., Song, J. H., Withers, P. J., McDonald, S. A., 2008. A plasticity model for powder compaction processes incorporating particle deformation and rearrangement. *International Journal of Solids and Structures*, **45**: 2056–2076.
- Chen, L.-J., Ting, L., Yi-min, L., Hao, H., You-hua, H., 2009. Porous titanium implants fabricated by metal injection molding. *Transactions of Nonferrous Metals Society of China*, **19**: 1174–1179.
- Chmielewski, M., Nosewicz, S., Pietrzak, K., Rojek, J., Strojny-Nedza, A., Mackiewicz, S., Dutkiewicz, J., 2014. Sintering behavior and mechanical properties of NiAl, Al<sub>2</sub>O<sub>3</sub>, and NiAl-Al<sub>2</sub>O<sub>3</sub> composites. *Journal of Materials Engineering and Performance*, **23**: 3875–3886.
- Das, S., Mukhopadhyay, A. K., Datta, S., Basu, D., 2009. Prospects of microwave processing: An overview. *Bulletin of Materials Science*, **32**: 1–13.
- Ding, M., Dalstra, M., Danielsen, C. C., Kabel, J., Hvid, I., Linde, F., 1997. Age variations in the properties of human tibial trabecular bone. *The Journal of Bone and Joint Surgery*, **79**: 995–1002.
- Duda, T., Raghavan, L. V., 2016. 3D metal printing technology. *IFAC-PapersOnLine*, **29**: 103–110.
- Dunand, D. C., 2004. Processing of titanium foams. *Advanced Engineering Materials*, **6**: 369–376.
- Elias, L. M., Schneider, S. G., Schneider, S., Silva, H. M., Malvisi, F., 2006. Microstructural and mechanical characterization of biomedical Ti–Nb–Zr(–Ta) alloys. *Materials Science and Engineering A*, **432**: 108–112.
- Esen, Z., Bor, Ş., 2007. Processing of titanium foams using magnesium spacer particles. *Scripta Materialia*, **56**, 341–344.
- Esen, Z., Bor, Ş., 2011. Characterization of Ti-6Al-4V alloy foams synthesized by space holder technique. *Materials Science and Engineering A*, **528**: 3200–3209.
- Esen, Z., 2007. *Production and Characterization of Porous Titanium Alloys* (Ph.D thesis). Middle East University, Ankara.
- Evans, F. G., 1976. Mechanical properties and histology of cortical bone from younger and older men. *Anat. Rec.*, **185**: 1–12.
- Frosch, K.H., Stürmer, K. M., 2006. Metallic biomaterials in skeletal repair. *European Journal of Trauma*, **2**: 149–159.
- Geetha, M., Singh, A. K., Asokamani, R., Gogia, A. K., 2009. Ti based biomaterials, the ultimate choice for orthopaedic implants—A review. *Progress in Materials Science*, **54**: 397–425.
- Gepreela, M. A-H, Niinomi, M., 2013. Biocompatibility of Ti-alloys for long-term implantation. *Journal of the Mechanical Behavior of Biomedical Materials*, **20**: 407–415.
- German, R. M., 1984. *Powder Metallurgy Science*, Metal powder industries federation,

- Princeton, New Jersey.
- German, R. M., 2013. Progress in Titanium Metal Powder Injection Molding. *Materials*, **6**: 3641–3662.
- Ghasali, E., Pakseresht, A., Rahbari, A., Eslami-Shahed, H., Alizadeh, M., Ebadzadeh, T., 2016. Mechanical properties and microstructure characterization of spark plasma and conventional sintering of Al-SiC-TiC composites. *Journal of Alloys and Compounds*, **666**: 366–371.
- Gómez, D., Palma, R., 2015. Phenomenological modeling of Mo in a Hot Isostatic Pressing (HIP) Process. *Procedia Materials Science*, **9**: 271–278.
- Gupta, M., Wong, W. L. E., 2005. Enhancing overall mechanical performance of metallic materials using two-directional microwave assisted rapid sintering. *Scripta Materialia*, **52**: 479–483.
- Hallab, N.J., Anderson, S., Stafford, T., Glant, T., Jacobs, J. J., 2005. Lymphocyte responses in patients with total hip arthroplasty. *Journal of Orthopaedic Research*, **23**: 384–391.
- Hao, Y.L., Niinomi, M., Kuroda, D., Fukunaga, K., Zhou, Y.L., Yang, R., Suzuki, A., 2003. Aging response of the Young's modulus and mechanical Properties of Ti-29Nb-13Ta-4.6Zr for biomedical applications. *Metallurgical and Materials Transactions A*, **34 A**: 1007–1012.
- He, G., Hagiwara, M., 2006. Ti alloy design strategy for biomedical applications. *Materials Science and Engineering C*, **26**: 14–19.
- Hrabe, N. W., 2010. *Characterization of Cellular Titanium for Biomedical Applications* (Ph.D thesis). University of Washington, Department of Materials, seattle, USA.
- Huiskes, R., Weinans, H., Rietbergen, B. V., 1992. The relationship between stress shielding and bone resorption around total hip stems and the effects of flexible materials. *Clinical Orthopaedics and Related Research*, **274**: 124–134.
- Hussein, M. A., Mohammed, A. S., Al-Aqeeli, N., 2015. Wear characteristics of metallic biomaterials: A review. *Materials*, **8**: 2749–2768.
- Hussein, M. A., Suryanarayana, C., Al-Aqeeli, N., 2015. Fabrication of nano-grained Ti-Nb-Zr biomaterials using spark plasma sintering. *Materials and Design*, **87**: 693–700.
- Ibrahim, A., Zhang, F., Otterstein, E., Burkel, E., 2011. Processing of porous Ti and Ti5Mn foams by spark plasma sintering. *Materials and Design*, **32**: 146–153.
- Jha, N., Mondal, D. P., Majumdar, J. D., Badkul, A., Jha, A. K., Khare, A. K., 2013. Highly porous open cell Ti-foam using NaCl as temporary space holder through powder metallurgy route. *Materials and Design*, **47**: 810–819.
- Kains, J. A., Melton, L. J., Christiansen, C., Johnston, C. C., Khaltsev, N., 1994. The diagnosis of osteoporosis. *Journal of Bone and Mineral Research*, **9**: (1137–1141).
- Kopas, P., Handrik, M. Sága, M., Melicher, R., 2007. Comparative analysis of influence selected geometrical parameters on stress concentration in the surrounding of inclusion. *Applied and Computational Mechanics*, 115–120.
- Kuroda, D., Niinomi, M., Morinaga, M., Kato, Y., Yashiro, T., 1998. Design and mechanical properties of new  $\beta$  type titanium alloys for implant materials. *Materials Science and Engineering A*, **243**: 244–249.
- Kurtz, S. M., Lau, E., Ong, K. Zhao, K. Kelly, M., Bozic, K. J., 2009. Future young patient demand for primary and revision joint replacement: National projections

- from 2010 to 2030. *Clinical Orthopaedics and Related Research*, **467**: 2606–2612.
- Lewis, G., 2013. Properties of open-cell porous metals and alloys for orthopaedic applications. *Journal of Materials Science: Materials in Medicine*, **24**: 2293–2325.
- Leyens, C., Peters, M., 2003. *Titanium and titanium alloys: fundamental and applications*. Wiley-VCH.
- Li, B.-Q., Li, Z.-Q., Lu, X., 2015. Effect of sintering processing on property of porous Ti using space holder technique. *Transactions of Nonferrous Metals Society of China*, **25**: 2965–2973.
- Li, S. J., Yang, R., Li, S., Hao, Y. L., Cui, Y. Y., Niinomi, M., Guo, Z. X., 2004. Wear characteristics of Ti–Nb–Ta–Zr and Ti–6Al–4V alloys for biomedical applications. *Wear*, **257**: 869–876.
- Li, Y.-H., Chen, R.-B., Qi, G.-x., Wang, Z.-T., Deng, Z.-Y., 2009. Powder sintering of porous Ti-15Mo alloy from TiH<sub>2</sub> and Mo powders. *Journal of Alloys and Compounds*, **485**: 215–218.
- Li, Y., Yang, C., Zhao, H., Qu, S., Li, X., Li, Y., 2014. New Developments of Ti-Based Alloys for Biomedical Applications. *Materials*, **7**: 1709–1800.
- Liang, S.X., Feng, X.J., Yin, L.X., Liu, X.Y., Ma, M.Z., Liu, R. P., 2016. Development of a new  $\beta$  Ti alloy with low modulus and favorable plasticity for implant material. *Materials Science and Engineering: C*, **61**: 338–343.
- Lin, J.-G., Zhang, Y.-F., MA, M., 2010. Preparation of porous Ti35Nb alloy and its mechanical properties under monotonic and cyclic loading. *Transactions of Nonferrous Metals Society of China*, **20**: 390–394.
- Liu, X., Chu, P. C., Ding, C., 2004. Surface modification of titanium, titanium alloys, and related materials for biomedical applications. *Materials Science and Engineering R*, **47**: 49–121.
- Liu, Y., Chen, L. F., Tang, H. P., Liu, C. T., Liu, B., Huang, B. Y., 2006. Design of powder metallurgy titanium alloys and composites. *Materials Science and Engineering A*, **418**: 25–35.
- Long, M., Rack, H. J., 1998. Titanium alloys in total joint replacement a materials science perspective. *Biomaterials*, **19**: 1621–1639.
- Manière, C., Durand, L., Estournès, C., 2016. Powder/die friction in the spark plasma sintering process: Modelling and experimental identification. *Scripta Materialia*, **116**: 139–142.
- Mansourighasri, A., Muhamad, N., Sulong, A. B., 2012. Processing titanium foams using tapioca starch as a space holder. *Journal of Materials Processing Technology*, **212**: 83–89.
- Maya, A. E A., Grana, D. R., Hazarabedian, A., Kokubu, G. A., Luppo, M. I., Vigna, G., 2012. Zr-Ti-Nb porous alloys for biomedical application. *Materials Science and Engineering C*, **32**: 321–329.
- Mendes, M. W. D., Agreda, C. G., Bressiani, A. H. A., Bressiani, J. C., 2016. A new titanium based alloy Ti-27Nb-13Zr produced by powder metallurgy with biomimetic coating for use as a biomaterial. *Materials Science and Engineering C*, **63**: 671–677.
- Moffat, D. L., Kattner, U. R., 1988. The stable and metastable Ti-Nb phase diagrams. *Metallurgical Transactions A*, **19A**: 2389–2397.
- Moffat, D.L., Larbalestier, D. C., 1988. The competition between the alpha and omega



- phases in aged Ti-Nb alloys. *Metallurgical Transactions A*, **19A**: 1687–1694.
- Moyen, B.J.-L., Lathey, P.J., Weinberg, E.H., Harris, W. H., 1978. Effects on intact femora of dogs of the application and removal of metal plates. *Journal of Bone and Joint Surgery*, **60–A**: 940–947.
- Murr, L. E., & Johnson, W. L., 2017. 3D metal droplet printing development and advanced materials additive manufacturing. *J Mater Res Technol.*, **6 (1)**: 77–89.
- Nakas G. I., Dericioglu, A. F., Bor, Ş., 2011. Fatigue behavior of TiNi foams processed by magnesium space holder technique. *Journal of Mechanical Behavior of Biomedical Materials*, **4**: 2017–2023.
- Niinomi, M., Akahori, T., Katsura, S., Yamauchi, K., Ogawa, M., 2007. Mechanical characteristics and microstructure of drawn wire of Ti–29Nb–13Ta–4.6Zr for biomedical applications. *Materials Science and Engineering C*, **27**: 154–161.
- Niinomi, M., 2002. Recent metallic materials for biomedical applications. *Metallurgical and Materials Transactions A*, **33A**: 477–486.
- Niinomi, M., 2008. Mechanical biocompatibilities of titanium alloys for biomedical applications. *Journal of the Mechanical Behavior of Biomedical Materials*, **I**: 30–42.
- Niinomi, M., & Nakai, M., 2011. Titanium-based biomaterials for preventing stress shielding between implant devices and bone. *International Journal of Biomaterials*, **2011**: 1–10.
- Niu, W., Gill, S., Dong, H., Bai, C., 2010. A two-scale model for predicting elastic properties of porous titanium formed with space-holders. *Computational Materials Science*, **50**: 172–178.
- Niu, W. Bai, C., Qiu, G., Wang, Q., 2009. Processing and properties of porous titanium using space holder technique. *Materials Science and Engineering A*, **506**: 148–151.
- Nnamchi, P. S., Obayi, C. S., Todda, I., Rainforth, M. W., 2016. Mechanical and electrochemical characterisation of new Ti–Mo–Nb–Zr alloys for biomedical applications. *Journal of the Mechanical Behavior of Biomedical Materials*, **60**: 68–77.
- Nosewicz, S., Rojek, J., Pietrzak, K., Chmielewski, M., 2013. Viscoelastic discrete element model of powder sintering. *Powder Technology*, **246**: 157–168.
- Nugroho, A. W., Leadbeater, G., Davies, I. J., 2010. Processing of a porous titanium alloy from elemental powders using a solid state isothermal foaming technique. *Journal of Materials Science: Materials in Medicine*, **21**: 3103–3107.
- Oghbaei, M., Mirzaee, O., 2010. Microwave versus conventional sintering: A review of fundamentals, advantages and applications. *Journal of Alloys and Compounds*, **494**: 175–189.
- Oh, I-H., Nomura, N., Masahashi, N., Hanada, S., 2003. Mechanical properties of porous titanium compacts prepared by powder sintering. *Scripta Materialia*, **49**: 1197–1202.
- Oliveira, C. S. S., Griza, S., Oliveira, M. V., Ribeiro, A. A., Leite, M. B., 2015. Study of the porous Ti35Nb alloy processing parameters for implant applications. *Powder Technology*, **281**: 91–98.
- Ontanon, C., Aparicio, C., Ginebra, M.P., Planell, J., 2000. *Structural Biological Material Design and structure-Property Relationship*, Edited by M. Elices, Pergamon Press, Oxford, 31-72.
- Ouchi, C., Iizuni, H., Mitao, S., 1998. Effects of ultra-high purification and addition of

- interstitial elements of properties of pure titanium and titanium alloy. *Materials Science & Engineering A*, **243**: 186–195.
- Ozaki, T., Matsumoto, H., Watanabe, S., Hanada, S., 2004. Beta Ti alloys with low **Young's modulus**. *Materials Transactions*, **45**: 2776–2779.
- Ozan, S. Lin, J., Li, Y. Ipek, R., & Wen, C., 2015. Development of Ti-Nb-Zr alloys with high elastic admissible strain for temporary orthopedic devices. *Acta Biomaterialia*, **20**: 176–187.
- Prado, R. F. D., Rabelo, S. B., Andrade, D. P. D., Nascimento, R. D., Henriques, V. A. R., Carvalho, Y. R., Cairo, C. A. A., Vasconcellos, L. M. R. D., 2015. Porous titanium and Ti-35Nb alloy: effects on gene expression of osteoblastic cells derived from human alveolar bone. *Journal of Materials Science: Materials in Medicine*, **26**: 259–270.
- Qi, Y., Contreras, K. G., Jung, H-D, Kim, H-E, Lapovok, R., Estrin, Y., 2016. Ultrafine-grained porous titanium and porous titanium/magnesium composites fabricated by space holder-enabled severe plastic deformation. *Materials Science and Engineering C*, **59**: 754–765.
- Ramakrishna, S., Mayer, J., Wintermantel, E., Leong, K. W., 2001. Biomedical applications of polymer-composite materials: A review. *Composites Science and Technology*, **61**: 1189–1224.
- Rho, J.-Y., Tsui, T. Y., Pharr, G. M., 1997. Elastic properties of human cortical and trabecular lamellar bone measured by nanoindentation. *Biomaterials*, **18**: 1325–1330.
- Risbud, S. H., Han, Y.-H., 2013. Preface and historical perspective on spark plasma sintering. *Scripta Materialia*, **69**: 105–106.
- Rubshtein, A. P., Makarova, E. B., Rinkevich, A. B., Medvedeva, D. S., Yakovenkova, L. I., Vladimirov, A. B., 2015. Elastic properties of a porous titanium-bone tissue composite. *Materials Science and Engineering C*, **52**: 54–60.
- Ryan, G., Pandit, A., Apatsidis, D. P., 2006. Fabrication methods of porous metals for use in orthopaedic applications. *Biomaterials*, **27**: 2651–2670.
- Sakaguchi, N., Niinomi, M., Akahori, T., Takeda, J., Toda, H., 2005. Relationships between tensile deformation behavior and microstructure in Ti-Nb-Ta-Zr system alloys. *Materials Science and Engineering C*, **25**: 363–369.
- Shibo, G., Bohua, D., Xinbo, H., Xuanhui, Q., 2009. Powder injection molding of pure titanium. *Rare Metals*, **28**: 261–265.
- Sidambe, A. T., Figueroa, I. A., Hamilton, H. G. C., Todd, I., 2012. Metal injection moulding of CP-Ti components for biomedical applications. *Journal of Materials Processing Technology*, **212**: 1591–1597.
- Sidambe, A. T., 2014. Biocompatibility of advanced manufactured titanium implants-A review. *Materials*, **7**: 8168–8188.
- Swinkels, F. B., Wilkinson, D. S., Arzt, E., Ashby, M. F., 1983. Mechanism of hot-isostatic pressing. *Acta Metall.*, **31**: 1829–1840.
- Tang, X., Ahmed, T., Rack, H. J., 2000. Phase transformations in Ti-Nb-Ta and Ti-Nb-Ta-Zr alloys. *Journal of Materials Science*, **35**: 1805–1811.
- Terayama, A., Fuyama, N., Yamashita, Y., Ishizaki, I., Kyogoku, H., 2013. Fabrication of Ti-Nb alloys by powder metallurgy process and their shape memory characteristics. *Journal of Alloys and Compounds*, **577s**, S408–S412.
- Tiwari, A., 2000. Liquid phase sintering in microgravity. *Current Science*, **79**: 334–335.

- Viceconti, M., Muccini, R., Bernakiewicz, M., Baleani, M., Cristofolini, L., 2000. Large-sliding contact elements accurately predict levels of bone-implant micromotion relevant to osseointegration. *Journal of Biomechanics*, **33**: 1611–1618.
- Wally, J. Z., Grunsven, W. V., Claeysens, F., Goodall, R., Reilly, G. C., 2015. Porous Titanium for Dental Implant Applications. *Metals*, **5**: 1902–1920.
- Wan, X.-J., 2011. Effects of alkali and heat treatment on strength of porous Ti35Nb. *Transactions of Nonferrous Metals Society of China*, **21**: 1335–1339.
- Wang, J. C., 1984. Young's modulus of porous materials. *Journal of Materials Science*, **19**: 809–814.
- Wang, K., 1996. The use of titanium for medical applications in the USA. *Materials Science and Engineering A*, **213**: 134–137.
- Węglewski, W., Basista, M., Chmielewski, M., Pietrzak, K., 2012. Modeling of thermally induced damage in the processing of Cr–Al<sub>2</sub>O<sub>3</sub> composites. *Composites: Part B*, **43**: 255–264.
- Wen, C. E., Mabuchi, M., Yamada, Y., Shimojima, K., Chino, Y., Asahina, T., 2001. Processing of biocompatible porous Ti and Mg. *Scripta Materialia*, **45**: 1147–1153.
- Wen, C. E., Yamada, Y., Shimojima, K., Chino, Y., Asahina, T., Mabuchi, M., 2002. Processing and mechanical properties of autogenous titanium implant materials. *Journal of Materials Science: Materials in Medicine*, **13**: 397–401.
- Wen, C. E., Yamada, Y., Shimojima, K., Chino, Y., Hosokawa, H., Mabuchi, M., 2002. Novel titanium foam for bone tissue engineering. *Journal of Materials Research*, **17**: 2633–2639.
- Wu, S., Liu, X., & Yeung, K. W. K. Liu, C., Yang, X., 2014. Biomimetic porous scaffolds for bone tissue engineering. *Materials Science and Engineering R*, **80**: 1–36.
- Xiong, J., Li, Y., Wang, X., Hodgson, P., Wen, C., 2008. Mechanical properties and bioactive surface modification via alkali-heat treatment of a porous Ti-18Nb-4Sn alloy for biomedical applications. *Acta Biomaterialia*, **4**: 1963–1968.
- Xu, J. L., Bao, L. Z., Liu, A. H., Jin, X. F., Luo, J. M., Zhong, Z. C., Zheng, Y. F., 2015. Effect of pore sizes on the microstructure and properties of the biomedical porous NiTi alloys prepared by microwave sintering. *Journal of Alloys and Compounds*, **645**: 137–142.
- Ye, B., Dunand, D. C., 2010. Titanium foams produced by solid-state replication of NaCl powders. *Materials Science and Engineering A*, **528**: 691–697.
- Zhang, F., Otterstein, E., Burkel, E., 2010. Spark plasma sintering, microstructures, and mechanical properties of macroporous titanium foams. *Advanced Engineering Materials*, **12**: 863–872.
- Zhang, L., Zhang, Y. Q., Jiang, Y. H., Zhou, R., 2015a. Mechanical behaviors of porous NiTi alloy with high porosity and large pore size prepared by one-step spark plasma sintering. *Journal of Alloys and Compounds*, **644**: 513–522.
- Zhang, L., Zhang, Y. Q., Jiang, Y. H., Zhou, R., 2015b. Mechanical behaviors of porous Ti with high porosity and large pore size prepared by one-step spark plasma sintering technique. *Vacuum*, **122**: 187–194.
- Zhao, D., Chang, K., Ebel, T., Nie, H., Willumeit, R., Pyczak, F., 2015. Sintering behavior and mechanical properties of a metal injection molded Ti-Nb binary alloy as biomaterial. *Journal of Alloys and Compounds*, **640**: 393–400.

- Zhao, D., Chang, K., Ebel, T., Qian, M., Willumeit, R., Yan, M., Pyczak, F., 2013. Microstructure and mechanical behavior of metal injection molded Ti-Nb binary alloys as biomedical material. *Journal of the Mechanical Behavior of Biomedical Materials*, **28**: 171–182.
- Zhao, X., Sun, H., Lan, L., Huang, J., Zhang, H., Wang, Y., 2009. Pore structures of high-porosity NiTi alloys made from elemental powders with NaCl temporary space-holders. *Materials Letters*, **63**: 2402–2404.
- Zhu, S. L., Yang, X. J., Fu, D. H., & Zhang, L. Y., Li, C. Y., Cui, Z. D., 2005. Stress-strain behavior of porous NiTi alloys prepared by powders sintering. *Materials Science and Engineering A*, **408**: 264–268.
- Zhuang, H., Han, Y., Feng, A., 2008. Preparation, mechanical properties and in vitro biodegradation of porous magnesium scaffolds. *Materials Science and Engineering C*, **28**: 1462–1466.
- Zhuravleva, K., Chivu, A., Teresiak, A., Scudino, S., Calin, M., Schultz, L., Eckert, J., Gebert, A., 2013. Porous low modulus Ti40Nb compacts with electrodeposited hydroxyapatite coating for biomedical applications. *Materials Science and Engineering C*, **33**: 2280–2287.
- Zhuravleva, K., Müller, R., Schultz, L., Eckert, J., & Gebert, A., Bobeth, M., Cuniberti, G. 2014. Determination of the Young's modulus of porous  $\beta$ -type Ti-40Nb by finite element analysis. *Materials and Design*, **64**: 1–8.

## APPENDIX

### EXTENDED TURKISH SUMMARY (GENİŞLETİLMİŞ TÜRKÇE ÖZET)

#### ÖZET

### BİYOMEDİKAL UYGULAMALAR İÇİN GÖZENEKLİ TİTANYUM NİYOBYUM ALAŞIMLARININ ÜRETİLMESİ

PALANI, Dana Kareem Hamee  
Yüksek Lisans Tezi, MakineMühendisliği Anabilim Dalı  
Tez Danışmanı : Doç. Dr. Tarık AYDOĞMUŞ  
Ocak 2018, 113 sayfa

Bu çalışmada, biyomedikal kemik implant uygulamaları için gözeneklilikleri %43-68 aralığında olan  $Ti_{74}Nb_{26}$  alaşımlarını üretmek için saf Ti, saf Nb ve küresel Mg tozları kullanılmıştır. Gözenekli numuneleri üretmek için ilk kez sıcak presleme işlemi ile boşluk oluşturuvcu metot birlikte kullanılmıştır. Öncelikle, Ti, Nb ve farklı miktarda Mg tozları (%40, %50, %60 ve %70, hacimce) 15 dakika süre ile karıştırılmıştır. Daha sonra toz karışımları, iç çapı 15 mm olan içi boş silindirik grafit kalıplara doldurulmuş ve 10 mm yüksekliğinde numuneler üretmek için 50 MPa sabit basınç altında Mg'nin erimesini (650 °C) önlemek için 600 °C'de 1 saat süre ile sıcak presleme işlemine tabi tutulmuştur. Oksidasyonu önlemek için üretim sırasında saf argon gazı kullanılmıştır. Sıcak presleme işleminden sonra numuneler dikey bir fırında 1200 °C'de 4 saat boyunca inört argon gazı atmosferi altında sinterlenmiştir. Sinterleme sırasında eşzamanlı olarak Mg da (1090 °C) buharlaştırılmış ve numunelerden uzaklaştırılarak makro gözenekler oluşturulmuştur. X-Işını Kırınımı ve Taramalı Elektron Mikroskobu incelemeleri, tüm numunelerin mikroyapısında ana faz olan  $\beta$  fazının yanı sıra az miktarda  $\alpha$  fazı ve saf Nb'un bulunduğunu göstermiştir. Üretilen gözenekli alaşımların mekanik özelliklerinin süngerimsi kemik implantasyonu uygulamaları için yeterli iken, yoğun (kortikal) kemik implantasyonları için uygun olmadıkları sonucuna ulaşılmıştır. Verimsiz sıcak presleme ve yetersiz sinterleme sıcaklığının bir sonucu olarak oluşan mikro gözeneklerin düşük mekanik özelliklere neden olduğu görülmüştür.

**Anahtar kelimeler:** Gözenekli Titanyum-Niyobyum alaşımları, Mg boşluk oluşturuvcu yöntemi, Mekanik özellikler, Sıcak presleme, Toz metalurjisi.



## 1. GİRİŞ

Sert dokuların zarar görmesi ve mariz hale gelmesi, yapay protezlere duyulan ihtiyacı doğurmaktadır. Bu doğrultuda dizlerde, kalçalarda, kalp kapakçıklarında (yapay kapaklar), damarlarda (stentler), dirseklerde, kulaklarda, omuzlarda veya diş yapılarında ikame protezler ve implant malzemeleri kullanılmaktadır (Ramakrishna, 2001; Aherwar, 2015). Sert dokuların bozulmalarına neden olan bir diğer etmen de yaşlılıktır. Birleşmiş Milletlerin 2013 tarihli bir raporuna göre, 60 yaş üzeri nüfus oranı giderek artmaktadır ve 2050 yılında dünyanın gelişmiş kesimlerinde yaşlı insan nüfusunun %45'e kadar yükselmesi beklenmektedir (Ozan, 2015). Son yıllarda arabalar, bisikletler ve mobilet ve motosiklet gibi diğer taşıtların kullanımının yaygınlaşmasına bağlı olarak bunlardan kaynaklanan kazaların sayısı da yükselmektedir. Tüm bunlar ortopedik ameliyatlara ve biyomedikal malzemelere duyulan ihtiyacı daha da artırmaktadır.

Protezler seramik, polimer ya da alaşımlı malzemelerden üretilebilmekte, ayrıca metalik malzemeler de biyomalzeme implantların %70-%80'inin üretiminde kullanılmaktadır. Son dönemlerde paslanmaz çelik ve Co-Cr alaşımlarına bir alternatif olarak CP Ti kullanımı önerilmektedir. CP Ti'nin insan kemiğiyle biyo-uyumluluğu daha yüksektir ve çok iyi aşınma direncine sahiptir (Wu, 2014; Zhuang, 2008).

İmplant malzemesi ile kemik arasında yüksek Young modülü uyumsuzluğu olduğunda implantların gevşemesi durumu ile karşılaşmaktadır ve bu durum "gerilim perdelenmesi" adı verilen kemik protez uygulamalarında sıklıkla rastlanılan bir sorunu teşkil etmektedir. Elastik katsayısı azaltma amacına yönelik olarak Ti temelli alaşımlar geliştirilmiştir. Arzu edilen gözenekli yapıya sahip TiNb alaşımlarının üretilebilmesi için "boşluk oluşturucu" adı verilen yöntem en uygun yöntem olarak görülmektedir. Bununla beraber boşluk oluşturucu yöntem kullanıldığında malzemede iki tür gözenek oluşmaktadır: boşluk oluşturucu malzemenin uzaklaştırılması ile elde edilen makro-gözenekler ve yetersiz sinterlemeden kaynaklanan mikro-gözenekler. Olası kirlilikleri önlemek ve küresel şekilli ve birbirleri ile bağlantılı gözenekler oluşturmak amacıyla magnezyum tozu yeni bir boşluk oluşturucu malzeme olarak kullanıma girmiştir.





## 2. LİTERATÜR TARAMASI

### 2.1. Biyomedikal Uygulamalar için Ti-Esaslı Alaşımların Temel Malzeme Gereksinimleri

İnsan vücudundaki metalik implantların uzun dönem yük dayanımı performansına etki eden çok sayıda etmen bulunmaktadır. Bunlardan en önemlisi mekanik uyumluluktur. Biyomedikal uygulamalarda kullanılacak herhangi bir implant malzemesinin sertlik, dayanıklılık, yıpranma ve aşınma dirençleri gibi biyomekanik özellikleri ile, toksisite (zehirlilik) gibi biyomedikal özelliklerine hassasiyetle önem verilmelidir (Long Ve Rack, 1998; Wang, 1996; Nnamchi, 2016). Ti-esaslı alaşımların mekanik özellikleri insan sert dokularının gereksinimlerini karşılayacak seviyede olmalıdır.

Bu amaçla Ti gibi malzemelerin alaşımları hazırlanırken en uygun karışım değerleri kullanılarak gerçek insan kemiğinin düşük esneklik katsayısı (modulus) ve yüksek dayanım değerlerine yakın özellikler elde edilmeye çalışılmaktadır.

“Biyomekanik uyumsuzluk” olarak bilinen olgu yetersiz mekanik dayanımı ya da implant ile insan dokusu arasında elastik katsayı (modulus) değeri uyumsuzluğunu ifade etmektedir. İnsan kemiklerinin stresten korunmasının arkasındaki ana gerekçe de implant malzemesi ile insan dokuları arasındaki bu biyomekanik uyumsuzluk ya da elastik katsayı farkıdır (Huiskes, 1992).

İnsan bedenine bu malzemeler yerleştirildiğinde meydana gelecek biyolojik değişikliklerin değerlendirilmesi de yüksek önem arz etmektedir. Fizyolojik ortamda polarizasyon direnci, ilgili metalin iyon salınım hızını ifade etmektedir. İmplantlarda kullanılan malzemeleri biyo-uyumluluklarına göre yaşamsal, nötr ve zararlı olarak üç sınıfta toplamak mümkündür (Liang, 2016).

### 2.2. Ti-Nb Faz Diyagramı

Ti-Nb denge diyagramında yalnızca iki kararlı katı faz bulunmaktadır, bunlar hep  $\alpha$ -fazı ve bcc  $\beta$ -fazıdır (Moffat ve Larbalestier, 1988). Bu diyagrama göre %3

Nb'de ve 400 °C sıcaklıkta hcp  $\alpha$ -fazı kararlı durumdadır. 400 °C'de  $\alpha + \beta$  fazları karışımı Nb içeriği artırıldığında kararlı hale gelmektedir. Nb içeriğinin 400 °C'de %38 Nb'ye çıkarılması ile kararlı  $\beta$  fazı elde edilebilmektedir (Aleksanyan, 2012). Saf Ti'de sıcaklık 882 °C'nin üzerine çıktığında hcp  $\alpha$  fazından bcc  $\beta$  fazına dönüşüm gerçekleşmektedir.

### 2.3. Ti-Nb sistemi: yapı ve özellikler arasındaki ilişki

Ti 882±2°C'de alotropik (eş özdekli) dönüşüme uğramaktadır; bu sıcaklıktaki saf Ti  $\alpha$  fazından  $\beta$  fazına dönüşür. 882±2°C'nin altında,  $\alpha$ -fazı hegzagonal sıkı paket kristal (HCP) yapısındayken, 882±2°C'de  $\beta$  fazı hacim merkezli kübik (BCC) yapıdadır. Titanyuma ilave edilebilecek alaşım maddeleri  $\beta$ -dönüşüm sıcaklıklarına olan etkileri açısından üç kategoride toplanmaktadır. Bunlar sırasıyla  $\beta$ -stabilizör,  $\alpha$ -stabilizör ve nötr maddelerdir (Leyens ve Peters, 2003).

$\beta$ -stabilizör maddeler ise faz dönüşümü üzerindeki doğrudan etkilerine göre  $\beta$ -izomorfik ve  $\beta$ -ötektik (eutectic) olarak ikiye ayrılmaktadır. Vanadyum, molibden, tantal ve niyobyum  $\beta$  fazında tamamen çözülebilen  $\beta$ -izomorfik elementlere örnektir. Bu elementlerin alaşımdaki oranlarını artırarak  $\beta$ -dönüşüm sıcaklığını daha da azaltmak mümkündür (Leyens ve Peters, 2003).

Nb miktarı ile Young katsayısı arasındaki ilişki tespit edilmiştir. Nb miktarını artırarak Young katsayısını düşürmek mümkündür. Ti-Nb alaşımında en düşük Young katsayısı Nb oranı kütleli olarak yaklaşık %40 olduğunda tespit edilmiştir (Ozaki, 2004).

### 2.4. Gözenekli TiNb

Gözenekli metal malzemeler üretebilmek için çok sayıda yöntem geliştirilmiş olup, en çok kullanılanları sıvı hal ve katı hal teknikleridir (Banhart, 2001). Sıvı hal teknikleri gözenekli titanyum ve alaşımlarını üretmek için uygun değildir çünkü titanyum yüksek sıcaklıklarda atmosferik gazlarla (ör: oksijen) reaksiyona girmektedir. Bu yöntem, alüminyum, çinko ve magnezyum gibi elementlerden ve daha ziyade basit

süreçlerle elde edilebilen (Banhart, 2001), düşük erime noktasına sahip gözenekli malzemelerin üretimi için kullanılabilir.

Ancak Ti alaşımlarının elde edilmesinde toz metalürjisi yöntemleri gibi yaklaşımlar kullanılmalıdır (Leyens ve Peters, 2003). Toz metalürjisi yöntemleri daha düşük sıcaklıklarda ve atmosferik gazlarla daha az kimyasal reaksiyona neden olacak şekilde üretim yapabilmektedir. Bu üretim süreçlerinin ve elde edilen gözenek ebatlarının ve şekillerinin kontrolü diğer yöntemlere göre daha kolay olmaktadır.

## 2.5. Toz Metalürjisi

Metal veya seramik tozlarının sinterlenmesi çeşitli parçaların üretiminde kullanılan en basit üretim yöntemlerinden birisidir. Sinterleme, kimi zaman ilave basınç kullanılarak erime noktasına oldukça yakın seviyelere yükseltilmiş sıcaklıklarda bağlanmış tozlar elde etme yöntemidir. Sinterlenen her tür malzeme için, uygulamada kullanılan sıcaklık yükseldikçe neticede elde edilen sinterleme seviyesi de yükselmektedir (Chmielewski, 2014). Yapılan yoğunluk ölçümlerine dayanarak, sinterlemenin sıcaklık, sinterleme süresi, basınç ve atmosfer gibi pek çok değişkenden etkilenen karmaşık bir süreç olduğu anlaşılmaktadır; tüm bu değişkenler elde edilecek sinterlenmiş malzemenin özelliklerine etki etmektedir (Węglewski, 2012).

Gözeneklenme seviyesi tozun fiziksel boyutu küçüldükçe azalmaktadır, çünkü yüksek yüzey alanına sahip parçacıklar daha yüksek enerji seviyesinde bulunmaktadır (Čapek, 2015). Bu da daha düşük sinterleme sıcaklıklarında bile daha hızlı şekilde sinterlenecekleri anlamına gelmektedir. Gözeneklenmenin yüksek olması elastik katsayıyı, dayanımı ve eğilme dayanımını azaltmaktadır. Boşluk oluşturucu yönteminde ise gözenek boyut ve şeklinin mekanik özelliklere etkileri farklıdır. Boşluk oluşturucular ile sinterlenmiş tozlarda, bahsi geçen bu gözenek oluşturucu maddelerin hacimsel oranları vasıtasıyla gözenek miktarı, gözenek şekli ve makro-gözenek ebatları kontrol edilebilmektedir (Čapek, 2015; Maya, 2012; Ryan, 2006).

## 2.6. Üretim Yöntemleri

Gözenekli malzemelerin üretiminde kullanılacak, kıvılcım plazma sinterlemesi (Spark Plasma Sintering, SPS) (Ghasali, 2016; Zhang, 2015b), mikrodalga

sinterleme, metal enjeksiyon kalıplama (Metal Injection Molding, MIM) (Zhao, 2013), konvansiyonel sinterleme (Conventional Sintering, CS) (Aydoğmuş, 2010), eklemeli üretim (additive manufacturing – 3D baskı) (Duda ve Raghavan, 2016) ve boşluk oluşturuvcu yöntemi gibi çok sayıda yöntem mevcuttur (Aydoğmuş, 2010).

Kesin sınırları olan gözenekli parçalar elde etme imkânı, gözeneklerin homojen dağılımını sağlaması ve farklı boyutlarda gözeneklerin kullanılabilmesi gibi nedenlerle, toz metalürjisi yöntemi Ti ve Ti alaşımı malzemeler elde edilmesinde tercih edilen bir yöntemdir. Gözenekli yapıların elde edilmesi için izlenen adımlar genellikle tozun hazırlanması, sıkıştırma ya da kalıplama, bağlayıcı ya da boşluk malzemesinin uzaklaştırılması ve sinterleme şeklindedir.

Boşluk oluşturuvcu yöntemi (Space holder technique, SHT) yüksek gözeneklilikte TiNb elde etmek için kullanılmaktadır. Metaller, seramik parçacıkları, polimer taneleri ve tuzlar yer tutucu malzeme (ya da gözenek oluşturuvcuları, yer doldurucuları, gözenek doldurucu malzemeler vb.) olarak kullanılabilir. SHT'nin gözeneklilik seviyesinin ve gözenek şekilleri ile bunların dağılımının ayarlanabilmesi gibi avantajları vardır (Wen, 2001; Esen ve Bor, 2007; Aydoğmuş ve Bor, 2009). Bu yöntem genellikle karıştırma, soğuk ya da sıcak sıkıştırma, sinterleme ve boşluk malzemesinin uzaklaştırılması adımlarından oluşmaktadır.

Yer tutucu malzemelerin kullanımında sıklıkla karşılaşılan bir sorun da yüksek miktarda yer tutucu malzemenin son üründen nasıl uzaklaştırılacağıdır. Bir diğer önemli husus ise doğru yer tutucu malzemenin seçilmesidir. Biyomedikal uygulamalar göz önüne alındığında sinterlemenin ardından üründe kalan yer tutucu maddenin zararlı veya zehirli olmaması gerekmektedir, zira bu maddelerin insan vücudu tarafından emilerek metabolik zararlara yol açması ihtimali bulunmaktadır. Üre (Andrade, 2015), amonyum hidrojen karbonat (Lin, 2010), tapyoka nişastası (Mansourighasri, 2012), sodyum klorür (Jha, 2013), polimer malzemeler (Nugroho, 2010) ve magnezyum (Nakas, 2011) da dâhil olmak üzere çok sayıda malzeme farklı araştırmacılar tarafından yer tutucu olarak denenmiştir. Sodyum klorür (Ye ve Dunand, 2010), potasyum sorbat (Esen ve Bor, 2011) ve potasyum klorür (Esen ve Bor, 2011) gibi çok sayıda suda çözülebilen yer tutucu maddeler de bulunmaktadır.

Magnezyumun avantajı buharlaştığında kontaminasyon riskinin de ortadan kalkmasıdır. Bu çalışmada gözenekli TiNb alaşımları elde edilirken yer tutucu olarak

magnezyumun tercih edilmesinin temelde üç nedeni vardır. Bunlardan ilki, magnezyumun TiNb içerisindeki çözünürlüğünün görmezden gelinebilecek kadar düşük seviyede olmasıdır. İkincisi, sinterleme aşamasında Mg indirgeyici bir ortam oluşturarak TiNb alaşımlarının oksitlenmesini önlemektedir. Son olarak, Mg vücutta düşük miktarlarda çözülmekte ve zehirli olmayan bileşikler oluşturmaktadır (Aydoğmuş, 2010).

## 2.7. Gözenekli Metalik Malzemelerin Basma Davranışları

Gözenekli metalik malzemeler, gösterdikleri deformasyon davranışlarına bağlı olarak elastomerik, plastik-elastik ve kırılğan-elastik olarak üç ana grupta toplanabilir (Esen, Z., 2007).

- Elastomerik: bu tipteki doğrusal elastikliğin çok düşük bir gerilimi vardır; gerilim seviyesi %5 ya da daha aşağıdadır. Bu yapıda eğer hücreler kapalı yapıda ise hücre yüzeyi ya da hücre duvarları genişleyerek doğrusal bir elastiklik sağlamaktadır. Gözeneklerin elastik olarak çökmesi ise hücre duvarlarının elastik bükülmesi sonucu meydana gelmektedir. Açık ve kapalı gözeneklerin elastik çökme gerilimi üzerinde farklı etkileri vardır.
- Plastik-elastik çökme ve yoğunlaşma: Polimerler ve plastik eğilme noktasına sahip metalik köpükler sahip oldukları doğrusal elastik rejimin ötesinde yüke maruz kaldıklarında çökmektedir. Plastik çökme sayesinde gerilim-gerinim eğrisinde uzun yatay düzlükler ortaya çıkmaktadır. Plastik deformasyon meydana geldikten sonra yoğunlaşma başlamaktadır ve gerilim oranı hızlı şekilde yükselmektedir.
- Elastik-kırılğan: bu tür basma davranışı genellikle seramik köpüklerinde ve kırılğan gözenekli malzemelerde gözlenmektedir.



### 3. YÖNTEM VE GEREÇLER

#### 3.1. Kullanılan Tozlar

Bu çalışmada gözenekli TiNb alaşımlarının elde edilmesinde Ti, Nb ve Mg tozları kullanılmıştır. Alaşımın atomik oranı  $Ti_{74}Nb_{26}$  (ağırlıkça %40 Nb, %60 Ti) olarak belirlenmiştir; bu oran ikili Ti-Nb alaşımında en düşük elastik katsayıyı sunmaktadır ve bu nedenle biyomedikal uygulamalarda kullanıma uygundur. Saf titanyum (%99.5) ve saf niyobyum (%99.8) tozlarının parçacık büyüklüğü -325 mesh (45 $\mu$ m'den küçük) olarak belirlenmiştir ve her iki toz da Alfa Aesar, Almanya'dan tedarik edilmiştir. Numunelerin içinde küresel gözenekler elde etmek içinse boşluk oluşturucu madde olarak magnezyum tozları (TangShan WeiHao Magnesium Powder Co., Ltd., Çin) kullanılmış ve magnezyumun (%99.8 saflıkta) tanecik boyutu 100-600  $\mu$ m olarak belirlenmiştir.

#### 3.2. Deney Yöntemi

Bu çalışma kapsamında yaygın toz metalürji yöntemlerinden ikisi olan sıcak presleme ve boşluk oluşturucu teknikleri kullanılmış, bu yöntemler birleştirilerek gözenekli TiNb alaşımları elde edilmiştir. Farklı oranlardaki Ti, Nb ve Mg tozları (hacimsel olarak %40, %50, %60 ve %70 Mg) bağlayıcı madde olarak az miktarda (birkaç damla) etanol kullanmak suretiyle elle karıştırılmış ve ardından sıcak preslemeye maruz bırakılmıştır. Kaba Mg parçacıklarının ince Ti ve Nb tozları ile muntazam bir şekilde kaplanabilmesi için etanol kullanılması gereklidir. Homojen bir dağılım elde edilmesi için karıştırma süresi 15 dakika olarak belirlenmiştir. Karıştırmanın ardından malzemeler çift taraflı grafit kalıpta sıcak pres fırını kullanılarak 50 MPa basınçta ve 600°C'de 1 saat boyunca sıkıştırılmıştır.

Sıcak presten sonra numunelerinin yüzeylerinin temizlenmesi için taşlama uygulanmıştır. Taşlamadan kaynaklanabilecek deformasyonların ortadan kaldırılması için ise perdahlama yapılmıştır.

Sıcak pres ve taşlama aşamalarından sonra numunelerin basınçsız şekilde sinterlenmesi için Protherm PTF 14/50/450 model dikey fırını kullanılmıştır.

Sinterleme esnasında aynı anda hem gözenekler oluşmuş hem de Mg uzaklaştırılmıştır. Sinterleme sıcaklığı 1200 °C, süresi ise 4 saat olarak uygulanmıştır. Tüm sinterleme ve Mg uzaklaştırma işlemleri yüksek saflıkta argon ortamında gerçekleştirilmiştir.

Sinterlenmiş gözenekli  $Ti_{74}Nb_{26}$  numuneleri dikey fırınının sıcak bölümünde yavaşça soğumaya bırakılmıştır. 1200°C'den 150°C'ye soğuma yaklaşık 8 saat sürmüştür. Saf Ti gaz gidericileri kullanılarak sinterleme esnasında oluşabilecek oksitlenmeler asgariye indirilmiştir. Tel erezyon EDM kullanılarak tüm gözenekli numuneler 5x5x10 mm ebatlarında kesilmiştir. Tüm numunelerin SEM ve XRD analizleri ile mikroyapıları ortaya çıkarılmış, yoğunluk ve gözeneklilikleri Arşimet yöntemiyle ölçülmüş ve basma testleri ile mekanik özellikleri belirlenmiştir.



#### 4. SONUÇ

Bu çalışmada gözenekli  $Ti_{74}Nb_{26}$  alaşımları ilk defa sıcak presleme ve boşluk oluşturuvcu yöntemlerinin birlikte kullanılması ile üretilmiştir. Bu çalışmadan elde edilen sonuçlar aşağıda belirtilmiştir.

- Elde edilen tüm numunelerde makro ve mikro gözenekler oluşmuştur. Makro-gözenekler Mg buharlaşması sonucu, mikro gözenekler ise verimsiz sıcak presleme ve sinterleme nedeniyle oluşmuştur. Sıcak presleme sıcaklığı Mg erime noktası ile sınırlıdır (650 °C). Çalışmada 600 °C olarak uygulanan sıcak presleme sıcaklığı bütün mikro-gözeneklerden arınmaya yetecek seviyede değildir. Ayrıca kullanılan 1200°C'lik sinterleme sıcaklığı da istenmeyen mikro-gözeneklerin engellenmesine yetmemiştir.
- Tüm gözenekli numunelerin mikro-yapıları esas olarak  $\beta$  fazından ve az miktarda da  $\alpha$  fazı ile çözünmemiş saf Nb'den oluşmaktadır. 1200°C sinterleme sıcaklığı Nb'nin tam çözünmesi için yeterli değildir. Ayrıca mikro-yapıdaki Nb dağılımı da tamamen homojen olarak gerçekleşmemiştir.  $\beta$  fazının farklı noktalarından alınan EDS nokta analizi farklı Nb içeriği değerlerini göstermiştir.
- Gözenekli numunelerin mikro-yapılarında oksitler, karbürler veya Mg kalıntıları gibi kirletici edici ürünler gözlenmemiştir ve sinterleme esnasında Mg tozları başarı ile uzaklaştırılmıştır. Kullanılan Mg ve Ti gaz alıcıları işlem esnasında oksitlenmenin engellenmesi konusunda yeterli olmuştur.
- Yoğunluk testi sonuçları gözenekliliğin %43'ten %68'e yükselmesi ile numunelerin yoğunluğunun azaldığını göstermektedir. Ayrıca toplam gözenekliliğin artması ile gözenekler arasındaki bağlantı ve açık gözenek oranları da yükselmiştir.
- Artan gözenekliliğe bağlı olarak  $Ti_{74}Nb_{26}$  alaşımının elastik katsayısı, akma ve basma dayanımı azalmıştır. %43, 54 ve 59 gözeneklilikteki numuneler gözenekli kemiklerin protezi için uygundur ancak düşük dayanıklılığı nedeniyle %68 gözeneklilikteki numune uygun değildir. Öte yandan

numunelerin hiçbirisi kortikal kemiklerin protezlerinde kullanmaya uygun mekanik özelliklere sahip değildir.

- Mikro-gözenek içeriğini ortadan kaldırmak ya da en azından asgari seviyeye indirmek ve Nb'nin homojenik dağılımını sağlamak için sinterleme sıcaklığı 1200 °C'den yüksek olmalıdır.



## CURRICULUM VITAE

### Personal Information

Name and Family	Dana Kareem Hameed PALANI
Gender	Male
Date of Birth	27 November 1986
Birth Town	Darandikhan - Sulaymaniyah

### Contact Information

Work Address	Sulaymaniyah - Darbandikhan Technical Institute
Home Address	Sulaymaniyah - Darbandikhan
Mobile	07701586845
E-mail	danakareem86@gmail.com

### Education

Degree	University/Town	Period (years)	Started - Ended
Master of Mechanical Engineer	Van Yuzuncu Yil Turkey	3	2015/ 2018
Bachelor/Mechanical Engineer	Salahadin/Erbil	4	2005/2009

### Work Experience

Position	Employer	Started	Ended
Technical Drawing Teacher	Darbandikhan Technical Institute	2009	2015
Head of Storage Part	Darbandikhan Technical Institute	2010	2012
Computer Teacher	Darbandikhan Technical Institute	2011	2013
Electricaldepartment division	Darbandikhan Technical Institute	2012	2015
Building cafeteria for Darbandikhan Technical Institute work as mechanical engineer at 2013			

### Foreign Language

Language	Conversation	Translation	Writing	Reading
Kurdish	Excellent	Excellent	Excellent	Excellent
English	Good	Good	Good	Good
Arabic	Good	Very good	Very good	Very good